UNIVERSITY OF HAWAII LIBRARY
JUN 20 '58

The
hilosophical Magazine

FIRST PUBLISHED IN 1798

A Journal of Theoretical Experimental and Applied Physics

Vol. 3 May 1958 No. 29
Eighth Series

£1 5s. 0d., plus postage
Annual Subscription £13 10s. 0d., payable in advance

ALERE FLAMMAM

Printed and Published by
TAYLOR & FRANCIS LTD
RED LION COURT, FLEET STREET, LONDON, E.C.4

THE PHILOSOPHICAL MAGAZINE

Editor

Professor N. F. Mott, M.A., D.Sc., F.R.S.

Editorial Board

Sir Lawrence Bragg, O.B.E., M.C., M.A., D.Sc., F.R.S.
Sir George Thomson, M.A., D.Sc., F.R.S.
Professor A. M. Tyndall, C.B.E., D.Sc., F.R.S.

Authors wishing to submit papers for publication in the Journal should send manuscripts directly to the Publishers.

Manuscripts should be typed in *double* spacing on one side of quarto (8 × 10 in.) paper, and authors are urged to aim at absolute clarity of meaning and an attractive presentation of their texts.

References should be listed at the end in alphabetical order of authors and should be cited in the text in terms of author's name and date. Diagrams should normally be in Indian ink on white card, with lettering in soft pencil, the captions being typed on a separate sheet.

A leaflet giving detailed instructions to authors on the preparation of papers is available on request from the Publishers.

Authors are entitled to receive 25 offprints of a paper in the Journal free of charge, and additional offprints can be obtained from the Publishers.

The *Philosophical Magazine* and its companion journal, *Advances in Physics*, will accept papers for publication in experimental and theoretical physics. The *Philosophical Magazine* publishes contributions describing new results, letters to the editor and book reviews. *Advances in Physics* publishes articles surveying the present state of knowledge in any branch of the science in which recent progress has been made. The editors welcome contributions from overseas as well as from the United Kingdom, and papers may be published in English, French and German.

On Whisker Growth Shapes†

By S. Amelinckx
Laboratorium voor Kristalkunde, Rozier, 6, Gent, Belgium

[Received January 17, 1958]

Brenner (1956) has observed helically twisted silver whiskers grown by thermal decomposition of the silver halide. From his photograph it is quite clear that the side faces of the whisker are formed by parallel facets, indicating that the whisker is most probably a single crystal.

Frank (1956) suggested that this particular shape results from the circular movement of a catalytic particle at the tip of the whisker. The present author suggested at that time that a helical dislocation of which the end point describes a circular path during growth, could provide an adequate explanation as well. Since then, vapour grown whiskers of PbTe, presenting the same striking shape, have been produced at the General Electric Laboratories (Apker 1957, private communication). It is doubtful that in the latter case catalytic action is responsible. We feel therefore that it is not unreasonable to assume that a helical dislocation is at the basis of this particular growth shape. In this note we describe in some detail a possible mechanism which would yield kinked and helically wound whiskers.

In view of the difficulty of representing the mechanism in space we illustrate it by means of two dimensional analogon, which can however immediately be transposed to three dimensions.

Suppose that we have a perfectly straight whisker, growing at the tip, by means of the screw dislocation mechanism (Frank 1949, Sears 1955). The screw dislocation is stable at the centre of the whisker, as shown by Eshelby (1953). There is even an attraction of the screw towards the axis of the cylindrical crystal. The screw will leave the cylinder only if it is brought by some externally applied stress nearer than about half way to the surface of the cylinder.

We further assume that the habit ‘ faces ’ of the ‘ two dimensional whisker ’ are (01) and (11). When we start with a whisker having the shape shown in fig. 1 the screw will have no tendency to be displaced, unless by some climb due to condensing vacancies, as the crystals cool. The dislocation may then acquire helical shape (Amelinckx *et. al.*, 1957) this however cannot be represented adequately in a plane.

As long as the end facet is present, the displacement of the emergence point will lengthen the dislocation. As the facet containing the emergence point of the screw will however grow faster than the others, the end facet will practically disappear at some moment, we then have the situation shown in fig. 2. The top facet has now the size of the critical nucleus, which is very small for the supersaturation of interest here.

---

† Communicated by Professor Dr. W. Dekeyser.

We now can distinguish between two possibilities : the screw maintains its direction or is able to move slightly. In the first case, it will stabilize the shape of the whisker tip. This will be such that the intersection point of all end facets coincides with the mean position of the emergence point of the screw. All end facets will grow alternatively by growth layers initiated at the screw as it moves on its circular path. The probability that this happens is largest at lower temperatures.

Figs. 1–7

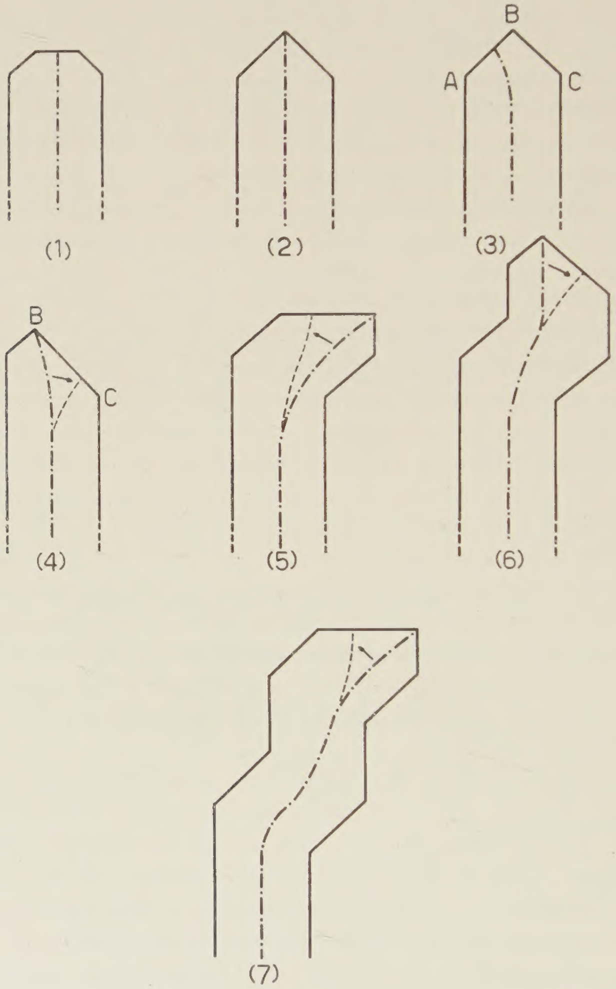

Successive stages of the developments of a (two dimensional) helical whisker. The displacement of the dislocation is indicated by the arrows.

If the screw is however able to move at higher temperatures it will do so because it implies a decrease in length. This leads to the configuration shown in fig. 3 where the screw now ends normally to one facet.

The actual shape is determined by a balance between the line tension which tends to shorten the dislocation, the surface energy which tends to shorten the exposed edge, and the attraction of the screw towards the axis of the cylinder.

The facet AB will now grow more rapidly than the other as it contains the screw ; a situation as fig. 4 results. At that point the screw can again shorten by moving over towards the centre of the facet BC. This facet can now serve as a base for the development of a little section of whisker, where again the same phenomenon will repeat. The sequence of events is represented schematically in figs. 1, 2, 3, 4, 5, 6 and 7. In the two dimensional model the dislocation ' wiggles ' from left to right and adopts a wavy shape, along the ' axis ' of the zig-zag shaped whisker. The movement of the screw is in great part conservative. If the plane of the drawing is a glide plane it is entirely a glide motion. In the three dimensional case however a small amount of climb will be necessary.

The driving force for the climb motion is in the first place the line tension and in the second place the small supersaturation of vacancies which one may expect immediately behind the growing tip. At the temperature of growth, the dislocation movement should not be too difficult. The vibration of the whiskers during growth may also favour displacement of the dislocation.

The fact that climb is involved induces the screw dislocations to adopt a helical shape, so that even in the absence of the line tension, the emergence point would tend to describe some circular path as the crystal lengthens.

The dislocation which is left in the coiled crystal, has helical shape and is of mixed character. Cottrell (1956) has demonstrated that such a situation is a stable one.

It is clear that not all whiskers will present this particular shape. It is quite well possible that the situation shown in fig. 2 subsists through the whole period of growth of the whisker especially at the lower temperature. In that case the whisker remains perfectly straight, with a tip exhibiting end facets. It may also happen that as a consequence of some growth accident the screw leaves partly or completely the whisker. In the first case the screw will end in a side face, and at high supersaturation a side branch may now develop on the whisker ; as Brenner has sometimes observed. At lower supersaturation the whisker may become a blade. A screw may also stabilize after one kink, e.g. in the situation shown in fig. 5. One will then end up with a kinked whisker. In fact the mechanism may stop accidently in any one of its phases, so that partially coiled and partially straight whiskers, may well occur. It is clear that this mechanism only applies to whiskers growing at the tip.

The square ' tubes ' of platinum described by Brenner (1956) probably originate in a normal whisker, where growth was inhibited in the centre of the terminal facet, e.g. by a foreign particle. A mechanism quite similar to the one described previously for the growth of ' hopper ' crystals (Amelinckx 1953) has probably operated in this case.

ACKNOWLEDGMENTS

This work is part of a research scheme supported by I.R.S.I.A. (Centre d'Etude de l'Etat Solide). We are grateful to Professor Dr. W. Dekeyser for his continuous interest and to Dr. R. Apker for showing the photographs of helical whiskers in PbTe, prior to publication.

REFERENCES

AMELINCKX, S., 1953, *Phil. Mag.*, **44,** 337.
AMELINCKX, S., BONTINCK, W., DEKEYSER, W., and SEITZ, F., 1957, *Phil. Mag.*, **2,** 355.
BRENNER, S. S., 1956, *Acta Met.*, **4,** 62.
COTTRELL, A. H., 1956, Lake Placid Conference on Dislocations.
ESHELBY, J. D., 1953, *J. appl. Phys.*, **24,** 176.
FRANK, F. C., 1949, *Disc. Faraday Soc.*, **5,** 48; 1956, Lake Placid Conference on Dislocations.
SEARS, G. W., 1955, *Acta. Met.*, **3,** 361.

The Electronic Structure of Diamond, Silicon and Germanium†

By G. G. Hall
Department of Mathematics, Imperial College,
South Kensington, London, S.W.7

[Received December 9, 1957 ; and in revised form January 3, 1958]

Abstract

The equivalent orbital method of describing the electronic structure of valence crystals, introduced in an earlier discussion of diamond, is extended in various ways. The interactions of more distant bonds are now included so that a more detailed description of the electronic structure can be given. The role of the equations as interpolation formulae is illustrated and used to deduce the effective masses of holes for diamond, silicon and germanium. The application of the method to the conduction bands is also considered.

§ 1. Introduction

The self-consistent field treatment of the electronic structure of a crystal is based on the use of a determinant as an approximate wave-function for the crystal as a whole. The elements in this determinant are the orbitals, functions of the position of one electron, each multiplied by a spin function. In order that a wave-function of this form should give the best energy, these orbitals must satisfy certain integro-differential equations. These equations alone do not define the orbitals uniquely; any unitary transformation of the orbitals is another solution and gives a determinantal wave-function of exactly the same form and value. This freedom is used in the equivalent orbital theory to define two different types of orbital. The crystal orbitals are defined by the additional condition that the equations should reduce to eigenvalue form and so make the orbitals independent of one another. The equivalent orbitals are defined by the additional condition that they should be invariant or permute into one another under the operations of the symmetry group of the crystal. Thus, in diamond, each equivalent orbital has a centre of inversion which leaves it invariant and every other operation permutes it into another equivalent orbital. It is not obvious that it is always possible to find such orbitals and the group theoretical conditions required have been discussed previously (Hall 1950). The remarkable fact is that these conditions are always satisfied in the equilibrium nuclear configuration of any molecule for which a classical valence diagram can be drawn, and that the symmetry of the bonds is the same as the symmetry of the equivalent orbitals. For

---

† Communicated by the Author.

this reason we may think of the equivalent orbitals as giving a quantum mechanical realization of the chemical bonds.

In diamond the transformation to equivalent orbitals is only possible within a limited range of CC internuclear distances. Thus, as the calculations of Kimball (1935) show, there is a crossing of some of the valence and conduction bands when the CC distance is about twice its equilibrium value and another when it is about half this value. Outside this range the conditions for a transformation to equivalent orbitals of this type are not satisfied and there are no chemical bonds. It is probable too that outside these limits the use of a wave-function consisting of a single determinant no longer corresponds to the ground state. This phenomenon of a definite internuclear distance at which bonds are broken, is also found in many molecules.

§ 2. THE ENERGY ZONES

The equivalent orbitals, from their definition, can be transformed exactly into the crystal orbitals by a unitary matrix. This gives a new method of discussing the band structure of crystals. The energies of the crystal orbitals are the eigenvalues of the matrix whose elements are the energies of interaction of the equivalent orbitals. The remarkable constancy of bond properties between small molecules and crystals suggests that in practice the equivalent orbitals are not widely spread, so that all but a finite number of these interactions between a bond and its neighbours will be negligible. In these circumstances the energies of the crystal orbitals can be deduced in terms of the remaining equivalent–orbital interaction energies. In principle all of these interactions could be included and knowledge of them is exactly equivalent to knowledge of the crystal orbital energies.

In an earlier paper (Hall 1952) this method was used to discuss the valence bands of diamond. Only two parameters were used a, the ionization energy of an equivalent orbital, and b, the interaction energy between two neighbouring equivalent orbitals. It was found that two of the four bands were broad, with widths depending on b, but two remained degenerate with energies independent of wave-vector. This was clearly an over-simplification but there was no information available then to enable further parameters to be estimated. Much more information about diamond-type crystals is now available and a more detailed treatment can be given.

Each bond in a diamond lattice has six nearest neighbours. These were discussed previously. There are also two kinds of next nearest neighbour. Six of these are parallel to the original bond and may be called trans bonds and twelve are non-parallel cis bonds. The corresponding interaction energies will be denoted by c and d respectively. The matrix of interactions e_{rs} between the equivalent orbitals χ_t can now be set up. The eigenvalues of this matrix, which are the energies of the crystal orbitals, are then found by solving the determinantal equation

$$|e_{rs}-E\delta_{rs}|=0. \qquad \ldots\ldots \quad (2.1)$$

Alternatively, the matrix T_{ts}, which reduces e_{rs} to diagonal form, may be found by solving the system of homogeneous linear equations

$$\sum_s e_{rs}T_{ts} - E_{tt}T_{tr} = 0, \quad r = 1, 2, \ldots \quad . \quad . \quad . \quad . \quad (2.2)$$

This matrix is largely determined by the translational symmetry of the crystal.

The unit cell of the diamond lattice is a parallelepiped spanned by three basic vectors $\mathbf{a}_1$, $\mathbf{a}_2$, $\mathbf{a}_3$, and containing two atoms. The two atoms in the (l, m, n) cell, where l, m, n are integers, are located at

$$\mathbf{a} = l\mathbf{a}_1 + m\mathbf{a}_2 + n\mathbf{a}_3$$

$$\mathbf{a}' = (l + \tfrac{1}{4})\mathbf{a}_1 + (m + \tfrac{1}{4})\mathbf{a}_2 + (n + \tfrac{1}{4})\mathbf{a}_3.$$

The unit cell contains four bonds. That joining the two atoms has an equivalent orbital which will be labelled $\chi\ (l, m, n, 0)$ and that joining $\mathbf{a}'$ to $\mathbf{a} + \mathbf{a}_r$ as $\chi(l, m, n, r)$. The translational symmetry suggests the substitutions

$$\begin{aligned} T_{\mathbf{K}, s} &= P_{\mathbf{K}, 0}\, e^{i\mathbf{K}\cdot\mathbf{a}}, \text{ if } s = (l, m, n, 0) \\ &= P_{\mathbf{K}, r}\, e^{i\mathbf{K}\cdot(\mathbf{a} + \frac{1}{2}\mathbf{a}_r)}, \text{ if } s = (l, m, n, r), \end{aligned} \quad . \quad . \quad . \quad (2.3)$$

where $\mathbf{K}$ labels the crystal orbitals and is a vector in the reciprocal lattice, viz.

$$\mathbf{K} = f\mathbf{b}_1 + g\mathbf{b}_2 + h\mathbf{b}_3 \quad . \quad . \quad . \quad . \quad . \quad . \quad . \quad . \quad (2.4)$$

and

$$\mathbf{a}_i \cdot \mathbf{b}_j = \delta_{ij}. \quad . \quad . \quad . \quad . \quad . \quad . \quad . \quad . \quad . \quad . \quad (2.5)$$

The effect of these substitutions is to reduce the infinite system of eqns. (2.2) to four equations

$$\sum_s \alpha_{rs}P_{\mathbf{K}, s} - E_{\mathbf{K}}P_{\mathbf{K}, r} = 0, \quad r = 0, 1, 2, 3. \quad . \quad . \quad . \quad (2.6)$$

In terms of the parameters a, b, c, d the symmetrical matrix α_{rs} has elements

$$\begin{aligned}
\alpha_{00} &= a + 2c\{\cos f + \cos g + \cos h\}, \\
\alpha_{11} &= a + 2c\{\cos f + \cos (g - f) + \cos (h - f)\}, \\
\alpha_{22} &= a + 2c\{\cos g + \cos (h - g) + \cos (f - g)\}, \\
\alpha_{33} &= a + 2c\{\cos h + \cos (f - h) + \cos (g - h)\}, \\
\alpha_{01} &= \alpha_{10} = 2b \cos \tfrac{1}{2}f + 2d\{\cos (g - \tfrac{1}{2}f) + \cos (h - \tfrac{1}{2}f)\}, \\
\alpha_{02} &= \alpha_{20} = 2b \cos \tfrac{1}{2}g + 2d\{\cos (h - \tfrac{1}{2}g) + \cos (f - \tfrac{1}{2}g)\}, \\
\alpha_{03} &= \alpha_{30} = 2b \cos \tfrac{1}{2}h + 2d\{\cos (f - \tfrac{1}{2}h) + \cos (g - \tfrac{1}{2}h)\}, \\
\alpha_{12} &= \alpha_{21} = 2b \cos \tfrac{1}{2}(g - f) + 2d\{\cos \tfrac{1}{2}(g + f) + \cos (h - \tfrac{1}{2}f - \tfrac{1}{2}g)\}, \\
\alpha_{13} &= \alpha_{31} = 2b \cos \tfrac{1}{2}(h - f) + 2d\{\cos \tfrac{1}{2}(h + f) + \cos (g - \tfrac{1}{2}h - \tfrac{1}{2}f)\}, \\
\alpha_{23} &= \alpha_{32} = 2b \cos \tfrac{1}{2}(h - g) + 2d\{\cos \tfrac{1}{2}(h + g) + \cos (f - \tfrac{1}{2}h - \tfrac{1}{2}g)\}.
\end{aligned} \qquad (2.7)$$

The elimination of the $P_{\mathbf{K},r}$ from eqn. (2.6) leads to a determinantal equation for the crystal orbital energies $E_{\mathbf{K}}$, viz.

$$|\alpha_{rs}-E_{\mathbf{K}}\delta_{rs}|=0. \quad . \quad . \quad . \quad . \quad . \quad . \quad . \quad . \quad (2.8)$$

This equation has four roots and these give the values of $E_{\mathbf{K}}$ in the four valence bands. The corresponding crystal orbitals will be

$$\psi_{\mathbf{K}}=\sum_{lmn}\{P_{\mathbf{K},0}\,e^{i\mathbf{K}.\mathbf{a}}\chi(l,m,n,0)+P_{\mathbf{K},1}\,e^{i\mathbf{K}.(\mathbf{a}+\frac{1}{2}\mathbf{a}_1)}\chi(l,m,n,1)$$
$$+P_{\mathbf{K},2}\,e^{i\mathbf{K}.(\mathbf{a}+\frac{1}{2}\mathbf{a}_2)}\chi(l,m,n,2)+P_{\mathbf{K},3}\,e^{i\mathbf{K}.(\mathbf{a}+\frac{1}{2}\mathbf{a}_3)}\chi(l,m,n,3)\}. \quad . \quad . \quad (2.9)$$

In the previous treatment it was always possible to factorize the eqn. (2.8) but this is no longer possible for arbitrary values of **K**. When **K** is restricted to certain lines, fixed by the symmetry of the energy surfaces, factorization is still possible. Thus, along the line $h=0$, $g=f$ the four energy bands are

$$E_{(f,f,0)}=a+2b+2c+4(c+d)\cos f\pm 4(b+2d)\ \cos\tfrac{1}{2}f, \quad . \quad (2.10)$$

$$a-2b+2c+4(c-d)\cos\ f\,(\text{twice}). \quad . \quad . \quad . \quad . \quad (2.11)$$

Similarly along the line $h=g=f$, or the line $g=h=0$, the four bands are

$$E_{(f,f,f)}=a+2b+2c+2d+(4c+2d)\cos f\pm 2\sqrt{\{[b+c+d+(d-c)\cos f]^2}$$
$$+3(b+2d)^2\cos^2\tfrac{1}{2}f\}, \quad . \quad . \quad . \quad . \quad . \quad . \quad . \quad . \quad . \quad . \quad . \quad . \quad . \quad (2.12)$$

$$a-2b+4c-2d+(2c-2d)\cos f\,(\text{twice}). \quad . \quad . \quad . \quad (2.13)$$

These formulae show that the two bands, which were degenerate before, now have a width proportional to $(c-d)$. At $(0,0,0)$ there are two energies, the lower at

$$E_{(0,0,0)}=a+6b+6c+12d \quad . \quad . \quad . \quad . \quad . \quad (2.14)$$

is singly degenerate, while the upper at

$$E_{(0,0,0)}=a-2b+6c-4d \quad . \quad . \quad . \quad . \quad . \quad (2.15)$$

is triply degenerate.

§ 3. DETERMINATION OF PARAMETERS

This description of the valence bands of a diamond-type crystal now contains four parameters which could be determined in various ways. In principle it might be possible to solve the equation defining one equivalent orbital since this one function defines all the matrix elements, but in practice this is too difficult. The previous paper used values of a and b which were determined purely empirically from the ionization potentials of paraffin molecules. Unfortunately these potentials are not known with sufficient accuracy or in sufficient numbers to enable further parameters to be determined.

There are many advantages in a purely empirical determination of the parameters. The greatest is that the labour of calculation is avoided. There are risks of overfitting or underfitting the experimental data but, if the experimental accuracy is known, these risks can be estimated by a χ^2 significance test. One method of determining the parameters empirically might be to use the x-ray emission spectra of the crystals. The width of the spectrum, for example, is a measure of

$$8b+16d \qquad (3.1)$$

but, unfortunately, the width is not well defined experimentally because of the background. The development of this method will depend on a better understanding of the details of these spectra.

Another method of determining the parameters is by using the formulae to fit the results obtained by other methods of calculation. This method was applied in the previous paper to the calculations of Kimball (1935) on diamond. The method has since been applied to metals (Hall 1953, Slater and Koster 1954). It is particularly useful as an interpolation formula to deduce the energy of any crystal orbital from the small number of energies which can be calculated directly by other methods. The calculations of Kimball are not accurate enough to determine c and d but those of Herman on diamond (1952) and germanium (1954) by the orthogonalized plane wave method, and of Jenkins on silicon (1956) by the variational cellular method, have been fitted in this way and the resulting values of the parameters are shown in table 1.

Table 1. Parameters Determined by Fitting other Calculations (in Rydbergs)

	Diamond	Silicon	Germanium
a	−1·547	−0·353	−0·248
b	−0·135	−0·058	−0·110
c	0·044	0·011	0·020
d	−0·032	−0·031	0·004

Despite the labour of their calculations, these authors do not claim high accuracy in their results, primarily because of the uncertainty of the crystal potential. For this reason these values of the parameters may not be very accurate despite the closeness of the fitting.

§ 4. SHAPE AT THE TOP OF THE VALENCE BANDS

In diamond, silicon and germanium the top of the valence bands occurs when $\mathbf{K}=0$ at the energy given by (2.15). The form of the energy surfaces in this neighbourhood are of considerable importance in understanding many physical properties of the crystals.

Three energy surfaces meet at the top of the valence band and in consequence they vary in a way too complicated to be described by an effective mass. To determine their form, the determinantal eqn. (2.8) is first transformed using the matrix

$$1/4 \begin{bmatrix} 1 & 1 & 1 & 1 \\ 1 & 1 & -1 & -1 \\ 1 & -1 & 1 & -1 \\ 1 & -1 & -1 & 1 \end{bmatrix}. \tag{4.1}$$

This is the matrix of eigenvectors appropriate to $\mathbf{K}=0$. The cosines in the elements of α_{rs} are then expanded up to the quadratic terms. Because of the transformation using (4.1) it is found that, to the same accuracy, one eigenvalue has separated from the others. This is the eigenvalue corresponding to the lower singly degenerate energy surface. The remaining equation is cubic and describes the upper three surfaces in the neighbourhood of $\mathbf{K}=0$.

It is convenient now to introduce rectangular coordinates in order to clarify the relation between $\mathbf{K}$ and the momentum. Unit vectors $\mathbf{i}$, $\mathbf{j}$, $\mathbf{k}$ are taken along the sides of the face-centred cubic lattice formed by the $\mathbf{a}$ atoms. If the distance between two neighbouring atoms is p, the basic lattice vectors can be expressed as

$$\left.\begin{aligned} \mathbf{a}_1 &= q(\mathbf{i}+\mathbf{j}), \\ \mathbf{a}_2 &= q(\mathbf{i}+\mathbf{k}), \\ \mathbf{a}_3 &= q(\mathbf{j}+\mathbf{k}), \end{aligned}\right\} \tag{4.2}$$

where

$$q\sqrt{3}=2p. \tag{4.3}$$

This implies that, if

$$\mathbf{K}=k_x\mathbf{i}+k_y\mathbf{j}+k_z\mathbf{k}, \tag{4.4}$$

its components are related by the equations

$$\left.\begin{aligned} f &= q(k_x+k_y), \\ g &= q(k_x+k_z), \\ h &= q(k_y+k_z). \end{aligned}\right\} \tag{4.5}$$

The cubic equation for the energy surfaces near $\mathbf{K}=0$ in terms of these new variables is

$$\begin{vmatrix} Ak^2+(B-A)k_x^2-\epsilon & Dk_xk_y & Dk_xk_z \\ Dk_xk_y & Ak^2+(B-A)k_y^2-\epsilon & Dk_yk_z \\ Dk_xk_z & Dk_yk_z & Ak^2+(B-A)k_z^2-\epsilon \end{vmatrix} = 0, \tag{4.6}$$

where

$$k^2=k_x^2+k_y^2+k_z^2 \tag{4.7}$$

and

$$A=2q^2(d-c), \tag{4.8}$$

$$B=D=q^2(\tfrac{1}{2}b-2c-d), \tag{4.9}$$

$$\epsilon=E-(a-2b+6c-4d). \tag{4.10}$$

An equation of the form (4.6) has also been deduced for these surfaces by Herman (1954) using perturbation theory and with a different interpretation of A, B, and D. This equation requires to be modified when the original Hamiltonian is modified by including spin orbit coupling terms. The effect of these terms has been considered by Elliott (1954) and he shows that at $\mathbf{K}=0$ the triplet is split into a doublet, which is uppermost, and a singlet. The shape of the surfaces in the neighbourhood of the doublet is given by eqn. (21) in his paper which should be corrected to read

$$\epsilon=\tfrac{1}{3}(2A+B)k^2\pm\tfrac{1}{3}\{(B-A)^2k^4+3[D^2-(B-A)^2](k_x^2k_y^2+k_y^2k_z^2+k_z^2k_x^2)\}^{1/2} \qquad (4.11)$$

and, near the singlet,

$$\epsilon=\tfrac{1}{3}(2A+B)k^2. \qquad (4.12)$$

Thus the singlet energy surfaces are spherical and can be described adequately by a single effective mass but the doublet energy surfaces vary with angle in a more complicated fashion than can be described adequately by effective masses. It has been found experimentally that cyclotron resonance measurements can be explained by using a formula of this type, viz.

$$\epsilon=-\hbar^2/2m[\alpha k^2\pm\{\beta^2k^4+\gamma^2(k_x^2k_y^2+k_y^2k_z^2+k_z^2k_x^2)\}^{1/2}], \qquad (4.13)$$

and experimental values of α, β, γ have been found for silicon and germanium.

A theoretical estimate of α, β, γ can now be given using the eqns. (4.8), (4.9) and identifying terms in (4.11) and (4.13). When a, b, c, d are given in Rydbergs and q in atomic units, the resulting equations for α, β, γ are

$$\left.\begin{aligned}\alpha&=-q^2(b/6-2c+d),\\ \beta&=-q^2(b/6-d),\\ \gamma^2&=\tfrac{2}{3}q^4(d-c)(b-2c-4d).\end{aligned}\right\} \qquad (4.14)$$

These equations show that α, β, γ depend sensitively on the values of c and d rather than on b and, unfortunately, they depend even more on the values of other smaller parameters which cannot yet be estimated. This sensitivity is clearly to be expected, since the higher order parameters describe the finer details of the surfaces, and the behaviour at a point is a fine detail.

The results of using (4.14) in conjunction with the values of b, c, d given in table 1 are shown in table 2 together with the experimental values (Lax, as quoted by Herman 1955). The calculation for diamond has been done in the same way as for silicon and germanium although the spin–orbit terms are much smaller and the separation of the doublet and singlet is very small. The calculations imply that the holes in the three bands of diamond all have effective masses of about 0·5 to 0·8 electron masses. The poor numerical agreement in table 2, particularly for germanium, is probably due to the inadequate accuracy of the calculations from which the parameters were determined. The eqn. (4.9) also contains the relation, $B=D$, and because of this only two of the experimental quantities are independent. The relation between them is

$$3\gamma^2=(\alpha-\beta)(\alpha+5\beta) \qquad (4.15)$$

and this relation is satisfied by the experimental values to within the experimental errors.

§ 5. The Conduction Bands

Slater (1956) has suggested that the conduction bands in these valence crystals should be considered using antibonding equivalent orbitals each of which has a node between the two atoms with which it is associated. Although this is probably possible, its justification is more difficult than that for the use of the bonding equivalent orbitals to describe the valence bands.

Table 2. Calculated and Experimental Values of α, β, γ

	Diamond calc.	Si calc.	Si expt.	Ge calc.	Ge expt.
α	1·61	1·63	4·1	1·54	13·0
$\lvert\beta\rvert$	0·11	0·56	1·4	0·63	8·7
$\lvert\gamma\rvert$	0·78	0·92	3·7	1·19	11·4

The conduction bands of a crystal may most easily be defined as the unoccupied bands obtained as higher solutions of the self-consistent equations for the crystal orbitals. The lowest of these bands should be good approximations to the orbitals occupied when extra electrons are added to the crystal. Since there are unlimited numbers of these unoccupied orbitals available, it will always be possible to select those of the correct symmetry to transform into equivalent orbitals but there may well be others, not so selected, whose energies are lower. There is some justification, however, for believing that these antibonding equivalent orbitals should have low energies. Their form is determined by the form of the effective potential in the self-consistent equations and this is completely defined by the occupied orbitals. Outside the atomic cores its most important part is the exchange potential. For these antibonding equivalent orbitals, this potential does provide a Coulomb attraction towards the nearest nuclei but it is rather weaker than for the occupied orbitals (Hall 1956). Furthermore, the unoccupied orbitals are higher solutions of the same equation and so will have more nodes and be more diffuse than the occupied orbitals. This reduced localization will mean that the interactions of higher order neighbours will be of greater importance and, hence, that the shapes of the bands will vary more from substance to substance. This general conclusion is well borne out both by experiment and by calculation.

If the phases of the antibonding equivalent orbitals are adjusted so that the four which meet at any one atom all have the same sign, then it is easily shown that they can be treated exactly like the occupied equivalent orbitals. The energies of the unoccupied crystal orbitals, for example, are given by equations identical in form with those given above except that the parameters a, b, c, d must now refer to the interactions of the antibonding equivalent orbitals. Values for a, b, c, d have been found, as before, by a least squares fitting of the formulae to the energies calculated by the same authors and are given in table 3.

Because of the uncertainties in the original calculations these results are not reliable. The values of c and d show, too, that further parameters would have to be included before the fitting became satisfactory. A positive value of a implies that the orbitals are already in the continuum. The antibonding equivalent orbitals will probably, therefore, be little more localized than if they had been constructed from plane waves. Since the calculated bands for silicon are certainly too low, the true value of a for silicon is probably positive also.

Table 3. Parameters Determined by Fitting Calculated Conduction Bands (in Rydbergs)

	Diamond	Silicon	Germanium
a	0·106	—0·070	0·538
b	—0·119	—0·010	—0·038
c	—0·072	0·025	—0·029
d	0·103	0·015	0·005

§ 6. COMPARISON WITH THE LINEAR COMBINATIONS OF ATOMIC ORBITALS METHOD

The method of equivalent orbitals, as given in previous papers, has been criticized adversely by Slater and Koster (1954). Unfortunately, most of their remarks are based on the assumption that an equivalent orbital is defined as the sum of two overlapping atomic hybrids one from each atom of the bond. Such a definition would indeed lead to an over-simplified treatment of the electronic structure and would deserve most of their comments, but it is not part of this theory. The equivalent orbitals are defined as transformations of the best possible crystal orbitals and so must give the most accurate description of the crystal which can be given using a determinantal wave-function. The expansion of equivalent orbitals in terms of atomic orbitals is not yet known but would probably be much more complicated than Slater and Koster have assumed.

The comparative simplicity of the equivalent orbital method makes it difficult to realize the number of difficult theoretical problems which it has solved or evaded. Some of these can be seen by comparing it with the linear combinations of atomic orbitals method, as applied by Slater and Koster to valence crystals. The use of atomic orbitals as a starting point might appear to make the method more concrete and easier to visualize than the equivalent orbital method, but, in fact, it leads to great difficulties.

In the first place, the best atomic orbitals to use for the solid are not known but it is clear from the example of the hydrogen molecule that the best orbitals for the atom need considerable modification, especially in scale, when a strong bond is formed. In the second place, the atomic orbitals on different atoms are not orthogonal and it is necessary either to include the overlap integrals or to transform to orthogonal orbitals. The inclusion of overlap would lead to very different equations from those used by Slater and Koster and to a difficult problem of finding independent parameters. The transformation to orthogonal orbitals is easier to carry out but has two disadvantages. It involves a delocalizing of the atomic orbitals and thus blurs the simple picture of atomic orbitals and makes necessary the inclusion of matrix elements between second and perhaps more distant neighbours. It also involves the danger of transforming away all the binding. In the hydrogen molecule, for example, the use of orthogonalized atomic orbitals fails to give any binding energy (Slater 1951). The reason for this is that, in a valence crystal, though not in an ionic solid nor in the standard-excited-state treatment of a metal (Hall 1953), the transformation to orthogonal atomic orbitals involves a genuine change in the value of the wave-function and, hence, in the form of the self-consistent potential. Some of these difficulties are masked in the Slater and Koster theory by the fact that they have not considered the self-consistent potential but treated it as independent of the orbital. In the accurate theory, the potential depends on the orbital so that the equations determining the coefficients of the atomic orbitals in the crystal orbital are cubic and not linear as they have assumed. A first approximation to the solution of the cubic equations can be found by linearizing them, as for example in the standard-excited-state method, but the energies of the crystal orbitals are no longer the eigenvalues of the linear equations but require various corrections.

The situation is, therefore, that the use of atomic orbitals involves an overlap problem, a problem of solving cubic equations and a problem of defining, even in principle, the best atomic orbitals. Also there is no reason, even then, to believe that the crystal orbitals can be expressed exactly as a linear combination of atomic orbitals, using a finite number on each atom. These problems are all solved in the equivalent orbital method. The orthogonalization of the equivalent orbitals leaves the total wave-function unchanged, the equations to be solved are rigorously linear, because of the definition as unitary transformations of the crystal orbitals, and the resulting crystal orbitals are exact. In practice, of course, the method involves approximations, due to the use of a finite number of parameters, but this is involved in any fitting method and refinements can be made as more accurate information becomes available.

ACKNOWLEDGMENT

This work was completed while the author was spending a year with the Quantum Chemistry Group, Uppsala, Sweden and he would like to express his thanks to Doc. P. O. Löwdin for his generous hospitality.

References

Elliott, R. J., 1954, *Phys. Rev.*, **96,** 266.

Hall, G. G., 1950, *Proc. roy. Soc.* A, **202,** 336 ; 1952, *Phil. Mag.*, **43,** 338 ; 1953, *Proc. phys. Soc. Lond.* A, **66,** 1162 ; 1956, *Ibid.*, **69,** 1124.

Herman, F., 1952, *Phys. Rev.*, **88,** 1210 ; 1954, *Physica*, **20,** 801 ; 1955, *Proc. Inst. Radio Engrs.*, **43,** 1703.

Jenkins, D.P., 1956, *Proc. phys. Soc. Lond.* A, **69,** 548.

Kimball, G. E., 1935, *J. chem. Phys.*, **3,** 560.

Slater, J. C., 1951, *J. chem. Phys.*, **19,** 220 ; 1956, *Handbuch der Physik*, **19,** 1 (Berlin : Springer-Verlag).

Slater, J. C., and Koster, G., 1954, *Phys. Rev.*, **94,** 1498.

The Twist in a Crystal Whisker Containing a Dislocation†

By J. D. ESHELBY
Department of Metallurgy, University of Birmingham

[Received February 10, 1958]

ABSTRACT

The twist due to a screw dislocation parallel to the axis of an isotropic cylinder of arbitrary cross section can be found from the solution of the ordinary torsion problem for the same cylinder. Some particular cases are worked out. The results are also valid for certain kinds of anisotropy.

§ 1. INTRODUCTION

It has been pointed out (Mann 1949, Eshelby 1953) that when a screw dislocation is introduced along the axis of a circular cylinder the cylinder suffers a uniform twist equal (in radians per unit length) to the Burgers vector of the dislocation divided by the area of the cross section of the cylinder. Recently twists have been observed and accurately measured in crystal ' whiskers ' whose cross sections are not circles but, for example, regular hexagons or rectangles (Webb *et al.* 1957, Webb and Forgeng 1958, Dragsdorf and Webb 1958).

In § 2 we give a general method for finding the twist due to a screw dislocation in a cylinder of general cross section. The dislocation line is parallel to the cylinder axis, but its position in the cross section is arbitrary. The problem reduces to the solution of the ordinary torsion problem for the cylinder. Some particular cases are discussed in § 3. These results refer to an elastically isotropic material, but in § 4 it is shown that they can also be applied with little or no modification to anisotropic crystals in a number of particular situations which are likely to occur in actual whiskers.

§ 2. SOLUTION OF THE TWIST PROBLEM

Let R denote the whisker cross section and C the curve bounding it, and let $\alpha(x, y)$ be the twist produced by a screw dislocation parallel to the whisker axis and passing through the point (x, y). In order to calculate α we give the whisker an arbitrary additional twist α_1 by applying couples to its ends.

To obtain the stresses associated with α_1 we have to find a function ψ satisfying

$$\nabla^2\psi=0 \text{ in } R, \qquad \psi=\tfrac{1}{2}(x^2+y^2) \text{ on } C. \quad . \quad . \quad . \quad . \quad (1)$$

---

† Communicated by the Author.

(See any book on the theory of elasticity: our notation agrees with that of Sokolnikoff 1946.) In terms of the auxiliary function

$$\Psi = \psi - \tfrac{1}{2}(x^2 + y^2) \quad . \quad . \quad . \quad . \quad . \quad . \quad . \quad . \quad . \quad (2)$$

the non-vanishing stresses are

$$\tau_{xz} = \mu\alpha_1\, \partial\Psi/\partial y, \qquad \tau_{yz} = -\mu\alpha_1\, \partial\Psi/\partial x \quad . \quad . \quad . \quad . \quad (3)$$

where μ is the shear modulus.

If the dislocation has a Burgers vector b these stresses exert a force

$$F_x = b\tau_{yz} = -\mu b\alpha_1\, \partial\Psi/\partial x$$
$$F_y = -b\tau_{xz} = -\mu b\alpha_1\, \partial\Psi/\partial y$$

on unit length of it. Thus Ψ is a potential whose gradient determines the force on the dislocation. (Compare the analogous role of the flexure function in a bent whisker (Eshelby 1953).)

The work done by the applied couples (per unit length of whisker) when the dislocation at (x, y) moves right out of the whisker along any path s is

$$\int (F_x\, dx + F_y\, dy) = -b\alpha_1\mu \int \frac{\partial\Psi}{\partial s}\, ds = -b\alpha_1\mu\, \Psi(x, y)$$

since $\Psi = 0$ on C. But this work may be calculated directly: if D is the torsional rigidity of the whisker it is simply $-\alpha_1\alpha(x, y)D$, the work done (per unit length of whisker) by the couple $\alpha_1 D$ as the twist due to the dislocation falls from its original value $\alpha(x, y)$ to the value zero when the dislocation reaches C. Thus $b\alpha_1\Psi = \alpha_1\alpha D$ and we have our basic result

$$\alpha(x, y) = \Psi(x, y)\mu b/D. \quad . \quad . \quad . \quad . \quad . \quad . \quad . \quad . \quad (4)$$

Since

$$D = 2\mu \int_R \Psi\, dx\, dy$$

we have

$$\alpha(x, y) = \tfrac{1}{2} b\Psi(x, y) \Big/ \int_R \Psi\, dx\, dy. \quad . \quad . \quad . \quad . \quad . \quad . \quad (5)$$

The integral of α over R is $\tfrac{1}{2}b$. This implies that a uniform distribution of small dislocations of total strength b per unit area spread over the cross section produces a total twist $\tfrac{1}{2}b$, in agreement with a result in the continuum theory of dislocations (see, for example, Nye 1952, Bilby *et al.* 1958).

This physical argument (which is equivalent to an application of Colonnetti's theorem), is, perhaps, formally unsatisfactory in that we have in effect subtracted the infinite self-energy of the dislocation from the two sides of the energy balance $-\alpha_1\alpha D = -b\alpha_1\Psi$, and so we sketch an analytical proof which also suggests a way to determine α when the Ψ-function is not available. It is adapted from the method used in a previous paper (Eshelby 1953). We imagine that we have obtained a solution of the elastic equations representing a dislocation in a whisker whose side-surfaces are stress-free, and in which the displacement w is required to be everywhere parallel to the whisker axis. In this state of anti-plane strain the whisker is not twisted but the stresses on its end-surfaces have a certain moment M about the whisker axis. If the necessary end-couples are not supplied the whisker will evidently have a twist $-M/D$.

Suppose that the dislocation is at $\boldsymbol{r}'=(x',y')$. Then the displacement is harmonic, behaves like $(b/2\pi)\tan^{-1}[(x-x')/(y-y')]$ near $\boldsymbol{r}'$, and, since the sides of the whisker are stress-free, its normal derivative $\partial w/\partial n$ vanishes on C (compare (6) below). It is most convenient to use the conjugate function χ related to w by

$$\frac{\partial w}{\partial x}=\frac{\partial \chi}{\partial y}=\tau_{xz}/\mu, \quad \frac{\partial w}{\partial y}=-\frac{\partial \chi}{\partial x}=\tau_{yz}/\mu. \quad . \quad . \quad . \quad . \quad (6)$$

If s denotes arc-length along C, (6) shows that $\partial\chi/\partial s=-\partial w/\partial n$, and so on C χ has a constant value which we may take to be zero. Further, χ is harmonic and behaves like $(b/2\pi)\ln|\boldsymbol{r}-\boldsymbol{r}'|$ near $\boldsymbol{r}'$. More compactly, χ is defined by the requirements:

$$\nabla^2\chi=b\delta(\boldsymbol{r}-\boldsymbol{r}') \quad \text{in } R, \quad \chi=0 \quad \text{on } C. \quad . \quad . \quad . \quad . \quad (7)$$

This implies that $-2\pi\chi/b$ is the Green's function which solves Dirichlet's problem for the contour C. That is to say, if $f(\boldsymbol{r})$ is some function defined only for values of $\boldsymbol{r}$ on C then the expression

$$F(\boldsymbol{r}')=\frac{1}{b}\int_C f(\boldsymbol{r})\frac{\partial}{\partial n}\chi(\boldsymbol{r},\boldsymbol{r}')\,ds(\boldsymbol{r}) \quad . \quad . \quad . \quad . \quad . \quad (8)$$

regarded as a function of $\boldsymbol{r}'$ is harmonic and takes the value $f(\boldsymbol{r}')$ on C.

The end couple required to maintain anti-plane strain is given by

$$M=\int_R (x\tau_{yz}-y\tau_{xz})\,dx\,dy=\mu\int_R\left(x\frac{\partial w}{\partial y}-y\frac{\partial w}{\partial x}\right)dx\,dy \quad . \quad . \quad (9)$$

or, in terms of χ,

$$M=-\tfrac{1}{2}\mu\int_R(\operatorname{grad} r^2)\,.\,(\operatorname{grad}\chi)\,dx\,dy$$

$$=\tfrac{1}{2}\mu\int_R r^2\nabla^2\chi\,dx\,dy-\tfrac{1}{2}\mu\int_C r^2\frac{\partial\chi}{\partial n}\,ds \quad . \quad . \quad . \quad . \quad (10)$$

by Green's theorem. According to (7) the first term is $\frac{1}{2}\mu b r'^2$. Equation (8) implies that the second term is harmonic in R and reduces to $-\frac{1}{2}\mu b r'^2$ on C; it is therefore identical with $-\mu b\psi(x',y')$(eqn. (1)). Thus, dropping the primes, $M(x,y)$ is identical with $-\mu b\Psi(x,y)$. To find the twist when the end couples are removed we divide $-M$ by the torsional rigidity D and so recover (4).

The sign convention we have used for the Burgers vector gives positive twist for positive b. The actual relation between Burgers vector and direction of twist is most simply stated thus. Suppose that there is a set of crystal planes perpendicular to the axis of a cylindrical whisker. When a screw dislocation is introduced they join up to form a spiral staircase. A creature ascending this staircase would follow a helical path with a certain sense. The helix formed by a generator of the undislocated cylinder has the opposite sense, and, naturally, a much coarser pitch.

When Ψ is not easily available it may be practicable to evaluate M by mapping the whisker cross section conformally on to the unit circle. Suppose that the dislocation is at the origin and that the relation

$$z \equiv x + iy = f(\zeta) \qquad . \quad . \quad . \quad . \quad . \quad . \quad . \quad . \quad . \quad (11)$$

maps the whisker contour C on to the circumference γ of the unit circle $|\zeta| \leqslant 1$ in the complex ζ-plane and in such a way that $z=0$ maps into $\zeta=0$. (The complex variable (11) is, of course, not the same as the z which appears as a suffix in (3).) We shall use a suffixed ζ to distinguish quantities taken in the ζ-plane from those in the z-plane. Let us associate with each point ζ the value of χ at the corresponding point in the z-plane. We obtain a function $\chi_\zeta(\zeta) = \chi[z(\zeta)]$ which is easily seen to be the χ-function for a dislocation at the centre of the unit circle γ, that is,

$$\chi_\zeta(\zeta) = (b/2\pi) \ln |\zeta|.$$

It follows from the theory of conformal mapping that

$$\frac{\partial \chi}{\partial n} ds = \frac{\partial \chi_\zeta}{\partial n_\zeta} ds_\zeta$$

if ds, ds_ζ are corresponding elements of C and γ. Since $\partial \chi_\zeta / \partial n_\zeta = \mu b / 2\pi$ eqn. (10) with $\boldsymbol{r}' = 0$ may be written as

$$|M| = \frac{\mu b}{4\pi} \int_\gamma |z|^2 \, d\theta.$$

If the transformation (11) can be expressed in the form

$$f(\zeta) = \sum_{n=1}^{\infty} a_n \zeta^n$$

then

$$|M| = \frac{\mu b}{4\pi} \int_\gamma \sum_m \sum_n a_m a_n^* \exp\{i(m-n)\theta\} \, d\theta$$

since $\zeta = \exp i\theta$ on γ. Thus we have the simple result

$$|M| = \tfrac{1}{2} \mu b \sum_1^\infty |a_n|^2 \qquad . \quad . \quad . \quad . \quad . \quad . \quad . \quad . \quad (12)$$

and $\alpha = |M|/D$.

The point $z=0$ can be chosen at will within C, and so our assumption that $z=f(\zeta)$ maps $z=0$ into $\zeta=0$ does not in principle limit the position of the dislocation in the whisker cross section. However, there will usually be one position of the origin for which $f(\zeta)$ takes on a manageable form, and this may not coincide with the position of the dislocation. We should then be faced with the general problem of determining ψ or Ψ at an arbitrary point within C using, for example, the analysis of Morris (1940) (see Sokolnikoff 1946) of which the above is a simple special case.

§ 3. Some Examples

It is convenient to express the twist in the form

$$\text{twist } \alpha = \kappa \times \frac{\text{Burgers vector } b}{\text{area of whisker cross section } A}.$$

We have, for example, $\kappa = 1$ for any ellipse, $\kappa = 10/9$ for an equilateral triangle, $\kappa = 1{\cdot}048$ for a square, $\kappa = 1{\cdot}015$ for a regular hexagon. In each case the dislocation is supposed to be at the centre of the cross section. The Ψ-functions for ellipse and equilateral triangle are simple expressions, (Sokolnikoff 1946, § 36, § 37) and for these and some other cross sections there is no difficulty in finding κ for a dislocation at any point in the cross section. The value for the square follows from the discussion of the rectangle below. In the case of the hexagon κ was calculated from (12) using the transformation

$$z(\zeta) = \int_0^\zeta \frac{dt}{(1-t^6)^{1/3}} = \zeta + \sum_{n=1}^{\infty} A_n \zeta^{6n+1}$$

with

$$A_n = \frac{2 \,.\, 8 \,.\, 14 \ldots \{2+6(n-1)\}}{n!\, 6^n (6n+1)}$$

which transforms a regular hexagon of side $a = z(1) = 2^{-5/2} 3^{-1/2} \pi^{-1} [\Gamma(\frac{1}{3})]^2$ into the unit circle (Kober 1957). For the torsional rigidity the value $D = 1{\cdot}0359\, \mu a^4$ quoted by Pólya and Szegő (1951) was used.

In the case of a rectangle there are rapidly-converging series for $\Psi(x, y)$ and D. (see, for example, Sokolnikoff 1946, § 38). The following values refer to a dislocation at the centre of a rectangle of sides l and $h \leqslant l$.

l/h	1	1·5	2	3	5	10	∞
κ	1·048	1·026	0·996	0·948	0·858	0·800	$\frac{3}{4}$

If we put

$$\Psi(0,0) = \tfrac{1}{4} - (8/\pi^3)\,\mathrm{sech}\,(\pi l/2h),$$
$$D/\mu l h^3 = \tfrac{1}{3} - (64/\pi^5)\{\tanh(\pi l/2h) + 3^{-5}\tanh(3\pi l/2h)\}$$

the error in

$$\kappa = \frac{\Psi(0,0)/h^2}{D/\mu l h^3}$$

will not exceed $\frac{1}{5}$%. If $l \geqslant 3h$ we have

$$\kappa = \tfrac{3}{4}/(1 - 0{\cdot}630 h/l)$$

to better than $\frac{1}{5}$%.

The twist due to a dislocation not at the centre of the cross section of the rectangle is easily found from the series for $\Psi(x, y)$. As an example, suppose that in a rectangle of sides 1 unit by 2 units the dislocation is displaced from the centre to a point equidistant from three sides. Then κ is reduced from 0·996 to 0·850, or by about 12%.

For any whisker cross section C a well known analogy enables us to visualize roughly how the twist varies with the position of the dislocation. A hole having C for boundary is cut in a plate and a membrane is stretched across it. If a uniform pressure is applied to one side the deflection of the membrane at (x, y) is proportional to $\Psi(x, y)$ and hence to α or κ. There is also a membrane analogy for the function χ of § 2. Let the uniform pressure be removed and instead let the membrane be deflected by a single point-force applied at a point corresponding to the position of the dislocation. Then the deflection at (x, y) is proportional to $\chi(x, y)$. The result following eqn. (5) says, in effect, that deflection by a multitude of point-forces and deflection by a pressure mean the same thing.

The expression for the twist needs modification if the dislocation has a hollow core. Suppose that this takes the form of a circular cylinder of radius r_0 small compared with the dimensions of the cross section. In the state of anti-plane strain described by χ (§ 2), there is no stress across a curve $\chi = \text{const.}$ Around the dislocation these curves will be very nearly circles, and so the elastic field will not be upset by the removal of the core, but $|M|$ will be reduced by $\frac{1}{2}\mu b r_0^2$. Thus (4) must be replaced by

$$\alpha(x, y) = \mu b \{\Psi(x, y) - \tfrac{1}{2} r_0^2\}/D.$$

Strictly, D as well as $|M|$ is decreased by the presence of the hole, but it is not so easy to calculate the correction. If the dislocation happens to be at a centre of high symmetry of the boundary curve C the curves $\Psi = \text{const.}$ around the dislocation will be nearly circular, and D is reduced by $\frac{1}{4}\pi\mu r_0^4$. Whether it has this simple form or not the correction to D will be negligible compared with the correction to $|M|$.

§ 4. ANISOTROPIC WHISKERS

If the whisker axis coincides with a four-fold or six-fold axis of the crystal the equations governing anti-plane strain and torsion are identical with those for an isotropic medium with $\mu = c_{55}$ (Voigt 1929, Eshelby *et al.* 1953) and our previous expressions for the twist can be used without modification.

Again, suppose that the whisker axis coincides with the z-axis of the crystal and that the elastic coefficients c_{14}, c_{15}, c_{16}, c_{24}, c_{25}, c_{26} and c_{45} vanish. Then it is possible to have a state of anti-plane strain with the displacement parallel to the whisker axis. The governing equation is

$$\frac{\partial \tau_{xz}}{dx} + \frac{\partial \tau_{yz}}{\partial y} = 0 \quad \text{with } \tau_{xz} = c_{55}\frac{\partial w}{\partial x}, \quad \tau_{yz} = c_{44}\frac{\partial w}{\partial y}.$$

We need to find a solution representing a screw dislocation and from it we have to calculate the end-couple required to maintain anti-plane strain. Suppose that the dislocation is at (x', y') and that the boundary of the whisker cross section is the curve

$$C : x = F(y);$$

for example, $x = \pm (a^2 - y^2)^{1/2}$ when C is a circle.

Introduce the variables

$$\xi=(c_{44}/c_{55})^{1/2}x, \quad \eta=y. \qquad (13)$$

When C is described in the (x, y) plane the curve

$$\Gamma : \xi=(c_{44}/c_{55})^{1/2}F(\eta)$$

is described in the (ξ, η) plane. It is easy to show that the substitution (13) reduces the anisotropic problem to the corresponding isotropic problem in the sense that we have to find a function w to satisfy $\partial^2 w/\partial\xi^2+\partial^2 w/\partial\eta^2=0$ with the boundary conditions $w\sim(b/2\pi)\tan^{-1}[(\xi-\xi')/(\eta-\eta')]$ near (ξ', η') and $\partial w/\partial\nu=0$ on Γ, regarding ξ, η as ordinary Cartesian coordinates. (ν is the normal to Γ.) The integral (9) translates into

$$M=c_{55}\int\left(\eta\frac{\partial w}{\partial\xi}-\xi\frac{\partial w}{\partial\eta}\right)d\xi\,d\eta$$

taken over the interior of Γ. This is the same as M for a fictitious isotropic whisker bounded by Γ and having a shear modulus $\mu=c_{55}$. On the other hand, it can be shown (Sokolnikoff 1946, § 51) that the torsional rigidity of the anisotropic whisker is $(c_{55}/c_{44})^{1/2}$ times the torsional rigidity of the fictitious whisker. Thus the twist in the real whisker is equal to the twist in the fictitious whisker mutiplied by the factor $(c_{44}/c_{55})^{1/2}$. This factor can be eliminated from the expression for the coefficient κ of § 3 (the fictitious whisker has $(c_{44}/c_{55})^{1/2}$ times the area of the real whisker) and we are left with the following simple result:

> Let the whisker axis coincide with the z-axis of a crystal in which the elastic constants c_{14}, c_{15}, c_{16}, c_{24}, c_{25}, c_{26} and c_{45} vanish. Let the dislocation be at the point $x=X$, $y=Y$ within the whisker contour $x=F(y)$. Then the coefficient κ is the same as κ for a dislocation at $x=(c_{44}/c_{55})^{1/2}X$, $y=Y$ in an isotropic whisker bounded by the curve $x=(c_{44}/c_{55})^{1/2}F(y)$.

In addition to the more obvious cases this also applies when the whisker axis is in the basal plane of a hexagonal crystal. (We use ‘ hexagonal ’ in the narrower sense, to denote a crystal which has only five independent elastic constants.) The direction of the axis in the basal plane is immaterial. What we have called c_{44} and c_{55} would in this case be the quantities normally tabulated as c_{44} and c_{66} respectively.

We may use our previous results for the isotropic case when the transformation (13) alters the shape of the whisker cross section but not its type. For example, an ellipse becomes an ellipse, and the rectangle $x=\pm\frac{1}{2}h$, $y=\pm\frac{1}{2}l$ becomes the rectangle $x=\pm\frac{1}{2}h(c_{44}/c_{55})^{1/2}$, $y=\pm\frac{1}{2}l$. On the other hand a rectangle whose sides are not parallel to the coordinate axes becomes a parallelogram, a figure we have not treated.

REFERENCES

BILBY, B. A., GARDNER, L. R. T., and SMITH, E., 1958, *Acta Met.*, **6,** 29.

DRAGSDORF, R. D., and WEBB, W. W., 1958 (to be published).

ESHELBY, J. D., 1953, *J. appl. Phys.*, **24,** 176.

ESHELBY, J. D., READ, W. T., and SHOCKLEY, W., 1953, *Acta Met.*, **1,** 252.

KOBER, H., 1957, *Dictionary of Conformal Representations* (New York : Dover Publications).

MANN, ELIZABETH H., 1949, *Proc. roy. Soc.* A, **199,** 376.

MORRIS, ROSA M., 1940, *Proc. London Math. Soc.*, **46,** 81.

NYE, J. F., 1952, *Acta Met.*, **1,** 153.

PÓLYA, G., and SZEGŐ, G., 1951, *Isoperimetric Inequalities in Mathematical Physics* (Princeton : University Press).

SOKOLNIKOFF, I. S., 1946, *Mathematical Theory of Elasticity* (New York : McGraw-Hill Book Company.)

VOIGT, W., 1929, *Lehrbuch der Kristallphysik* (Leipzig : Teubner).

WEBB, W. W., DRAGSDORF, R. D., and FORGENG, W. D., 1957, *Phys. Rev.*, **108,** 498.

WEBB, W. W., and FORGENG, W. D., 1958, *J. appl. Phys.*, **28,** 1449.

The Structure of Strong Collision-Free Hydromagnetic Waves†

By J. H. Adlam and J. E. Allen
A.E.R.E., Harwell, Didcot, Berks.

[Received January 1, 1958]

Abstract

A theoretical study has been made of the structure of strong 'hydromagnetic' waves which are propagated, across a magnetic field, in a low density plasma where collisions can be neglected. Under these conditions the ions are accelerated in the direction of propagation and then brought to rest again. The thickness of the wave is determined by the characteristic distance $\surd(mc^2/4\pi ne^2)$ and the wave velocity lies between the Alfvén speed and twice the Alfvén speed.

§ 1. Introduction

Åström (1950 a, b) has discussed the propagation of hydromagnetic waves through a low density plasma, where collisions are unimportant. The direction of propagation was taken at an arbitrary angle to the magnetic field, but the treatment referred to small-signal waves, i.e. it was assumed that the magnetic field was unaffected by the induced currents flowing in the plasma. Ferraro (1956) has described the propagation of strong collision-free waves which travel along the magnetic field; this type of wave is the collision-free analogue of the Alfvén wave (Alfvén 1942, 1950). The analysis presented in this paper is complementary to that of Ferraro‡, and pertains to the structure of strong collision-free waves which are propagated across a magnetic field.

The physical situation considered in this paper is that of a disturbance travelling into undisturbed plasma. Figure 1 is a schematic diagram of the disturbance (or wave) showing the trajectories of the electrons and ions; it is convenient to use a coordinate system moving with the wave, so that the plasma appears to flow through the wave, from left to right. The energy associated with the wave is partly kinetic energy and partly magnetic energy. It is assumed that the energy which a particle acquires in the wave is much greater than its original thermal energy, so that the latter can be ignored. The increase in the magnetic field strength is due to the transverse electron currents shown in fig. 1. A small difference between the electron and ion densities produces an electrostatic field in the direction of propagation.

---

† Communicated by the Authors.

‡ It was stated in Ferraro's paper that the waves are 'hydromagnetic' if the frequency is small compared with the plasma frequency and the velocity is small compared with the speed of light. The correct limit on the frequency is that it should be small compared with the gyrofrequency of a positive ion in the guiding field.

In the laboratory frame of reference the massive positive ions are accelerated by the electrostatic field, and then brought to rest again. Both the ion density and magnetic field increase within the wave, and then return to their initial values. The plasma returns to its initial state after the passage of the wave, except that each particle has been displaced in the direction of propagation. The thickness of the wave is determined by the characteristic distance $\sqrt{(mc^2/4\pi ne^2)}$ and the wave velocity lies between the Alfvén speed and twice the Alfvén speed, the velocity increasing with the strength of the wave.

Fig. 1

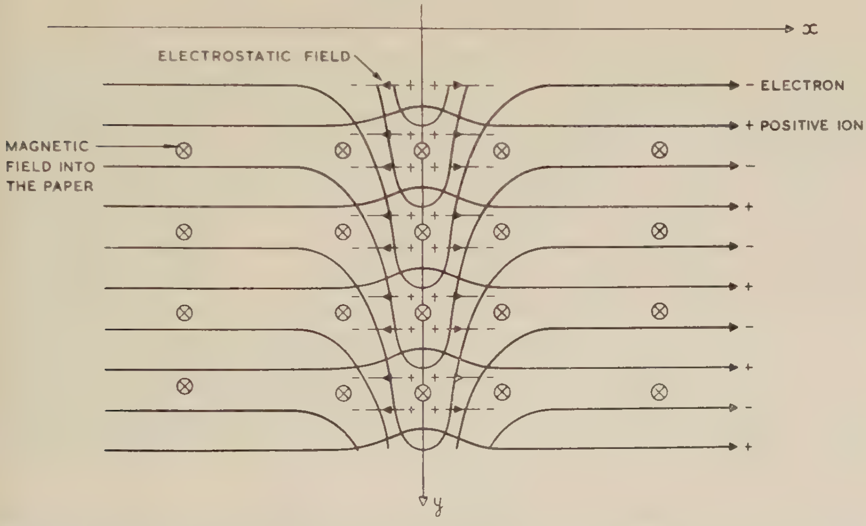

Schematic diagram showing the trajectories of the electrons and ions, viewed in a coordinate system moving with the wave. An induced electric field exists in the y-direction.

§ 2. FUNDAMENTAL EQUATIONS

The coordinate system is chosen so that the magnetic field is in the z-direction. The case considered is that of a plane wave with no variations in the y-direction or the z-direction. Thus the equations of motion for the electrons and ions can be written as follows, where suffixes 1 and 2 refer to the electron and ion respectively, and u and v are the velocity components in the x- and y-directions.

$$\frac{\partial u_1}{\partial t}+u_1\frac{\partial u_1}{\partial x}=\frac{e_1}{m_1}\left[E_x+\frac{v_1B_z}{c}\right], \quad . \quad . \quad . \quad . \quad . \quad (1)$$

$$\frac{\partial v_1}{\partial t}+u_1\frac{\partial v_1}{\partial x}=\frac{e_1}{m_1}\left[E_y-\frac{u_1B_z}{c}\right], \quad . \quad . \quad . \quad . \quad . \quad (2)$$

$$\frac{\partial u_2}{\partial t}+u_2\frac{\partial u_2}{\partial x}=\frac{e_2}{m_2}\left[E_x+\frac{v_2B_z}{c}\right], \qquad (3)$$

$$\frac{\partial v_2}{\partial t}+u_2\frac{\partial v_2}{\partial x}=\frac{e_2}{m_2}\left[E_y-\frac{u_2B_z}{c}\right]. \qquad (4)$$

The field equations, neglecting the displacement currents, are

$$\frac{\partial H_z}{\partial x}=-\frac{4\pi}{c}[n_1e_1v_1+n_2e_2v_2] \qquad (5)$$

$$\frac{\partial E_x}{\partial x}=\frac{4\pi}{k}[n_1e_1+n_2e_2] \qquad (6)$$

and

$$\frac{\partial E_y}{\partial x}=-\frac{1}{c}\frac{\partial B_z}{\partial t}. \qquad (7)$$

The numerical values of μ and k (the permeability and dielectric constant of a vacuum) are both unity, but they are retained in the equations.

These equations are much simplified by the use of the fundamental property of a plasma, namely that $|n_1-n_2|\ll n_1$ (Tonks and Langmuir 1929). Thus both n_1 and n_2 will be replaced by n in all equations except eqn. (6); the difference between n_1 and n_2 produces the electrostatic field E_x which plays an important role in this type of wave. It has been assumed that the ions are singly charged, so that $e_1=-e_2$.

Only waves of constant profile will be considered in this paper, and it is convenient to use a coordinate system moving with the wave, as already mentioned. The undisturbed plasma has a density n_0 and velocity u_0 in this coordinate system, and is situated in a uniform magnetic field B_0 at large negative values of x (see fig. 1). As the charge separation is small, it follows that $u_1=u_2=u$, to a high degree of approximation.

The relative velocity between the electrons and ions will be denoted by v, i.e. $v=(v_1-v_2)$ and the suffix z will be dropped from B_z, since the magnetic field has no other component. Eliminating E_x between eqns. (1) and (3) and putting $\partial/\partial t=0$ gives

$$u\frac{du}{dx}=-\frac{e_2vB}{(m_1+m_2)c}. \qquad (8)$$

Equations (2) and (4) give

$$u\frac{dv}{dx}=-\frac{e_2(m_1+m_2)}{m_1m_2}\left[E_y-\frac{uB}{c}\right] \qquad (9)$$

and eqn. (5) reduces to

$$\frac{dH}{dx}=\frac{4\pi n_0u_0e_2v}{uc} \qquad (10)$$

since $n=(n_0u_0)/u$.

The electric field in the undisturbed plasma is u_0B_0/c, when measured in the coordinate system moving with the wave. Equation (7) shows that $\partial E_y/\partial x=0$ when $\partial B_z/\partial t=0$, thus E_y has the constant value u_0B_0/c for all values of x.

§ 3. Solution of the Equations

The dimensionless quantities $x_n=x/d$, $u_n=u/v_A$, $\alpha=u_0/v_A$, $v_n=v/v_*$ and $B_n=B/B_0$ where

$$d=\sqrt{\left[\frac{m_1m_2c^2}{4\pi n_0\mu e_2{}^2(m_1+m_2)}\right]},\qquad v_A=\sqrt{\left[\frac{B_0{}^2}{4\pi n_0\mu(m_1+m_2)}\right]}$$

and

$$v_*=\sqrt{\left[\frac{B_0{}^2(m_1+m_2)}{4\pi n_0m_1m_2\mu}\right]}$$

will be introduced so that eqns. (8), (9) and (10) can be written

$$u_n\frac{du_n}{dx_n}=-v_nB_n, \qquad . \quad . \quad . \quad . \quad . \quad . \quad . \quad . \qquad (8\,a)$$

$$u_n\frac{dv_n}{dx_n}=-(\alpha-u_nB_n) \qquad . \quad . \quad . \quad . \quad . \quad . \quad . \qquad (9\,a)$$

and

$$\frac{dB_n}{dx_n}=\frac{\alpha v_n}{u_n}. \qquad . \quad . \quad . \quad . \quad . \quad . \quad . \quad . \quad . \qquad (10\,a)$$

Eliminating v_n between (8 *a*) and (10 *a*) gives

$$\frac{du_n}{dB_n}=-\frac{B_n}{\alpha}. \qquad . \quad . \quad . \quad . \quad . \quad . \quad . \quad . \quad . \qquad (11)$$

Integration gives

$$u_n=\alpha-(B_n{}^2-1)/2\alpha \qquad . \quad . \quad . \quad . \quad . \quad . \quad . \quad . \qquad (12)$$

where the constant of integration is chosen so that $u_n=\alpha$ when $B_n=1$.

Eliminating x_n between eqns. (8 *a*) and (9 *a*), and substituting for u_n and du_n/dB_n using (11) and (12) gives

$$v_n{}^2=-\frac{B_n{}^4}{4\alpha^2}+\left(1+\frac{1}{2\alpha^2}\right)B_n{}^2-2B_n+C$$

where C is a constant of integration. In the undisturbed plasma, $B_n=1$, $v_n=0$ so that C can be evaluated and the resulting expression for v_n is

$$v_n=\pm\frac{(B_n-1)}{2\alpha}\sqrt{[(2\alpha+1+B_n)(2\alpha-1-B_n)]}. \qquad . \quad . \qquad (13)$$

Substituting for u_n and v_n in eqn. (10 *a*), using (12) and (13) gives

$$\frac{dB_n}{dx_n}=\pm\frac{\alpha(B_n-1)\sqrt{[(2\alpha+1+B_n)(2\alpha-1-B_n)]}}{2\alpha^2+1-B_n{}^2} \qquad . \quad . \qquad (14)$$

which shows that B_n has stationary values at $B_n=1$ and $B_n=(2\alpha-1)$.

The positive sign in (14) will be used for the present, and the reason for this choice will appear later.

Inversion and integration of eqn. (14) gives

$$x_n=\frac{1}{\alpha}\sqrt{\{(2\alpha+1+B_n)(2\alpha-1-B_n)\}}+\frac{\alpha}{\sqrt{(\alpha^2-1)}}$$
$$\times\ln\left[\frac{(2\alpha^2-1-B_n)-\sqrt{\{(\alpha^2-1)(2\alpha+1+B_n)(2\alpha-1-B_n)\}}}{\alpha(B_n-1)}\right]. \qquad (15)$$

The constant of integration has been chosen so that x is measured from the point where B_n has the stationary value $(2\alpha-1)$.

Examination of (15) shows that $B_n\to 1$ as $x_n\to-\infty$, which is the required boundary condition for the undisturbed plasma; this justifies the choice of the positive sign in (14) since the negative sign leads to the result $B_n\to 1$ as $x_n\to+\infty$. In order to determine B_n for positive values of x_n, however, the negative sign of (14) must be used, since the positive sign yields no further information. The resulting curve is an even function of x_n, and is plotted in fig. 2 (*a*) for different values of α.

Figure 2 also contains plots of the electric field (fig. 2 (*b*)), the relative velocity (fig. 2 (*c*)), and the ion density (fig. 2 (*d*)). The relative velocity v was calculated using (13), and the ion density n_0u_0/u was obtained from (12). The electric field was eliminated from the initial equations, but it is easily shown that

$$E_x=-\left(\frac{m_2-m_1}{m_2+m_1}\right)\frac{vB}{c} \quad . \quad . \quad . \quad . \quad . \quad . \quad . \quad . \quad (16)$$

or, using dimensionless quantities,

$$E_n=-v_nB_n \quad . \quad . \quad . \quad . \quad . \quad . \quad . \quad . \quad . \quad . \quad (17$$

where the unit of electric field strength is

$$\left(\frac{m_2-m_1}{m_2+m_1}\right)\frac{v_*B_0}{c}.$$

The range of values of α, the parameter denoting the strength of the wave, is $1\leqslant\alpha\leqslant 2$. This can be shown as follows: substituting $B_n=(2\alpha-1)$ into eqn. (12) shows that $u_n=(2-\alpha)$ at $x_n=0$. Waves containing multiple streams of ions are not considered in this paper, so that u_n is always positive and $\alpha\leqslant 2$. Equation (13) shows that $v_n\to(B_n-1)\{(\alpha+1)(\alpha-1)\}^{1/2}/\alpha$ as $B_n\to 1$, so that $\alpha\geqslant 1$. Thus $1\leqslant\alpha\leqslant 2$, i.e. $v_A\leqslant u_0\leqslant 2v_A$ for a wave of this type.

§ 4. Examination of the Plasma Property $|n_1-n_2|\ll n_1$

The net charge responsible for the electrostatic field E_x is described by eqn. (6), viz.

$$\frac{dE_x}{dx}=\frac{4\pi e_2}{k}(n_2-n_1)\,. \quad . \quad . \quad . \quad . \quad . \quad . \quad . \quad . \quad (6)$$

This quantity is greatest at the centre of the wave, as shown by fig. 2 (*b*); furthermore it increases with the value of α. Differentiation of eqn. (16) gives dE_x/dx, and at $x=0$ (where $dB/dx=0$)

$$\left(\frac{dE_x}{dx}\right)_{x=0}=-\left(\frac{m_2-m_1}{m_2+m_1}\right)\frac{B}{c}\frac{dv}{dx}. \quad . \quad . \quad . \quad . \quad . \quad . \quad (18)$$

In the strongest waves, in which α is slightly less than two, $E_y\gg uB/c$ at $x=0$. Using this condition eqn. (9) shows that

$$\left(\frac{dv}{dx}\right)_{x=0}=-\frac{e_2(m_1+m_2)u_0B_0}{um_1m_2c}$$

since $E_y=u_0B_0/c$.

Fig. 2

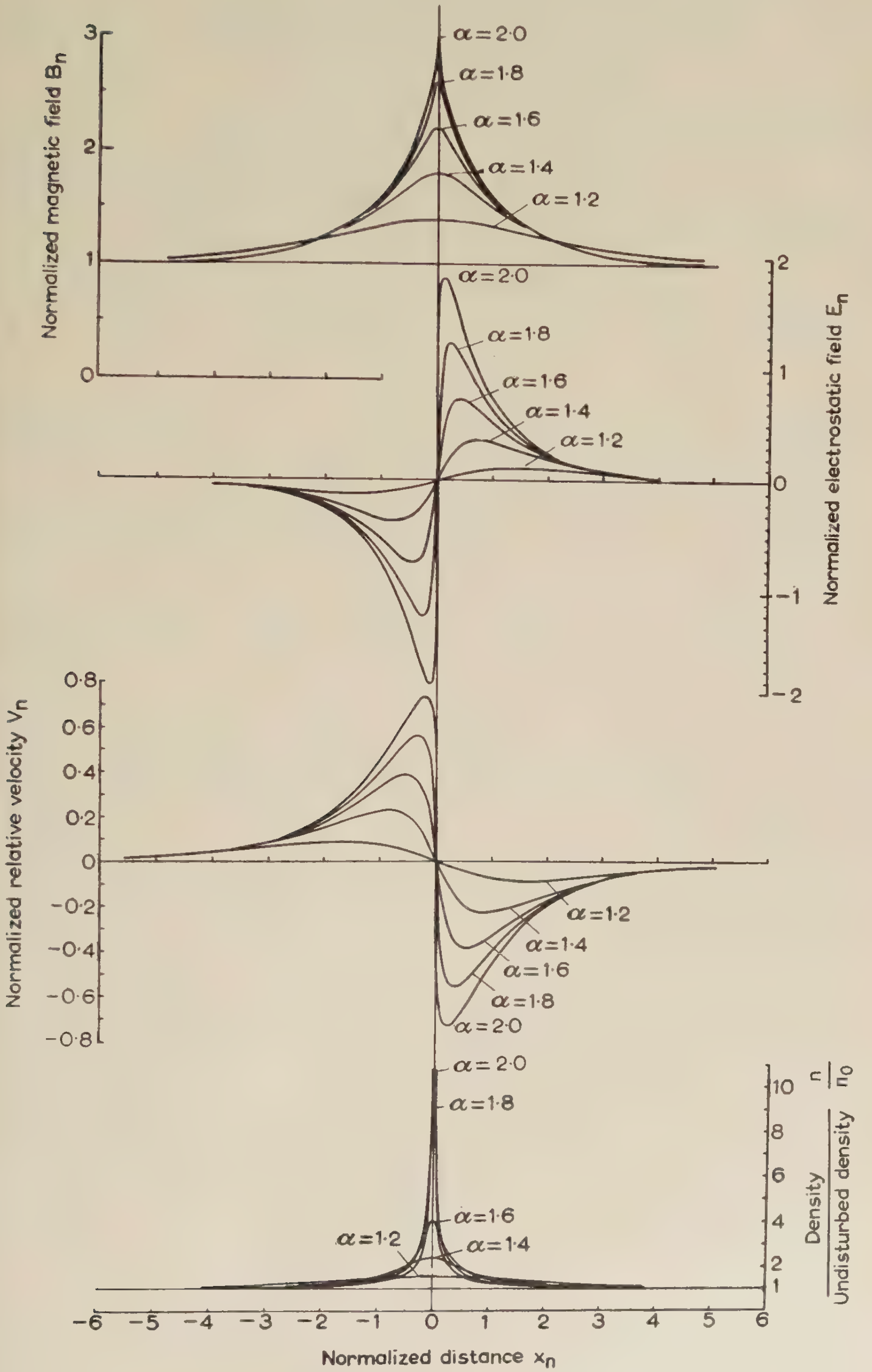

The variation throughout the wave of (*a*) the magnetic field, (*b*) the electrostatic field, (*c*) the relative velocity between electrons and ions, and (*d*) the ion density.

Substituting this expression in (18) and combining the result with (6) gives

$$\left(\frac{n_2-n_1}{n}\right)=\left(\frac{m_2-m_1}{m_2}\right)\left(\frac{(2\alpha-1)kB_0{}^2}{4\pi n_0 m_1 c^2}\right) \quad . \quad . \quad . \quad . \quad (19)$$

since $B=(2\alpha-1)\,B_0$ and $n_0u_0=nu$. As $\alpha\to 2$

$$\left(\frac{n_2-n_1}{n}\right)\to 3\left(\frac{m_2-m_1}{m_2}\right)\left(\frac{kB_0{}^2}{4\pi n_0 m_1 c^2}\right). \quad . \quad . \quad . \quad . \quad (20)$$

which can be written

$$\left(\frac{n_2-n_1}{n}\right)\to 3\left(\frac{m_2-m_1}{m_2+m_1}\right)\left(\frac{\mu k v_*{}^2}{c^2}\right).$$

Thus the assumption that $|n_1-n_2|\ll n_1$ is justified if $(v_*/c)^2\ll 1$.

§ 5. DISCUSSION

Three conditions must be satisfied if waves of the type illustrated in figs. 1 and 2 are to be excited.

(*a*) $(v_*/c)^2\ll 1$. It has been shown in § 4 that this condition must hold if $|n_1-n_2|\ll n$; it is also the condition for non-relativistic equations to be valid. An alternative form is $B_0{}^2/4\pi n_0\mu\ll m_1c^2$.

(*b*) $kT_1\ll B_0{}^2/4\pi n_0\mu$. The initial random energy is negligible if this condition holds, since the electrons are given a velocity of the order of v_*. Combination of (*a*) and (*b*) gives $kT_1\ll B_0{}^2/4\pi n_0\mu\ll m_1c^2$.

(*c*) $(d/v_A)\ll(n_0vQ)^{-1}$ where v is the random velocity of the electrons and Q is the positive ion cross section for momentum transfer. This is the criterion for collisions to be unimportant, since the time which an ion (or electron) spends in the wave is $\sim(d/v_A)$, and the mean time between collisions is $(n_0vQ)^{-1}$.

An interesting result of the present work is the emergence of the characteristic distance $d(\simeq 5\times 10^5\,n^{-1/2}$ cm). It is identical with the collision-free ‘ skin-depth ’ of a plasma, for frequencies well below the plasma frequency (Spitzer 1956).

A strong wave imparts an energy of $4(B_0{}^2/8\pi n_0\mu)$ to ions which it encounters. This energy may be appreciable, for example if $n_0=10^{13}$ ions/cm^3 and $B=1000$ gauss the ions are accelerated to an energy of 10^4 electron volts. Such waves may be excited if a plasma containing a magnetic field is rapidly compressed; the energy given to the plasma at the boundary is conveyed to the interior, partly as magnetic energy, and partly as kinetic energy of organized motion. In certain cases, some of this energy will eventually be degraded into thermal energy, by coulomb collisions or collisions with neutral atoms.

ACKNOWLEDGMENT

The authors wish to thank Dr. P. C. Thonemann for helpful comments on the first draft of this paper.

Note added in proof.—The characteristic distance d is an important parameter in Rosenbluth's recent theory of the pinch effect.

Rosenbluth, M., 1957, *Magnetohydrodynamics*, ed. R. K. M. Landshoff, p. 57, (Stanford).

References

Alfvén, H., 1942, *Nature, Lond.*, **150,** 405; 1950, *Cosmical Electrodynamics*, Ch. 4 (Oxford : Clarendon Press).
Åström, E., 1950 a, *Nature, Lond.*, **165,** 1019 ; 1950 b, *Ark. Fys.*, **2,** 443.
Ferraro, V. C. A., 1956, *Proc. roy. Soc.* A, **233,** 310.
Spitzer, L., 1956, *Physics of Fully Ionized Gases* (New York : Interscience), p. 51.
Tonks, L., and Langmuir, I., 1929, *Phys. Rev.*, **34,** 876.

Nuclear Orientation of Praseodymium 142†

By M. A. Grace, C. E. Johnson‡, R. G. Scurlock and
R. T. Taylor §
Clarendon Laboratory, Oxford

[Received January 29, 1958]

The theoretical prediction by Lee and Yang (1956) that parity might not be conserved in β-decay has stimulated an interest in the study of the angular distribution of β-rays from polarized nuclei. This was further increased by the experiment at the National Bureau of Standards (Wu *et al.* 1957), which first confirmed this hypothesis. As a result we were led to consider possible β-emitters which could be polarized by the low temperature method. One of these, ^{143}Pr seemed to be a favourable isotope since it is a pure β-emitter and if the β-intensity is recorded by the blackening of a photographic film (Grace *et al.* 1957) the absence of γ-radiation could be an advantage. To test whether polarization of ^{143}Pr was likely to be obtained we have carried out experiments on the neighbouring 19 hr isotope ^{142}Pr whose orientation can be detected and measured by observation of its γ-radiation.

In earlier experiments (e.g. Ambler *et al.* 1956, Cacho *et al.* 1955) isotopes of some rare earth elements have been oriented in both the double nitrate and ethyl sulphate salts. Paramagnetic resonance experiments on Pr^{3+} (Baker and Bleaney 1955, Duffus 1954, Cooke and Duffus 1955) show that the lowest electronic level is a magnetic doublet in both salts and that the observed spectrum can be represented by the spin Hamiltonian,

$$\mathscr{H} = g_{\parallel}\beta H_z S_z + A S_z I_z + \Delta_x S_x + \Delta_y S_y \qquad . \quad . \quad . \quad . \quad (1)$$

with an effective spin $S=\frac{1}{2}$. It is seen that the hyperfine structure is is completely anisotropic and therefore axial alignment should arise in zero magnetic field when the crystal is cooled to sufficiently low temperatures. The quantity $\Delta=\sqrt{(\Delta_x^2+\Delta_y^2)}$ is not sharply defined but has a two dimensional Gaussian distribution of standard deviation $\bar{\Delta}$ centred on zero, and has been ascribed to distortions of the local crystal field (Bleaney and Scovil 1952); its magnitude is difficult to measure accurately from the paramagnetic resonance spectrum and may be expected to depend sensitively on concentration and nature of the constituents of the crystal. The measurements on ^{141}Pr in lanthanum magnesium nitrate at 4°K show that $A = 0{\cdot}077\ \text{cm}^{-1}$, $g_{\parallel} = 1{\cdot}55$ and $\bar{\Delta}$ is about $0{\cdot}1\ \text{cm}^{-1}$ (Cooke and Duffus 1955, Duffus 1953). For ^{141}Pr in lanthanum ethyl sulphate at 20°K, $A = 0{\cdot}075\ \text{cm}^{-1}$, $g_{\parallel} = 1{\cdot}52$ and $\bar{\Delta}$ is about $0{\cdot}04\ \text{cm}^{-1}$ (Baker and Bleaney 1955).

---

† Communicated by the Authors.

‡ Now at the Radiation Laboratory, University of California, Berkeley, California, U.S.A.

§ Now at the Randall Laboratory of Physics, University of Michigan, Ann Arbor, Michigan, U.S.A.

For any particular ion, the energy levels are given by

$$W = \pm \tfrac{1}{2}\sqrt{\{(g_{\parallel}\beta H_z + Am)^2 + \Delta^2\}},$$

where m is the nuclear magnetic quantum number. As Δ increases, the different m-states are crowded together so that the degree of alignment at any given temperature is reduced. The effect of Δ can be removed by the application of an external magnetic field such that $g_{\parallel}\beta H_z \gg \Delta$, when the separation between the different m-states will approach the full value of $\frac{1}{2}A$. From the expression for the level positions the relative population distribution of the nuclear magnetic states is easily calculated as a function of temperature for given values of the parameters Δ, A and $g_{\parallel}\beta H_z$. The population distribution for a given value of $\bar{\Delta}$ is obtained by a Gaussian averaging over all Δ. The γ-ray anisotropy can then be calculated as a function of temperature for any particular decay scheme.

Since the values of A for ^{141}Pr are similar for the two crystal lattices we decided to incorporate ^{142}Pr into cerium magnesium nitrate. This choice was governed by the following considerations; firstly, temperatures down to a few millidegrees can be reached by adiabatic demagnetization o cerium magnesium nitrate (Daniels and Robinson 1953); and secondly, since $g_{\parallel}$ for Ce^{3+} in this salt is small it is possible to apply the axial magnetic field necessary for overcoming the effect of Δ without producing a prohibitive rise in temperature.

The decay scheme of ^{142}Pr, which is formed by neutron capture in stable ^{141}Pr, is shown in fig. 1. (Pohm *et al.* 1954). The unique first forbidden β-transition to the ground state of ^{142}Nd shows that ^{142}Pr has a spin of 2^-. The β-transition to the 1·57 MeV level in ^{142}Nd is classified by its comparative half-life as first forbidden with $i_{\beta} = 0$ or 1 and hence the spin of the 1·57 MeV level is 1^+, 2^+ or 3^+: the choice of 2^+ was made by Pohm *et al.* on the basis of the general systematics of the energies of the first 2^+ excited states of even–even nuclei. This spin sequence has been used for the interpretation of the present experiments.

In the experiment a single crystal of cerium magnesium nitrate (about 1 g) was grown from solution containing ^{142}Pr and this was mounted in the demagnetization cryostat: it was estimated that about $\frac{1}{2}\%$ of the Ce^{3+} ions had been replaced by Pr^{3+}. The crystal was then cooled by adiabatic demagnetization and the γ-ray anisotropy $\epsilon\{= 1 - I(0)/I(\frac{\pi}{2})\}$ was measured as a function of temperature in zero field. These measurements were also repeated with axial magnetic fields of 300 and 600 gauss and the results are shown in fig. 2. The amount of activity which can be incorporated in the crystal is determined by the heating up rate due to β-activity and in this case was chosen to be about $50\,\mu\text{c}$. Because only 5% of the decays are accompanied by γ-rays the counting rate is necessarily small, and gives rise to the large statistical errors. As can be seen the

Fig. 1

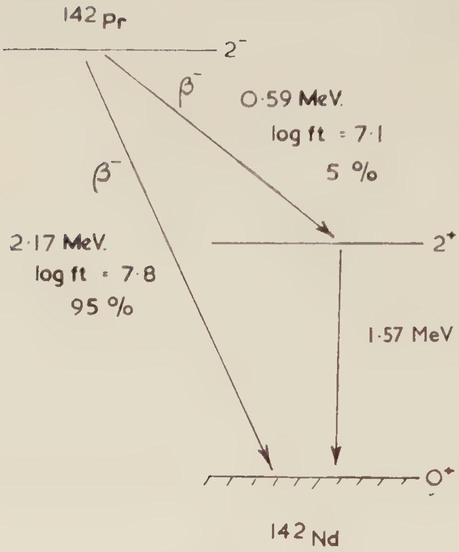

The decay scheme of ^{142}Pr.

Fig. 2

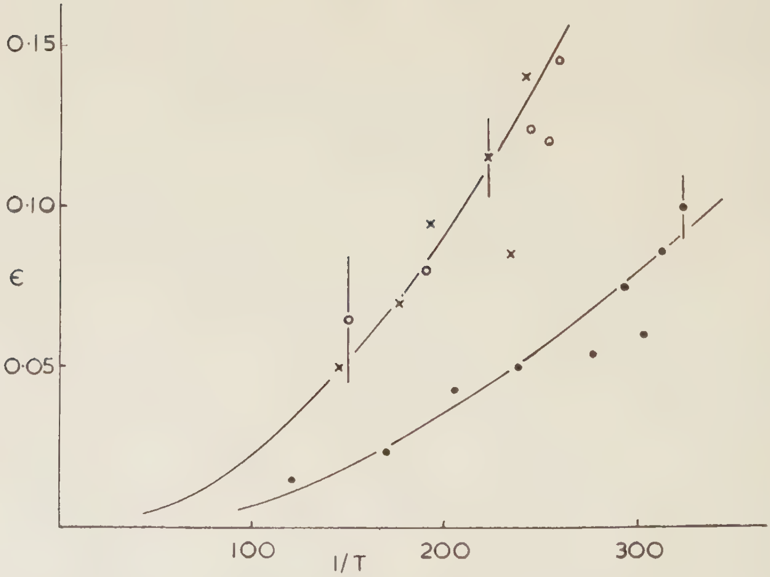

The dependence on temperature ($1/T$ in degrees K^{-1}) of the anisotropy of the 1·57 MeV γ-ray from ^{142}Pr in zero field (●) and with axial magnetic fields of 300 gauss (O) and 600 gauss (X). For each of the three experiments, a typical statistical error is indicated.

anisotropy at a given temperature is increased by the application of the field. This change in γ-ray anisotropy shows that the degree of nuclear alignment, $\langle I_z^2 \rangle$, has been increased. Since the nuclear orientation arises through a magnetic hfs coupling, any appreciable increase in $\langle I_z^2 \rangle$ through the application of a small magnetic field must be accompanied by a nuclear polarization $\langle I_z \rangle$. Thus, although we have not performed an experiment specific to nuclear polarization, the increase in γ-ray anisotropy associated with the applied magnetic field implies that a nuclear polarization has been produced. The figure also shows that the observed anisotropies in 300 and 600 gauss are closely the same. This indicates that the effect of $\bar{\Delta}$ has been largely removed by these fields. The sign of the anisotropy rules out the possibility of dipole radiation and confirms that the 1·57 MeV level must have a spin greater than one. This is in accord with the assignment of 2^+ made by Pohm *et al.* The temperatures in the applied field have been calculated from the susceptibility assuming $g_{\parallel} = 0{\cdot}03$ for Ce^{3+} (Wheatley and Estle 1956). There is an apparent contradiction between the relatively large temperature rise on application of the magnetic field, and the small value of $g_{\parallel}$. There are two possible explanations: either the $g_{\parallel}$ value is larger than that given by Wheatley and Estle, or application of the field produces irreversible heating through some secondary processes. The existence of this rise in temperature does not, however, lead to any uncertainty in the interpretation of the results which depend only on the knowledge that the effect of the Δ term has been removed by the magnetic field.

From the anisotropy of the γ-radiation in the magnetic field the hfs constant A and hence the nuclear magnetic moment can be determined. Since the angular momentum change (i_β) accompanying the β-transition can be 0 or 1, two possible sets of values are obtained. Taking

$$\epsilon = +0{\cdot}140 \pm 0{\cdot}015 \text{ at } 1/T = 250$$

we find

	A cm^{-1}	μ n.m.
$i_\beta = 0$	$0{\cdot}0027 \pm 0{\cdot}0003$	$0{\cdot}11 \pm 0{\cdot}01$
$i_\beta = 1$	$0{\cdot}0042 \pm 0{\cdot}0005$	$0{\cdot}17 \pm 0{\cdot}02$.

With these values of A, the calculated nuclear polarization ($\langle I_z/I \rangle$) of ^{142}Pr in fields above 300 gauss and at $1/T = 250$ are $0{\cdot}44$ ($i_\beta = 0$) or $0{\cdot}62$ ($i_\beta = 1$). By comparing the ϵ–$1/T$ curves with and without field we find that $\bar{\Delta}$ is about $0{\cdot}004\,\mathrm{cm}^{-1}$ if $i_\beta = 0$ and $0{\cdot}006\,\mathrm{cm}^{-1}$ if $i_\beta = 1$. The curves shown have been calculated using these values of $\bar{\Delta}$ and A.

The known spins and moments of ^{141}Pr and ^{143}Nd are in accord with shell model predictions and suggest that in ^{142}Pr the odd proton and neutron are in $d5/2$ and $f7/2$ states respectively. The use of free proton and neutron moments leads to a value for the nuclear moment of ^{142}Pr of about 1·5 n.m.; this is about ten times greater than that observed experimentally. However, calculations by Caine (1957) show that the effect of configurational mixing is to reduce this value substantially and it may be possible, therefore, to understand the small moment on this basis.

From the present experiment, the following conclusions may be drawn.

(i) A substantial nuclear polarization of ^{142}Pr has been obtained.

(ii) The orientation of ^{142}Pr in cerium magnesium nitrate is satisfactorily described by the spin Hamiltonian of eqn. (1).

(iii) The nuclear moment of ^{142}Pr is estimated to be 0·11 n.m. ($i_\beta=0$) or 0·17 n.n ($i_\beta=1$).

(iv) Since the nuclear moment of ^{143}Pr is likely to be larger than that of ^{142}Pr and similar to that of stable ^{141}Pr ($\mu=3{\cdot}9$ n.m.) we can expect to obtain a large nuclear polarization in this isotope by the present method.

ACKNOWLEDGMENTS

We are most grateful to Professor Bleaney for discussions on the interpretation of the results and to Dr. N. Kurti for his stimulating interest in the experiments.

REFERENCES

AMBLER, E., HUDSON, R. P., and TEMMER, G. M., 1956, *Phys. Rev.*, **101**, 196.
BAKER, J. M., and BLEANEY, B., 1955, *Proc. phys. Soc., Lond.* A, **68**, 936.
BLEANEY, B., and SCOVIL, H. E. D., 1952, *Phil. Mag.*, **43**, 999.
CACHO, C. F. M., GRACE, M. A., JOHNSON, C. E., KNIPPER, A. C., SCURLOCK, R. G., and TAYLOR, R. T., 1955, *Phil, Mag.*, **46**, 1287.
CAINE, C. A., 1957, *Thesis, Oxford.*
COOKE, A. H., and DUFFUS, H. J., 1955, *Proc. roy. Soc.* A, **229**, 407.
DANIELS, J. M., and ROBINSON, F. N. H., 1953, *Phil. Mag.*, **44**, 630.
DUFFUS, H. J., 1953, *Thesis*, Oxford.
GRACE, M. A., JOHNSON, C. E., SCURLOCK, R. G., and SOWTER, C. V., 1957, *Phil. Mag.*, **2**, 1050.
LEE, T. D., and YANG, C. N., 1956, *Phys. Rev.*, **104**, 254.
POHM, A. V., LEWIS, W. E., TALBOY, J. H., and JENSEN, F. N., 1954, *Phys. Rev.*, **95**, 1523.
WHEATLEY, J. C., and ESTLE, T. L., 1956, *Phys. Rev.*, **104**, 264.
WU, C. S., AMBLER, E., HAYWARD, R. W., HOPPES, D. D., and HUDSON, R. P., 1957, *Phys. Rev.*, **105**, 1413.

Some Thermal Properties of Helium and their Relation to the Temperature Scale†

By R. Berman and C. F. Mate
Clarendon Laboratory, Oxford

[Received January 11, 1958]

Abstract

Values have been obtained for the latent heat and saturated vapour density of helium between 2·2°K and 5·2°K, and the critical constants have been re-assessed. It is shown how the calculated vapour density may be used to examine the consistency of a liquid helium temperature scale.

§ 1. Introduction

In a previous paper (Berman and Poulter 1952—referred to as I), some values were given for the amount of heat required to liberate a mole of helium vapour from a calorimeter containing liquid helium. The quantity actually determined, L_a, in such measurements is related to the latent heat, L, as usually defined, by the equation

$$L = L_a(1 - \rho_V/\rho_L) \quad . \quad . \quad . \quad . \quad . \quad . \quad . \quad . \quad (1)$$

where ρ_V and ρ_L are the densities of saturated vapour and of liquid respectively. The factor $(1-\rho_V/\rho_L)$ arises because a fraction, ρ_V/ρ_L, of the vapour produced occupies the space in the calorimeter vacated by the evaporated liquid.

The measurements reported in I were made in order to calibrate a calorimeter in which the volume of gas liberated was used to measure enthalpy changes. It was later shown (Berman and Swenson 1954) that if a liquid helium temperature scale (the temperature–vapour pressure relation) is assumed, then the saturated vapour density can be derived, without a knowledge of the liquid density, from the relation

$$\rho_V = T(dP/dT)/L_a. \quad . \quad . \quad . \quad . \quad . \quad . \quad . \quad . \quad (2)$$

The vapour density can also be obtained from the virial equation, or measured directly, and a comparison of such values with those calculated from eqn. (2) can be used to examine the consistency of the assumed temperature scale. We have reported this work briefly (Berman and Mate 1957), and in the present paper we describe some experimental details and present the results in full.

---

† Communicated by the Authors.

§ 2. The Experiments

The essentials of the apparatus were described in I, so that here we mention only the changes made for the present series of experiments. The relevant part is shown in fig. 1, in which S is the high pressure pot of a Simon liquefier. A is a small annular vessel into which helium can be condensed through B, which leads to a helium supply and a burette system. F is the dropping tube used in the enthalpy measurements, and H is the small heating coil needed for determinations of L_a. E is a heat exchanger used to increase the efficiency of condensation into A.

Fig. 1

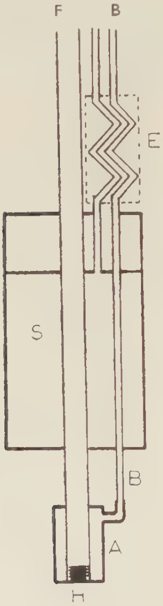

Sketch of calorimeter.

It had been found that with helium boiling at atmospheric pressure, the evaporation from the pot S sometimes became so large that it emptied before readings could be completed. At higher pressures this occurred more frequently, and experiments in the temperature range from the boiling point to the critical temperature were usually abortive. It was concluded that the well known oscillations of a helium gas column were responsible for these effects, since the onset of high evaporation rates was quite sudden and the instability increased with pressure (see ter Haar 1955). Several changes were made in the apparatus in attempts to eliminate the oscillations, which were eventually shown to be associated with the heat exchanger, E. The oscillations appeared to arise in the tubing B, connected to the tail but their main effect was to convey heat to S, increasing the evaporation from the tail only slightly. Replacement of the heat exchanger by two separate straight tubes to the pot and to the tail entirely eliminated oscillations at all pressures. Naturally, more helium was evaporated from S during condensation; nevertheless several latent heat determinations were still possible for each expansion. Later, to reduce the background evaporation, the central tube, F (required for enthalpy measurements), was cut above S and sealed, preventing radiation from reaching the tail; the elimination of conduction along this tube halved the evaporation from the pot, more than compensating for the loss during condensation.

§ 3. RESULTS

All calculations have been made using the temperature scale T_{55E} proposed by Clement (see reference).

Fig. 2

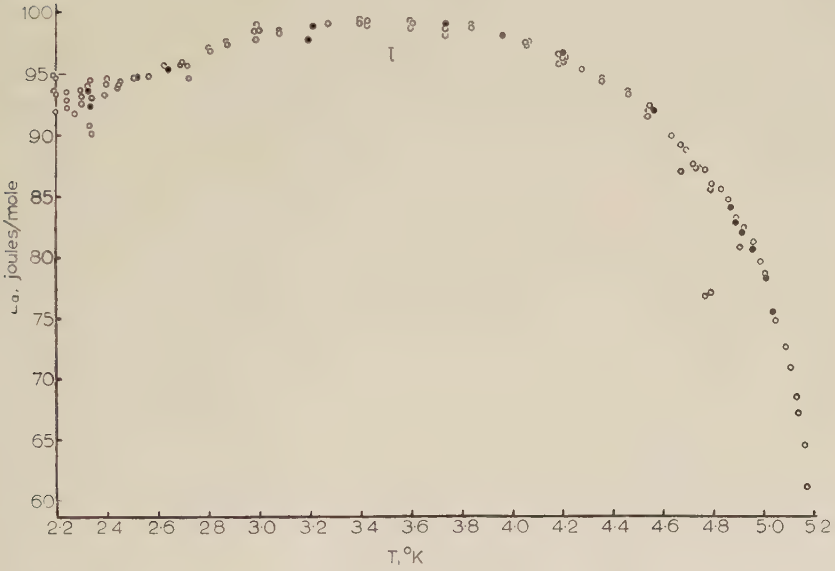

Experimental points. Full circles correspond to several measurements. Vertical line represents 1%.

3.1. *Experimental Values of L_a*

The experimental results are shown in fig. 2. They extend over a greater temperature range than the few measurements reported in I, and the values are of the order of 1% higher, the discrepancy being greater at higher temperatures. A discrepancy of 0·4% is accounted for by the neglect in I of the variation of mercury density with temperature. (The pressure of the collected gas was measured with mercury at room temperature.) Other systematic errors which might arise (e.g. calibration of the burette tubes, manometer scales, stop watch and electrical standards) were thoroughly investigated during the present series of measurements, and were not found to account for any appreciable fraction of the remaining discrepancy.

At the beginning of the present experiments only one completely satisfactory run was made with the apparatus in the same condition as for the earlier measurements. This gave a value of L_a differing from the corresponding value in I only by the mercury correction discussed above. After the heat exchanger was eliminated higher values of L_a were obtained, and at the same time several improvements in the behaviour of the apparatus were noticed: The evaporation from A returned to its background value much more rapidly after the heater current was switched off; also the final and initial backgrounds, which previously had nearly always differed, were now usually the same. A constriction in the heat exchanger could account for the first observation and the pressure built up in A could lead to low values of L_a as well as encourage oscillations. As the apparatus can now be used up to the critical pressure with no sign of oscillations, it seems safe to assume that these are absent at all lower pressures too, and we believe the present, higher, values of L_a to be correct.

It should be noted that the previous values seem to be in error systematically, so that calibration of the apparatus for enthalpy measurements is not affected.

The scatter of the experimental points is seen from fig. 2 to be of the order of 0·5% over most of the temperature range. At the lower temperatures ($< 2{\cdot}5^\circ$K) the scatter is greater due to the increase in volume of the background evaporation (the same mass of gas must be acommodated in the burette at a lower pressure) which, even for the largest burette tube we had, became a large fraction of the total evaporation measured. At the lower pressures involved, fluctuations in pressure also have more effect. As the general scatter was rather larger than expected we attempted to trace its cause, and looked for a dependence of L_a on the rate of heating or on the height of liquid helium in vessel A. In I measurements were made at different heating rates, but on examining the results more critically it was not considered certain that this had no effect. A variation with rate of heating would suggest that the background correction applied was not appropriate, as the extra flow of cold gas during the heating period alters the temperature gradient in tube B. By varying the temperature difference between S and A and finding the change in background rate it was concluded that an insignificant part of the heat leak flows down B, and indeed no change in L_a was found in the present measurements when the rate of heating was varied by a factor of 5. If there is insufficient liquid in A to extract the heat efficiently, some heat from the heater will pass up the metal walls and reach the vapour instead of evaporate liquid. There was no change in L_a when the height of liquid was varied by a factor of 20.

In the course of the work three heaters were used with resistances varying from 100 to 600 ohms, and the electrical wiring was altered. In addition, runs were made for different lengths of time for fixed rates of heating. Again, none of these variations was reflected in the values of L .

3.2. *The Latent Heat*

Smoothed values of L_a taken from fig. 2 are given in the table; these should be accurate to a few tenths of 1%. From L_a and the T_{55E} vapour pressure–temperature relation we have calculated ρ_V by eqn. (2). ρ_V derived in this way is denoted by ρ_{L_a} in the table. Below 4·4°K the liquid densities shown in the table are taken from Kerr (1957). The only data for ρ_L at higher temperatures are from the measurements of Mathias *et al.* (1925) and Clement has tabulated values from them by taking account of the change in temperature scale. As these values are only 0·25% higher than Kerr's at 4·4°K, we use them to complete the table above this temperature without further adjustment.

These values of L_a, ρ_V and ρ_L have been used in eqn. (1) to calculate the latent heat, L, which is also shown in the table. Vapour densities derived from the equation of state are possibly slightly more accurate than our values below about 3°K as the non-ideality is small, while our values are dependent on a knowledge of dP/dT. We have, however, used our values throughout since at the lower temperatures the error produced in L is negligible (even at 3·8°K $\rho_V/\rho_L \sim 0{\cdot}1$, so that an error of 1% in ρ_V will only affect L by 0·1%), and at higher temperatures, where ρ_V/ρ_L is large, the saturated vapour density can not be calculated from a virial equation with the present knowledge of the virial coefficients.

Our latent heats differ from those tabulated as L_{exp} by van Dijk and Durieux (1957) throughout the common temperature range. L_{exp} was derived from the experimental data of Dana and Kamerlingh Onnes (1926) and Berman and Poulter, and the smoothed values given by Keesom (1942). At 2·4°K our values are about 0·5% higher and the difference increases steadily to 1·7% at 4·2°K.

3.3. *Critical Data*

In fig. 3 we have plotted the vapour density, ρ_V, the liquid density, ρ_L, and the diameter, $\frac{1}{2}(\rho_V+\rho_L)$, using as before our calculated values of ρ_V.

The critical density obtained from fig. 3 is $\rho_C = 0{\cdot}0680 \pm 0{\cdot}0003\,\mathrm{g/cm^3}$. This is in extremely good agreement with the value of $0{\cdot}0675 \pm 0{\cdot}0005\,\mathrm{g/cm^3}$ which Kerr suggests as most likely, from a discussion of several possible ways in which his values of ρ_L can be used to obtain ρ_C.

Above 5°K the liquid density, as tabulated by Clement, decreases rapidly and the critical temperature is fixed fairly closely by the shape of this curve. Since we now have, in addition, values for the vapour density and can construct the diameter, it is possible to narrow the limits of uncertainty of T_C. On the T_{55E} scale we find $T_C = 5{\cdot}194 \pm 0{\cdot}002$°K and the critical pressure $P_C = 172{\cdot}4 \pm 0{\cdot}3$ cm Hg at 20°C. The critical coefficient $(RT_C\rho_C)/P_C = 3{\cdot}20$. Kamerlingh Onnes (1911) determined P_C directly as $172{\cdot}4 \pm 1{\cdot}0$ cm Hg, which corresponds on the T_{55E} scale to $5{\cdot}194 \pm 0{\cdot}008$°K.

§ 4. THE VAPOUR DENSITY AND THE TEMPERATURE SCALE

The density of a vapour can be represented by a virial equation of the form

$$PV = RT(1 + B/V + C/V^2 + D/V^3 + \ldots) \quad . \quad . \quad . \quad . \quad (3)$$

Table of Smoothed Values.

P cm Hg 20°c	L_a J/mole	ρ_L g/cm^3	T_{55E} °K	dP/dT_{55E} cm Hg 20°c per °K	L J/mole	ρ_{La} g/cm^3	ρ_{VIR} g/cm^3	$\Delta\rho$ % (smoothed)	$\frac{1}{2}(\rho_{La}+\rho_L)$ g/cm^3	$T_{La}-T_{55E}$ 10^{-4} deg
4·054	92·2	0·14646	2·200	9·767	91·4	0·001239	0·001243	+0·33	0·07385	3
5·114	92·9	14601	2·3	11·474	—	1510	1512	+0·18	—	1
6·353	93·6	14550	2·4	13·324	92·5	1816	1818	+0·05	0·07366	0
7·783	94·3	—	2·5	15·311	—	2159	2158	−0·05	—	0
9·421	95·05	14430	2·6	17·44	93·4	2538	2536	−0·05	0·07342	0
11·276	95·8	—	2·7	19·71	—	2955	2959	+0·05	—	0
13·37	96·5	14285	2·8	22·12	94·2	3413	3419	+0·22	0·07313	−1
15·71	97·2	—	2·9	24·67	—	3913	—	+0·39	—	−4
18·31	97·8	14114	3·000	27·35	94·7	4462	4484	+0·49	0·07280	−8
21·18	98·3	—	3·1	30·18	—	506	—	+0·55	—	—
24·35	98·7	13918	3·2	33·16	94·6	572	5735	+0·58	0·07245	—
27·81	98·9	—	3·3	36·26	—	643	—	+0·59	—	
31·60	99·15	13694	3·4	39·53	93·9	721	7251	+0·60	0·07208	—
35·73	99·25	—	3·5	—	—	—	—	+0·64	—	—
40·20	99·3	13443	3·6	46·52	92·7	897	9036	+0·72	0·07170	—
45·03	99·2	—	3·7	—	—	—	—	+0·83	—	—
50·25	99·0	13164	3·8	54·12	90·7	0·01105	0·01116	+0·98	0·07135	—
55·87	98·6	—	3·9	—	—	—	—	—	—	-
61·89	98·0	12856	4·000	62·38	87·7	1354	1375	—	0·07105	—
68·35	—	—	4·1	—	—	—	-	—	—	—
75·25	96·6	12518	4·2	71·33	83·8	1650	1701	—	0·07084	—
82·62	—	—	4·3	—	—	—	—	—	—	—
90·46	94·4	12150	4·4	81·00	78·8	2008	—	—	0·0708	—
98·83	—	—	4·5	—	—	—	—	—	—	—
107·71	91·1	1170	4·6	91·47	72·0	2456	—	—	0·0708	—
117·13	—	—	4·7	—	—	—	—	—	—	—
127·1	86·15	1107	4·8	102·7	62·5	3042	—	—	0·0706	—
137·7	—	—	4·9	—	—	—	—	-	—	—
148·9	78·4	1006	5·000	114·9	48·1	3896	—	—	0·0698	—
160·7	71·4	0·0928	5·1	121·4	36·0	4610	—	—	0·0695	—
166·2	66·0	0·0866	5·15	124·2	26·8	515	—	—	0·0691	—
170·6	60·4	0·0786	5·18	126·7	16·0	0·0578	—	—	0·0682	—

where the virial coefficients B, C, D ... can be derived from measurements of PV as a function of V for fixed temperatures. Keller (1955) has measured such isotherms for helium at several temperatures. At 4°K the highest vapour pressure used corresponded to about 40% of the saturation pressure, and near 2°K the highest pressure was over 90% of saturation pressure. Within the limits of the experimental uncertainties Keller found that the measured densities could be represented by eqn. (3), using only the second virial coefficient B. We would not necessarily expect, however, that the saturated vapour can be represented in the same way when the temperature and consequently the vapour pressure is high enough for large departures from ideality to exist. Using B alone, the saturated vapour at 4·2°K would have a density 40% greater than an ideal gas at the same temperature and pressure, and at 4·4°K the calculated density becomes imaginary. Even at 3·0°K the departure from ideality is still 15%. As the saturated density decreases the vapour behaves more like an ideal gas, and the small departures should be adequately represented by the term in B.

Fig. 3

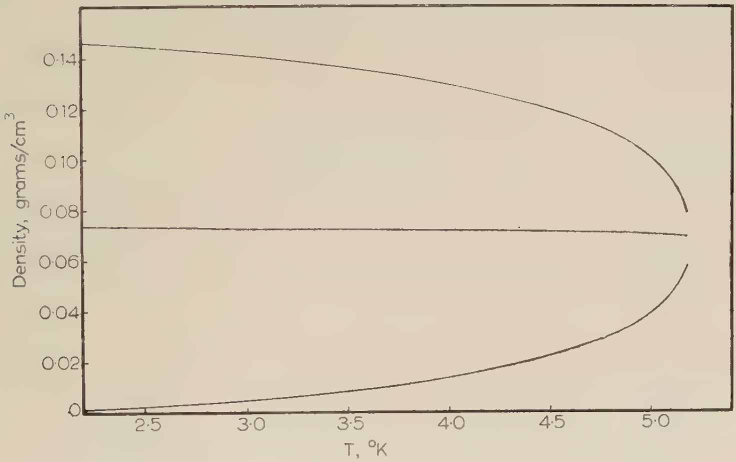

Liquid density, vapour density and the diameter.

We have calculated ρ_{VIR} the saturated vapour density derived from eqn. (3), when only the first two terms are used. We have taken for B the values tabulated by Kilpatrick *et al.* (1955) which are based on Keller's measurements. Any adjustments of B which might be necessary on account of changes in the temperature scale have a negligible influence on ρ_{VIR}. Figure 4 shows the difference, $\Delta\rho = \rho_{VIR} - \rho_{La}$, between the densities derived from eqns. (2) and (3). The rapid increase of $\Delta\rho$ above 3·3°K merely indicates the inadequacy of using only two terms in eqn. (3) and shows that if the third term is responsible then C must be positive. We, would expect $\Delta\rho$ to approach zero at lower temperatures in a regular way, and the irregular shape of the curve found here must reflect some errors in the parameters entering eqns. (2) and (3). The irregularities can not be accounted for by the small uncertainties in the values of B, and except at the lowest temperatures, where the curve has been drawn as a broken line, they are greater than the uncertainties in L_u. For a measured pressure it is unlikely that T_{55E} is wrong by more than a few millidegrees, an error which could only account for about one tenth of 1% discrepancy. We therefore ascribe the shape of the $\Delta\rho$ curve to errors in the values of dP/dT used to calculate $\rho_{L,u}$. If one point on the P-T curve were known, we could find and integrate corrections to dP/dT to give corrections to T at other temperatures. Failing this knowledge, we have assumed that at 2·55°K—the centre of the region where $\Delta\rho$ is small—T_{55E} is correct. We have then calculated corrections to T_{55E} which are shown in the table. We do not give values above 3·0°K as it is not known how much of $\Delta\rho$ is due to the inadequacy of calculating ρ_{VII} from B alone. The table does show, however, that between 2·3 and 2·8°K T_{55E} can only be in error by a constant amount, apart from a variation of the order of 1/10 millidegree. Above this range the correction seems to start as a positive quantity, relative to any correction at 2·55°K, but we cannot make any deductions for temperatures above 3°K for the reason discussed. There is only a slight suggestion that below 2·3°K the correction is in the opposite sense.

Fig. 4

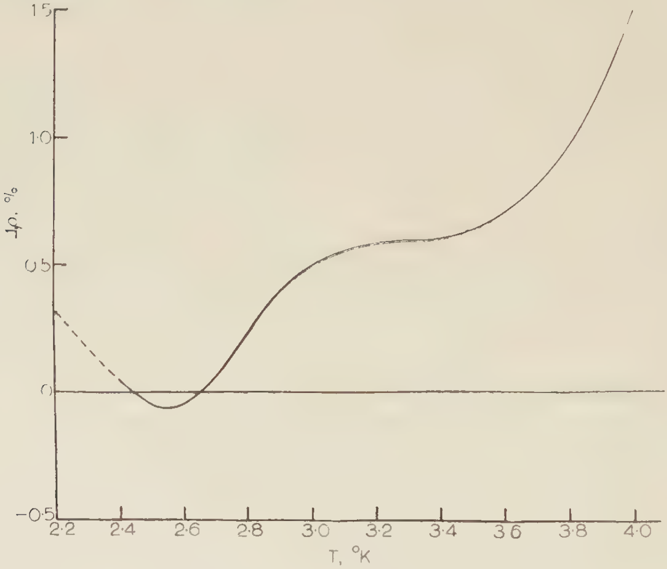

Variation of $\Delta\rho$ with temperature.

Sydoriak and Roberts (1957) give a vapour pressure equation for ^{3}He which fits experimental data between 0·45°K and the critical point (3·3°K). They show a graph of the difference between T_{55E} and T_{3He}, which bears a striking resemblance to the corrections we have suggested in the neighbourhood of 2·5°K.

We will not pursue further the relation of our measurements to the temperature scale in view of the proposals to make another attempt to produce an accurate scale. It is evident, however, that our results, when used in the manner we have outlined, will be useful in examining the consistency of any future scale.

ACKNOWLEDGMENTS

We are indebted for research grants to Industrial Distributors (1946) Ltd. (R.B.) and to the Department of Scientific and Industrial Research (C.F.M.)

REFERENCES

BERMAN, R., and MATE, C. F., 1957, *Proc. 5th Int. Conf. on Low Temp. Phys. and Chem., Madison.*

BERMAN, R., and POULTER, J., 1952, *Phil. Mag.*, **43,** 1047.

BERMAN, R., and SWENSON, C. A., 1954, *Phys. Rev.*, **95,** 311.

CLEMENT, J., private communication, see W. E. Keller, 1956, *Nature, Lond.*, **178,** 883.

DANA, L. I., and ONNES, H. K., 1926, *Leiden Comm.*, 179 c.

VAN DIJK, H., and DURIEUX, M., 1957, *Progress in Low Temperature Physics*, Vol. II (North-Holland Publishing Co.), p. 431.

TER HAAR, D., 1955, *4th Int. Conf. on Low Temperature Physics*, Paris.

KEESOM, W. H., 1942, *Helium* (Amsterdam : Elsevier).

KELLER, W. E., 1955, *Phys. Rev.*, **97,** 1 ; 1955, *Ibid.*, **98,** 1571.

KERR, E. C., 1957, *J. chem. Phys.*, **26,** 511.

KILPATRICK, J., KELLER, W., and HAMMEL, E., 1955, *Phys. Rev.*, **97,** 9.

MATHIAS, E., CROMMELIN, C. A., ONNES, H. K., and SWALLOW, J. C., 1925, *Leiden comm.*, 172 b.

ONNES, H. K., 1911, *Leiden Comm.*, 124 b.

SYDORIAK, S. G., and ROBERTS, T. R., 1957, *Phys. Rev.*, **106,** 175.

Density Changes of Crystals containing Dislocations†

By A. Seeger and P. Haasen
Max-Planck-Institut für Metallforschung, Stuttgart, Germany

[Received January 13, 1958; and in revised form February 12, 1958]

Abstract

Zener's theory of the volume expansion of self-strained elastic bodies is applied to screw and edge dislocations in isotropic media. The important physical parameters entering are the pressure dependence of the shear modulus, and, to a lesser extent, that of the bulk modulus. Numerical results for a number of materials are given. The volume expansion per atomic length of a dislocation line is found to be of the order of magnitude of one to two atomic volumes, thus confirming an earlier estimate by Stehle and Seeger.

In 1942 Zener published a theory relating the volume expansion of a self-strained elastic body to the stored elastic energy. The present authors (Haasen and Lawson 1955, Seeger 1957 a) subsequently have pointed out that Zener's theory can be employed to calculate the decrease in density of a crystal upon introduction of dislocations. It is the purpose of the present note to give the results of such a calculation. We shall compare these with a formula recently proposed by Lomer (1957) and shall show that Lomer's result can be obtained from Zener's more general approach by making the following assumptions: the total elastic energy is dilatational energy; there is no energy due to shear strains.

According to Zener (1942) the average dilation of a self-strained isotropic body is given within the framework of second order elasticity theory by

$$\overline{\Theta} = -\frac{1}{K}\left(\frac{d\log K}{d\log V}+1\right)W_d - \frac{1}{K}\left(\frac{d\log G}{d\log V}+1\right)W_s. \quad . \quad . \quad . \quad (1)$$

Here K denotes the (isothermal) bulk modulus, G the shear modulus, V the specific volume. W_d and W_s are the average work done on the unit volume in establishing the dilation and shearing strains, respectively. It will be demonstrated below that for practical purposes W_d and W_s can be replaced by the average densities of the stored energies of dilation and shear strains. The physical basis of eqn. (1) lies in the fact that in a self-strained body W_d and W_s are proportional to K and G, respectively. These elastic constants depend on the specific volume. Therefore the free energy of the strained body can be lowered by a volume expansion.

Treating a number of pertinent problems E. Mann (to be published) has shown that eqn. (1) gives the same result as Murnaghan's (1951) theory of second order elasticity the application of which, however, is much more tedious than that of eqn. (1).

---

† Communicated by the Authors.

Equation (1) will now be applied to a straight dislocation of strength b which is, as usual, assumed to lie in the axis of an isotropic elastic cylinder (Poisson's ratio ν) with outer radius R and inner radius r_0. In this case it is convenient to consider the volume expansion per unit length of the dislocation, which is given by

$$\delta v=\frac{1}{K}\left(\frac{dK}{dp}-1\right)E_d+\frac{1}{G}\left(\frac{dG}{dp}-\frac{G}{K}\right)E_s. \qquad (2)$$

In going from eqn. (1) to eqn. (2) we have used the relation

$$K=-V\frac{dp}{dV} \qquad (3)$$

between bulk modulus, volume, and hydrostatic pressure p. E_d and E_s are the dilatation and shear contributions to the dislocation line energy. They are given by

$$\left.\begin{aligned}E_d&=0,\\ E_s&=\frac{Gb^2}{4\pi}\log\frac{R}{r_0}\end{aligned}\right\} \qquad (4)$$

for a screw dislocation, and by

$$\left.\begin{aligned}E_d&=\frac{1}{3}\frac{Gb^2}{4\pi}\frac{1-\nu-2\nu^2}{(1-\nu)^2}\log\frac{R}{r_0}\\ E_s&=\frac{2}{3}\frac{Gb^2}{4\pi}\frac{1-\nu+\nu^2}{(1-\nu)^2}\log\frac{R}{r_0}\end{aligned}\right\} \qquad (5)$$

for an edge dislocation†. As is well known the total line energy of an edge dislocation is

$$E_{\text{tot}}=E_d+E_s=\frac{Gb^2}{4\pi}\frac{1}{(1-\nu)}\log\frac{R}{r_0}. \qquad (6)$$

Inserting these expressions for the line energies into eqn. (2) we obtain for the volume expansion per unit length due to a screw dislocation

$$\delta v=\frac{b^2}{4\pi}\left(\frac{dG}{dp}-\frac{G}{K}\right)\log\frac{R}{r_0}, \qquad (7)$$

due to the dilatational strains of an edge dislocation

$$\delta v_d=\frac{b^2}{4\pi}\frac{1}{2}\left(\frac{1-2\nu}{1-\nu}\right)^2\left(\frac{dK}{dp}-1\right)\log\frac{R}{r_0}, \qquad (8)$$

and due to the shearing strains of an edge dislocation

$$\delta v_s=\frac{b^2}{4\pi}\frac{2}{3}\frac{1-\nu+\nu^2}{(1-\nu)^2}\left(\frac{dG}{dp}-\frac{G}{K}\right)\log\frac{R}{r_0}. \qquad (9)$$

Total volume expansion δv and total line energy E_{tot} of an edge dislocation are related by

$$\delta v=\frac{1}{3}\left[\frac{1-\nu-2\nu^2}{1-\nu}\frac{1}{K}\left(\frac{dK}{dp}-1\right)+\frac{1-\nu+\nu^2}{1-\nu}\frac{2}{G}\left(\frac{dG}{dp}-\frac{G}{K}\right)\right]E_{\text{tot}}. \qquad (10)$$

---

† For the sake of simplicity we have neglected boundary terms in eqn. (5) which for $R/r_0 \sim 10^4$ are an order of magnitude smaller than those retained.

Table 1

Metal	Author and technique	$d \log K/dp$ or $\frac{d \log \frac{1}{3}(c_{11}+2c_{12})}{dp}$	$\frac{d \log G}{dp}$	$\frac{d \log c_{44}}{dp}$	$\frac{d \log \frac{1}{2}(c_{11}-c_{12})}{dp}$
Cu polycrystalline	Birch (1937) torsional vibration	—	2·71	—	—
	Bridgman (1935) static	3·65	—	—	—
Cu single crystal	Lazarus (1949) supersonic pulses	2·84	—	1·13	2·45
Ni polycrystalline	Birch (1937) torsional vibration	—	1·82	—	—
	Bridgman (1935) static	2·83	—	—	—
	Bridgman (1929) static	—	1·8	—	—
Al polycrystalline	Birch (1937) torsional vibration	—	7·61	—	—
	Bridgman (1935) static	5·83	—	—	—
	Hughes and Maurette (1956) supersonic pulses	5·2	9·8	—	—
Al single crystal	Lazarus (1949) supersonic pulses	5·47	—	7·49	—
Fe polycrystalline	Hughes and Maurette (1956) supersonic pulses	2·54	4·14	—	—
NaCl single crystal	Lazarus (1949) supersonic pulses	24·6	—	2·1	25·3

Experimental values for the pressure dependence of the elastic constants, in units of 10^{-6} cm^2/kg $= 10^{-6}$ bars^{-1}. Bridgman's (1935) data are corrected for the redetermination of the compressibility of steel (Bridgman 1940) as given by Birch (1942). Misprints in table V of Lazarus (1949) have been corrected.

In table 1 we have collected experimental data of the pressure dependence of the elastic constants of a number of f.c.c. metals, of α-Fe and of NaCl†. Lazarus' (1949) results on Cu single crystals are seen to differ appreciably from the polycrystalline data obtained by Birch (1937) and Bridgman (1935). Since we were unable to decide between the two sets of data we carried through the evaluation of eqn. (7) to eqn. (9) for both of them.

Table 2

	K kg/mm²	G kg/mm²	ν	$\dfrac{dK}{dp}$	$\dfrac{dG}{dp}$	Γ^{screw}	Γ_d^{edge}	Γ_s^{edge}	Γ^{edge}
Cu – Lazarus	15440	4590	0·36	4·38	0·80	0·056	0·034	0·07	0·10
Cu – Birch, Bridgman				5·64	1·24	0·106	0·047	0·13	0·18
Ni	18000	7850	0·31	5·10	1·42	0·11	0·069	0·12	0·19
Al	6780	2600	0·33	3·69	1·94	0·17	0·039	0·20	0·24
Fe	16640	8060	0·29	4·23	3·40	0·30	0·060	0·32	0·38
NaCl	2340	1500	0·24	5·77	2·05	0·317	0·25	0·30	0·55

The physical constants used in the calculations are given in table 2. As the results of the numerical evaluation we list the dimensionless quantities

$$\Gamma=\frac{\delta v\, b}{\Omega \log (R/r_0)}. \qquad (11)$$

$\Gamma \log R/r_0$ has the meaning of the volume expansion due to a dislocation line of length b, measured in atomic volumes Ω ($\Omega=b^3/2^{1/2}$ for f.c.c. crystals; $\Omega=4b^3/3^{3/2}$ for b.c.c. crystals; $\Omega=b^3/2^{3/2}$ for the NaCl-structure). Γ^{screw} refers to screw-dislocations (calculated from eqn. (7)), Γ_d^{edge} (calculated from eqn. (8)) and Γ_s^{edge} (calculated from eqn. (9)) refer to the expansion due to the dilatational and shear parts of the strain-field of an edge dislocation, respectively. Finally we give the sum $\Gamma^{\text{edge}}=\Gamma_d^{\text{edge}}+\Gamma_s^{\text{edge}}$. Comparing the contributions of dilatational and shearing strains to the volume expansion of an edge dislocation the latter is seen to be dominant (particularly for the metals) and of the same magnitude as the total volume expansion of a screw dislocation.

The dislocation densities in undeformed crystals correspond to $\log R/r_0=8-10$. The volume expansions of f.c.c. metals per dislocation length b are accordingly found to be of the magnitude one to two, in agreement with the results of Stehle and Seeger (1956) derived from a model based on inter-atomic forces. Stehle and Seeger's results can be approximated by an expression of the form of eqn. (11), namely

---

† For data on other materials see Birch (1942), Lazarus (1949) and Bridgman (1952, p. 386).

$$\Gamma^{\mathrm{screw}} = \frac{1}{\sqrt{2}\,.\,\pi}\left\{\frac{\alpha^2}{12(\alpha+1)} - \frac{1}{4}\right\}. \quad . \quad . \quad . \quad . \quad . \quad . \quad (12)$$

Here α is the exponent in the repulsion potential between neighbouring atoms. A reasonable value for metals is $\alpha = 14$. This gives $\Gamma^{\mathrm{screw}} = 0{\cdot}18$.

Lomer's (1957) relation between volume expansion and stored elastic energy, involving Grüneisen's constant γ, reads in our notation

$$\overline{\Theta} = \frac{2\gamma}{K} W_{\mathrm{tot}}, \quad . \quad . \quad . \quad . \quad . \quad . \quad . \quad . \quad (13)$$

where $W_{\mathrm{tot}} = W_d + W_s$ is the average density of the elastic energy. Assuming Hookeian forces between nearest neighbours the following relation between γ and dK/dp can be derived (Leibfried 1955)†:

$$2\gamma = \frac{dK}{dp} - 1. \quad . \quad . \quad . \quad . \quad . \quad . \quad . \quad . \quad (14)$$

Lomer's expression, which takes the form

$$\overline{\Theta} = \frac{1}{K}\left(\frac{dK}{dp} - 1\right) W_{\mathrm{tot}}, \quad . \quad . \quad . \quad . \quad . \quad . \quad . \quad (15)$$

can now be compared with eqn. (1), which we rewrite as

$$\overline{\Theta} = \frac{1}{K}\left(\frac{dK}{dp} - 1\right) W_{\mathrm{tot}} + \left(\frac{d\log G}{dp} - \frac{d\log K}{dp}\right) W_s. \quad . \quad . \quad (16)$$

We see that Lomer's formula yields either too large or too small values for $\overline{\Theta}$, depending on whether $d\log K/dp$ is larger or smaller than $d\log G/dp$. From table 1 we see that the first possibility obtains in the case of Cu and Ni, whereas the second possibility applies to Al and Fe. In an isotropic medium with $\nu = \frac{1}{3}$ shear strains contribute 7/9 of the line energy of an edge dislocation. If we consider an equal number of edge and screw dislocations we find that 13/15 of the stored energy is due to shear strains. In the application of eqn. (16) to dislocations the term due to W_s is therefore in general not negligible.

W_d and W_s have been defined as the reversible work done per unit volume in establishing the strains. The stored energy measured in a calorimetric experiment differs from the W's by the heat absorbed from the temperature bath if the deformation is done isothermally. The heat Q absorbed per unit volume is proportional to the average dilatation $\overline{\Theta}$ and given by (Darken and Gurry 1953, p. 183)

$$Q = T\alpha K^T \overline{\Theta}, \quad . \quad . \quad . \quad . \quad . \quad . \quad . \quad . \quad . \quad (17)$$

---

† Equation (14) is obtained by combining Leibfried's equations (83.6) and (83.11). The latter equation has been corrected according to a private communication by G. Leibfried and W. Ludwig.

where T denotes the absolute temperature, α the coefficient of thermal volume expansion and K^T the isothermal bulk modulus. Using the thermodynamic equation

$$\frac{K^S}{K^T} = 1 + K^S \frac{T\alpha^2}{c_p} \quad . \; . \; . \; . \; . \; . \; . \; . \; . \quad (18)$$

(K^S = adiabatic bulk modulus, c_p = specific heat at constant pressure per unit volume) and Grüneisen's relation

$$\gamma = K_S \, \alpha / c_p , \quad . \; . \; . \; . \; . \; . \; . \; . \; . \quad (19)$$

we obtain from eqn. (17)

$$Q = \frac{K^S - K^T}{K^T} \frac{K^T \overline{\Theta}}{\gamma} . \quad . \; . \; . \; . \; . \; . \; . \quad (20)$$

By combining eqn. (1) and eqn. (14) it is found that $K^T \overline{\Theta}/\gamma$ is of the order of magnitude of W_{tot}. Since $(K^S - K^T)/K^T$ is of the order of 10^{-2} (e.g. 3×10^{-2} for Cu at room temperature, see Overton and Gaffney 1955) we see that W_{tot} can be taken equal to the stored elastic energy, as originally asserted by Zener (1942). A comparison between the theory and measurements of volume expansion and stored energy due to cold-work has been given elsewhere (Seeger 1957 b).

ACKNOWLEDGMENT

The authors should like to thank cand. phys. E. Mann, Stuttgart, for helpful discussions.

REFERENCES

BIRCH, F., 1937, *J. appl. Phys.*, **8,** 129; 1942, *Handbook of Physical Constants*, Geological Society of America Special Papers No. 36.

BRIDGMAN, P. W., 1929. *Proc. Amer. Acad.*, **64,** 39; 1935, *Ibid.*, **70,** 285; 1940, *Ibid.*, **74,** 11; 1952, *Physics of High Pressure*, 2nd ed. (New York: Macmillan Co.).

DARKEN, L. S., and GURRY, R. W., 1953, *Physical Chemistry of Metals* (New York : McGraw-Hill).

HAASEN, P., and LAWSON, A. W., JR. 1955, *8th Annual Report on High Pressure Research* (University of Chicago), p. 67.

HUGHES, D. S., and MAURETTE, CH., 1956, *J. appl. Phys.*, **27,** 1184.

LAZARUS, D., 1949, *Phys. Rev.*, **76,** 545.

LEIBFRIED, G., 1955, *Encyclopedia of Physics* (Berlin : Springer), vol. VII 1, p. 277.

LOMER, W. M., 1957, *Phil. Mag.*, **2,** 1053.

MURNAGHAN, F. D., 1951, *Finite Deformation of an Elastic Solid* (New York : J. Wiley & Sons).

OVERTON, W. C., and GAFFNEY, J., 1955, *Phys. Rev.*, **98,** 969.

SEEGER, A., 1957 a, *Dislocations and Mechanical Properties of Crystals* (New York : J. Wiley & Sons), p. 504; 1957 b, *Varenna Summer School on Solid State Physics* (Suppl. to *Nuovo Cimento*, in press).

STEHLE, H., and SEEGER, A., 1956, *Z. Phys.*, **146,** 217.

ZENER, C., 1942, *Trans. Amer. Inst. min. met. Engrs.*, **147,** 361.

Small Angle Scattering from Cold-Worked and Fatigued Metals†

By H. H. Atkinson
Crystallographic Laboratory, Cavendish Laboratory, Cambridge

[Received March 3, 1958]

Abstract

Experiments have been made on the small angle scattering of x-rays from polycrystalline copper and single grains of aluminium deformed by cold work or fatigued by pulsating tension. The results confirm in a direct and conclusive way that almost all of the scattering is due to double Bragg reflections as proposed by Beeman *et al.* No surface scattering has been observed. Double Bragg reflections have been eliminated in small angle scattering experiments using cold neutrons: the results indicate the magnitude of the scattering from defects in the volume of the metal. The magnitude of the effect is consistent with scattering from dislocations. There was no observable effect from fatigued metals. Hence there is no direct evidence for the existence of cavities in metals as a result of small angle scattering experiments with either x-rays or neutrons.

§ 1. Introduction

The density changes associated with lattice imperfections which extend over several atomic dimensions can give rise to small angle scattering of x-rays or thermal neutrons. Hence, it should be possible to obtain information from small angle scattering experiments about dislocations and also about small voids which may be introduced into crystals by cold work, fatigue, quenching or radiation damage.

Quantitative small angle scattering experiments on pure metals using x-rays (of wavelength 1·54 Å) were first carried out by Blin and Guinier (1951, 1953) and Blin (1954, 1955) who examined the scattering from polycrystalline aluminium, nickel, copper and zinc in the range of scattering angles 55′ to 7°, i.e. in the range of s from 0·010 to 0·079 Å^{-1}, where $s = 2\sin\theta/\lambda \simeq 2\theta/\lambda$; 2θ is the scattering angle, and λ is the wavelength. They found substantial scattering from metals which had been plastically deformed in tension or by cold rolling. Blin and Guinier considered the observed intensities too large to be due to dislocations (Dexter 1953) and interpreted their results in terms of a concentration of 10^{15} to 10^{17} per cm^3 of cavities of a size corresponding to about 300 to 7000 atomic volumes; each of these cavities might have been formed by the aggregation of vacancies produced during deformation. However, Brammer (1955) found an immediate increase in scattering from a nickel foil stretched and examined at 77°K. Since vacancies are not thought to be mobile at this temperature, it is difficult to see how voids could be formed by clustering of vacancies.

---

† Communicated by the Author.

More recently Blin (1957) has suggested that his results can be explained as being due to scattering from density changes associated with the first order elastic strains around edge dislocations. Seeger (1957 a, b) also believes that the observed scattering is due to dislocations, but considers that second order elastic effects predominate. Both these theories have been discussed recently by Atkinson and Hirsch (1958) who showed that the previous theoretical calculations either contained errors or were incomplete, and that the theoretically expected scattering from a reasonable arrangement and density of dislocations is in fact very much less than that observed in x-ray experiments.

Quite apart from these theoretical considerations it is difficult to interpret certain features of the x-ray scattering in terms of defects introduced during cold work. Thus, for example, the original results of Blin (1954) and recent more detailed studies by Smallman (private communication) and Wild *et al.* (private communication) show that the scattering (at a fixed angle) at first increases with increasing degree of cold rolling, but that a maximum is reached after 10 to 20% reduction in thickness, beyond which the intensity *decreases* steeply and continuously with increasing deformation up to 95%, the maximum reduction used. In contrast to this variation of the intensity of scattering it is expected that the density of defects, and therefore the intensity scattered, should increase with increasing deformation.

Recent experiments by Beeman *et al.* (1957) have shown conclusively that a large proportion of the scattering from cold-worked metals can be explained in terms of a double Bragg reflection mechanism (Neynaber 1955). Thus, for example, Webb (1956) found that x-rays (FeK$_\alpha$ radiation) scattered at 1½° are partially polarized with their strong electric vectors in a direction radial to the undeviated beam. This polarization can only be explained by two successive large-angle Bragg reflections. The direction of the electric vector suggests that the process is one in which a ray reflected from one region of a grain suffers a further reflection by another region in which the reflecting planes are somewhat misaligned by a simple rotation about the direction of the once-reflected beam. The particle size- and strain-broadening were considered to be negligible. However, the polarization decreases as the degree of deformation is increased. This can be explained by taking into account the particle size- and strain-broadening of the Bragg reflections which become important at the larger deformations. Defects associated with the surface have also been shown to cause scattering at small angles (Robinson and Smoluchowski 1956, Zhurkov and Slutsker 1957).

On the basis of these experiments it appears therefore that the major part of the small angle x-ray scattering from metals deformed by cold rolling or in tension is due to double Bragg reflections and possibly also partly to the surface effect.

More recently, small angle scattering has also been measured from metals which have been deformed by fatigue. Franks and Holden (1955) have observed the effect of about $3{\cdot}5\times10^5$ cycles of pulsating tension (between 0 and 9·5 kg mm^{-2}) on the scattering from copper foil of thickness 60 μ. An individual grain was examined with CuK$_\alpha$ radiation, and x-ray photographs showed streaks through the central spot extending out to about 2°. These streaks were interpreted as being due to disc shaped cavities, about 100 Å in diameter, lying on (111) planes. No measurement was made of the absolute intensity of the effect.

Since 1955 the present author has studied the small angle scattering from deformed metals with the following aims in view. Firstly, it was thought desirable to demonstrate the double Bragg reflection mechanism by means of more direct experiments, and to determine whether this effect could also account for the scattering from metals deformed in fatigue. Secondly, a series of experiments were undertaken to study the small angle scattering with cold neutrons. By using neutrons of sufficiently long wavelength the possibility of double Bragg reflections was eliminated, and since the specimens examined were very large, surface effects were negligible. In this way it was possible to measure the true small angle scattering due to density changes associated with defects. A preliminary account of the neutron experiments has been published elsewhere (Atkinson and Lowde 1957).

In the present paper the x-ray experiments will be described and some new neutron scattering results discussed. The neutron scattering experiments will be published in more detail elsewhere.

§ 2. THE X-RAY EXPERIMENTS

2.1. *Equipment*

A point focusing monochromator and camera have been used in this work. Only a brief description of the instrument will be given here as full details are to be published elsewhere. A schematic diagram of the equipment is shown in fig. 1. Radiation from the copper target of the x-ray tube (operated at 20 mA and 30 kv) passes through a slit S_1 onto a single crystal of lithium fluoride plastically bent to conform to a toroidal surface so that the CuK$_\alpha$ radiation is reflected from the (200) planes and brought to a point focus 23 cm away. The specimen, placed midway between the crystal and the focus, is irradiated over a region of about 1·8 mm × 7 mm. Immediately behind the specimen is a second slit S_2 to limit the effect of parasitic radiation from the LiF crystal. This slit is carefully adjusted so that it just does not touch the direct beam. With the slit settings used in this experiment the parasitic scattering is reduced in one direction; the area indicated by the dotted lines in fig. 1 and by the elongated region about the direct beam in figs. 2, 9, 11 and 14, Plates 14, 16, 17 and 18 respectively, is obscured by parasitic radiation. This limits the smallest angle observable to $1\frac{1}{2}$°. The whole instrument is evacuated to eliminate air scattering.

The small angle scattering is recorded on a photographic film placed in a plane perpendicular to the direct beam. A round beam stop, of diameter 6 mm, intercepts the direct beam; this can be moved momentarily to obtain a picture of the direct beam. Measurements of the absolute intensity were made with a Geiger counter with a 1·2 mm square aperture.

Fig. 1

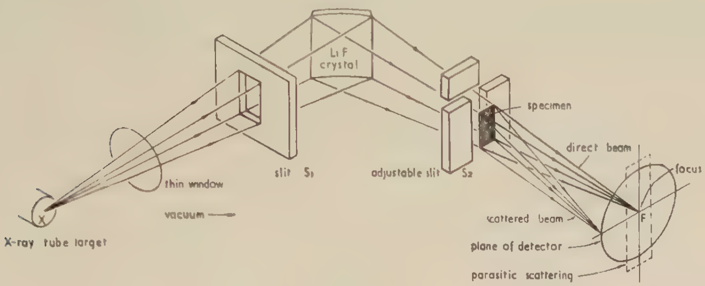

Schematic diagram of the x-ray point focusing monochromator and camera.

The direct beam intensity, about 10^7 counts per second, was measured with a counter, using nickel foil absorbers; a correction was made for radiation of higher orders reflected from the LiF crystal.

2.2. *Deformation by Cold Work*

2.2.1. *Cold rolled copper*

A photograph of the small angle scattering from heavily cold-rolled copper foil, 30 μ thick, is shown in fig. 2, Pl. 14 (exposure 70 hours). The material used was of commercial purity. (Material from the same batch will henceforth be referred to as ‘ commercial copper ’.) It is seen that streaks are produced, some of which do not pass through the trace of the direct beam. It will now be shown that all these streaks are due to double Bragg scattering.

As the x-ray beam passes through the polycrystalline metal, the rays which are Bragg reflected must lie on cones centred about the direct beam (e.g. C_{200} in fig. 3). Consider a particular singly reflected ray, e.g. OA: in passing through the rest of the specimen this ray itself may again be reflected (as described in § 1). The twice reflected ray will also lie on one of a series of cones (e.g. $C_{200,\ 200}$ or $C_{200,\ 111}$ in fig. 3, corresponding to successive reflections from planes of the same and different spacings, respectively) only one of which, $C_{200,\ 200}$ will intersect the direct beam in the forward direction. If the crystal consists of many randomly orientated grains and if there is no strain broadening, the resultant scattering will have circular symmetry about the direct beam, and will decrease steadily as $1/2\theta$ with increasing scattering angle 2θ. However, for angles $2\theta \geqslant |2\theta_{hkl} - 2\theta_{h'k'l'}|$, a new term is added to the intensity, for it is then possible for a single reflection described by the Bragg angle θ_{hkl} to be followed by a second reflection at a different set of planes $({}_{h'k'l'})$ and *vice versa*. Also, an abrupt increase in the intensity at small angles will occur at $2\theta=(2\pi-4\theta_{abc})$, if there is a Bragg angle θ_{abc} near to $\frac{1}{2}\pi$. For copper and aluminium with CuK$_\alpha$ radiation, the first increase should occur at 5° and $3\frac{1}{2}$° respectively, given by $2\theta=(2\theta_{222}-2\theta_{311})$. On the other hand, the copper foil used in this experiment showed strong preferred orientation, and the small angle pattern expected from the double Bragg scattering effect no longer has circular symmetry. The preferred orientation of the grains in the specimen is evident from figs. 4 and 5, Pl. 15. Figure 4 shows a transmission photograph taken in the point focusing instrument by placing a film parallel to the specimen and about 2 cm from it. This shows some of the first 111 and 200 reflections occurring under conditions the same as those in which fig. 2, Pl. 14 was taken. (The central blackening is caused by the direct beam which is out of focus at this point. The size of the direct beam also causes some of the spreading of the reflections.) Most of the other Bragg reflections occurring are shown in fig. 5, Pl. 15. In this case the film was bent in the form of a half cylinder. The x-ray beam (from a copper target with a nickel filter) passed along the axis of the cylinder onto a small piece of the copper foil. The normal to the

Fig. 3

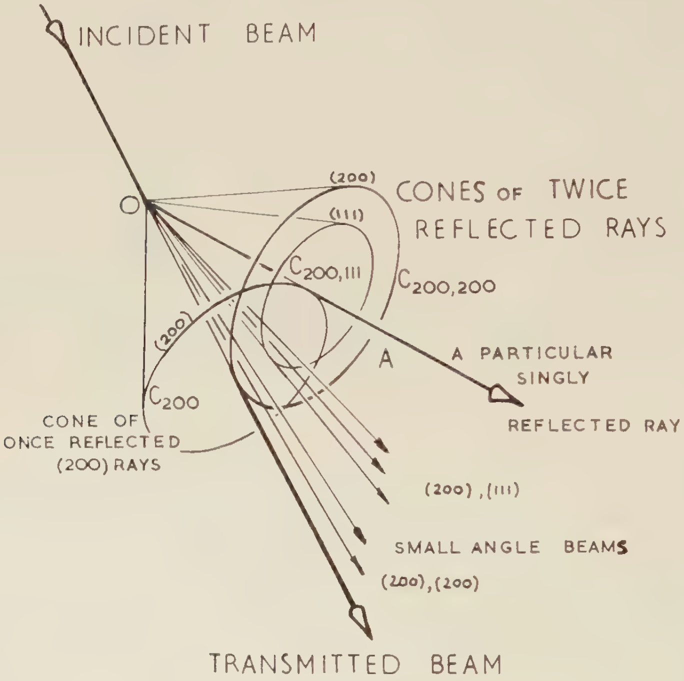

plane of the foil was parallel to the beam. The plane containing the x-ray beam and the rolling direction of the foil cuts the film along a line marked 0°; when this plane is rotated 90° about the beam it then intersects the film along the lines marked ± 90°.

A qualitative examination of figs. 4 and 5, Pl. 15, suggests that the small angle streaks which pass through the trace of the direct beam in fig. 2, Pl. 14, are associated with strong large angle Bragg reflections. To explain the details of the pattern, pole figures of the normals to the (111) and (200) planes have been determined photographically, and are shown in figs. 6 and 7. Using these pole figures, it is possible to predict the nature of the small angle scattering pattern expected; this predicted pattern is shown in fig. 8, Pl. 14. The dotted lines on fig. 8 indicate the positions of other double reflections deduced from fig. 5, Pl. 15, but for which pole figures have not been determined. The streaks which do not pass through the origin are due to reflections first at (200) planes and then at (111) planes: the pole figures show that reflections in the reverse order, 111 and then 200, occur in a range of angles not covered by the photograph. Comparison

Fig. 6

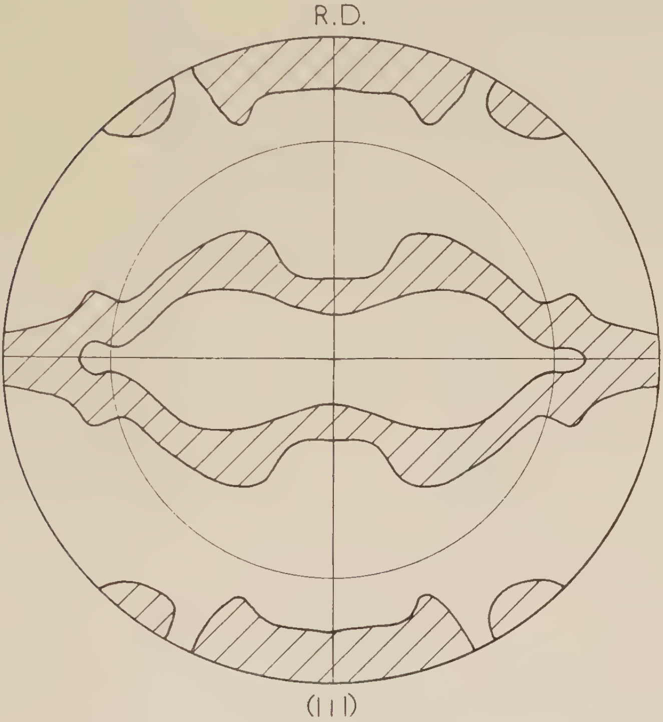

Pole figure of the preferred orientations of the normals to 111 planes for cold rolled commercial copper. The plane of the foil is parallel to the plane of the paper. 'R.D.' indicates the rolling direction.

of fig. 2 with fig. 8, Pl. 14 shows that all the observed streaks are explained completely by the double Bragg reflection mechanism.

The intensities of the scattering at some points of the pattern (fig. 2) have been measured with the Geiger counter; at *a* the intensity is 160 electrons/atom and at *b*, 85 electrons/atom, i.e. of the same order of magnitude as found previously by Blin. The intensity of the scattering was unaffected by removing a surface layer 2·5 μ thick from each side of the specimen by electropolishing. Removal of a further 2·5 μ from each side reduced the intensity slightly, but not by more than would be expected from the consequent reduction of the quantity of material in the beam.

Fig. 7

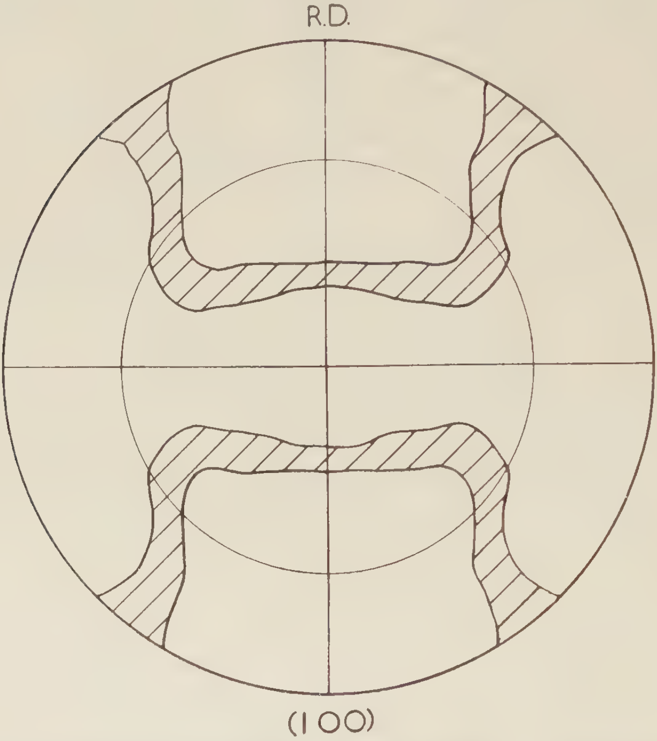

Pole figure of the preferred orientations of the normals to 100 planes for cold rolled commercial copper. The plane of the foil is parallel to the plane of the paper. 'R.D.' indicates the rolling direction.

2.2.2. *Aluminium deformed in tension*

Figure 9, Pl. 16 shows the scattering (64 hour exposure) from a large single grain of Al which has been extended ~ 18% by a tensile load. After deformation, the large grain concerned was reduced to a thickness of 100 μ by removing 100 μ from each side by electropolishing. Using a Geiger counter, the grain was orientated so that it would give a strong 200 reflection for CuK$_\alpha$ radiation when placed in the point focusing instrument. Figure 10, Pl. 16 shows that in fact two strong single 200 reflections occurred; the spot *a* on this photograph produces the intense streak marked *a* in fig. 9: the second 200 spot (*b*) probably produces streak *b* (fig. 9). Three other strong reflections have been observed (outside the range of fig. 10): two are of the type 311, producing streaks *c* and *d* (fig. 9); the third (of type 331) may also contribute to *b* and *c*. Spot *e* is due to the 311 reflection giving rise to streak *d*, followed by a 220 reflection.

2.3. *Deformation by Fatigue*

A small fatigue machine was constructed to apply to a thin foil a tensile load which alternated between a value of about zero and a fixed value, at a rate of 1200 cycles per minute (' pulsating tension '). The machine was automatically switched off when the specimen stretched more than a certain amount.

In these experiments the full load was applied immediately and in each case the previously recrystallized specimen would stretch considerably during the first few cycles and then more slowly during the rest of its life.

2.3.1. *Copper*

Figure 11, Pl. 17 shows the small angle scattering (45 hour exposure), from a piece of pure copper foil (supplied by Johnson, Matthey & Co. Ltd.) 30 μ thick, which had broken after $\sim 5 \times 10^5$ cycles of pulsating tension between 0 and about 7 kg mm^{-2}. The specimen stretched a total of at least 10% during the fatiguing. The corresponding 111 and 200 reflections are evident in fig. 12, Pl. 17. This shows that the numerous grains in the specimen have a wide range of orientations. Hence the small angle pattern has streaks occurring at many different angles. Streaks marked *b* in fig. 11 are due to double reflections of the type 200, 111. The intense scattering produced (e.g. 400 electrons/atom at *a*) shows that such a wide array of orientations increases the probability of the double scattering process.

The intensity of scattering at *a* is approximately the same as that resulting from a foil of the same material which had been stretched by the same amount (about 10%) but not fatigued. Removal by electropolishing of 5 μ from each side of either of these foils resulted in a negligible change in scattering.

A piece of the commercial foil was fatigued under similar conditions to the above. It produced no observable small angle scattering. This can be understood by referring to fig. 13, Pl. 18, taken under conditions identical with those corresponding to fig. 12. It is seen that the few 111 or 200 reflections which occur are not sufficiently wide to produce scattering observable at angles greater than $1\frac{1}{2}°$.

2.3.2. *Aluminium*

A piece of aluminium foil 250 μ thick, with very large grain size (~1 cm) was fatigued; during this process a selected grain stretched ~14%. The specimen did not break. This grain was then orientated to produce a strong 111 reflection. The small angle scattering is shown in fig. 14, Pl. 18 (22 hour exposure): the streak is produced by the strong 111 reflection shown in fig. 15, Pl. 19.

A photograph of the same grain orientated so that no strong 111 or 200 reflections occurred showed very little small angle scattering. Because of the heavy distortion of the lattice it is difficult to find an orientation for which there is no scattering at all.

The removal by electropolishing of 50 μ from each side of the specimen diminished only slightly the intensity of the streak in fig. 14.

2.4. *Discussion of X-Ray Scattering Results*

The experiments described above leave little doubt that nearly all the small angle x-ray scattering from metals deformed in tension, by cold rolling, and by fatigue stresses is due to double Bragg reflections. This mechanism, first suggested and investigated by Beeman, Brammer, Neynaber and Webb, has therefore been confirmed for several different types of deformation. It follows from the neutron scattering results (§ 3) that the x-ray scattering due to defects contributes not more than about 1% to the total scattered intensity. It is therefore doubtful whether this scattering can ever be detected with x-rays.

The present results also indicate that surface scattering is relatively unimportant.

In view of these results it should be noted that there is now no evidence, from x-ray scattering experiments, for the possible existence of cavities or cracks as a result of cold work or fatigue.

§ 3. THE NEUTRON SCATTERING EXPERIMENTS

In order to prevent entirely the occurrence of double Bragg scattering in a metal specimen, it is necessary to use radiation of wavelength greater than the Bragg cut-off wavelength, λ_c, for the metal used ($\lambda_c = 2d_{\max}$, where $d_{\max}$ is the maximum interplanar spacing: for copper $\lambda_c = 4{\cdot}17$ Å and for aluminium $\lambda_c = 4{\cdot}67$ Å). Long wavelength x-rays are so heavily absorbed that specimens only a few microns thick would have to be examined. However, for long wavelength neutrons, thick (~1 cm) specimens can be used.

In collaboration with R. D. Lowde at the A.E.R.E., Harwell, experiments have been carried out recently to measure the small angle scattering of cold neutrons from aluminium and copper deformed by tension, cold rolling and fatigue. The results of these experiments are now reported together with brief description of the experimental arrangement. A full description of the experiment will be given elsewhere.

The cold neutrons used came from the liquid hydrogen moderator (Butterworth *et al.* 1957) in the Harwell pile B.E.P.O. Filters of Be and Bi were placed between the source and the specimen to remove all the neutrons of wavelength $\lambda < 6{\cdot}5$ Å (Egelstaff and Pease 1954). For $\lambda > 6{\cdot}5$ Å, the intensity of the beam incident on the specimen is approximately proportional to λ^{-5}.

The flux of neutrons available even from this very intense source is still several orders of magnitude smaller than the x-ray flux used in the experiments described in § 2. Hence it is necessary to relax considerably the resolution of the apparatus so that, at the setting of the ‘ small-angle ’ counter used, neutrons could be detected over a range of scattering angles between 3° and 11°.

Fig. 16

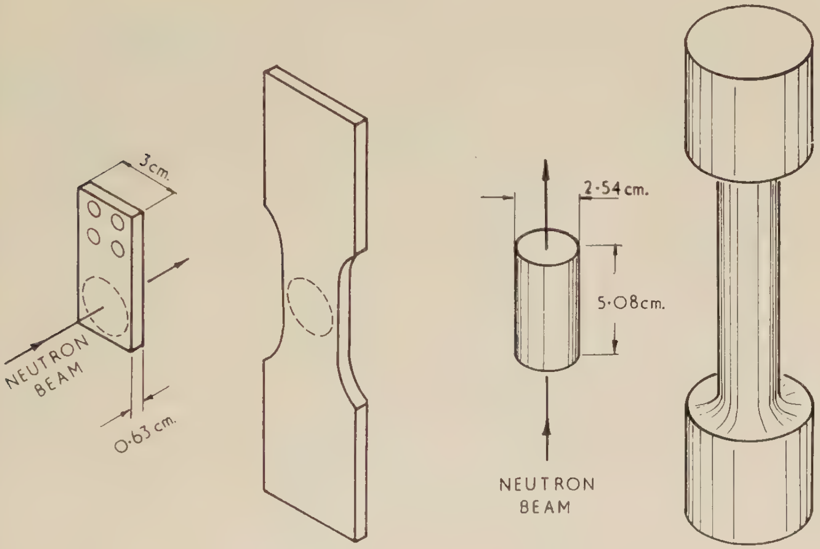

COPPER

ALUMINIUM

Fatigue test-pieces used in the neutron experiment. To the left of each test-piece is shown a finished specimen.

The aluminium specimens were prepared from a length of rod of 99·99% purity from the Northern Aluminium Company. The copper specimens were from a batch of metal of 99·995% purity supplied by I.C.I. (Metals Division) Birmingham. This material was cut into suitably shaped test-pieces (the fatigue test-pieces are shown in fig. 16), and then recrystallized. One piece of each metal was kept as a standard ‘ recrystallized ’ specimen. The tensile and fatigue test-pieces were deformed using a 10 ton Losenhausen fatigue machine. Each specimen was then carefully machined from the gauge length of the test-piece. Finally, the copper specimens were electropolished; 50 μ were removed from each side of the tensile specimen (the only copper specimen which had been machined on surfaces normal to the neutron beam) and 12 μ from each side of the fatigue specimen.

The final forms of the aluminium and copper specimens are shown in fig. 16. Details of the deformations are shown in table 1.

In the actual experiment, a deformed specimen was compared with a recrystallized but otherwise identical one; the difference in the scattering from the deformed and recrystallized specimens should be due solely to defects produced in the volume of the metal by the deformation. The magnitude of this 'defect' scattering, expressed as a differential scattering cross section for neutrons in units of millibarns steradian^{-1} atom^{-1}† is shown in the last column of table 1. The standard deviation is also shown. The absolute magnitude of the results may be in error by ±50%: however this does not effect the relative values of the quantities or the relative statistical errors.

Table 1. Small Angle Scattering of Neutrons from Deformed Aluminium and Copper

Metal	State	Details	Nuclear differential cross section for scattering by defects (millibarns/steradian/atom
Aluminium	Recrystallized	at 550° c for 1 hour.	—
	Extended	about 50%.	$0·03 \pm 0·08$
	Fatigued	in push–pull to fracture after $3·17 \times 10^5$ cycles at $\pm 2·3$ kg/mm^2	$-0·05 \pm 0·08$
Copper	Recrystallized	at 700°c for 4 hours in a vacuum of about 10^{-5} mm Hg.	—
	Extended	about 50%.	$1·5 \pm 0·8$
	Cold rolled	thickness reduced by 90%.	$1·9 \pm 0·8$
	Fatigued	in push–pull. The specimen fractured after being subjected successively to the following treatments: 17×10^5 cycles at $\pm 4·7$ kg/mm^2 $1·2 \times 10^5$ cycles at $\pm 5·8$ kg/mm^2 $1·0 \times 10^5$ cycles at $\pm 6·9$ kg/mm^2 $4·2 \times 10^5$ cycles at $\pm 7·6$ kg/mm^2	$-0·3 \pm 0·8$

It is seen that the cross section for small angle scattering by cold-worked or fatigued aluminium is probably less than 0·08 mb str^{-1} atm^{-1}. A small effect is observed for cold-worked copper. The statistical probability that this effect is real, and is not due to chance, is 92% for the extended and 98% for the cold rolled specimens. The fatigued copper gives no observable scattering.

---

† A table relating the scattering expressed in neutron or x-ray units to I_v/I_a, where I_v is the scattering per cm^3 and I_a is the intensity scattered from one atom under the same conditions, is given in Atkinson and Hirsch (1958).

For comparison, the x-ray results have been converted to average differential cross sections for neutrons, for the range of wavelengths and angles used in the neutron experiment. Table 2 shows average cross sections calculated in this way from the results of Blin (1954) and Smallman (private communication). The present x-ray experiments confirm these values.

It is seen that not more than about 1% of the scattering observed in the x-ray experiments is due to true small angle scattering from defects in the volume of the metal.

Table 2. Some X-Ray Scattering Results Converted to Equivalent Differential Cross Sections for Neutron Scattering

Specimen	Observer	Equivalent cross section for neutron scattering (millibarns/steradian/atom)
Copper		
Cold rolled 20%	Smallman	>150
90%	Smallman	> 70
95%	Blin	> 35
Extended 5%	Blin	>350
Aluminium		
Extended 5%	Blin	> 70

As for the magnitude of 'true' scattering, the neutron experimental sensitivity seems to be just sufficient to detect an effect for copper. Although no scattering was observed from aluminium, this experiment enables an upper limit to be set for the effect. To determine whether these results are consistent with scattering from dislocations, average neutron scattering cross sections have been calculated using the theoretical treatment of Atkinson and Hirsch (1958), assuming reasonable dislocation densities of 10^{11} and 10^{10} cm^{-2} for heavily cold-worked copper and aluminium, respectively, and supposing that half the dislocations are in the edge orientation. The values obtained, 2 mb str^{-1} atm^{-1} for copper and 0·04 mb str^{-1} atm^{-1} for aluminium, are in order of magnitude agreement with the experimental neutron scattering cross sections of table 1.

§ 4. CONCLUSIONS

The x-ray experiments show that most of the scattering at small angles is due to double Bragg reflections. No surface scattering effect has been detected.

The neutron scattering experiments show that the true scattering from defects is very small, and that the scattering detected for rolled and extended copper can be explained satisfactorily in terms of scattering from a density of about 10^{11} dislocations cm^{-2}. Thus there is no evidence for the existence of cavities in cold-worked or fatigued specimens of copper or aluminium.

In view of the small neutron scattering intensities, and considering the large effect of the double Bragg scattering mechanism for X-rays, it seems doubtful whether the small angle scattering method can be usefully applied at present to the study of dislocations.

ACKNOWLEDGMENTS

I wish to thank Professor N. F. Mott, F.R.S., Dr. W. H. Taylor and Dr. R. D. Lowde for their interest and encouragement, Dr. P. A. Egelstaff for making available the cold neutron source and especially Dr. P. B. Hirsch for suggesting the problem and for many invaluable discussions. I am indebted to the Master and Fellows of Corpus Christi College for the award of the Plumian Research Studentship and to I.C.I. for a grant.

REFERENCES

ATKINSON, H. H., and HIRSCH, P. B., 1958, *Phil. Mag.*, **3,** 213.
ATKINSON, H. H., and LOWDE, R. D., 1957, *Phil. Mag.*, **2,** 589.
BEEMAN, W. W., KAESBERG, P., ANDREGG, J. W., and WEBB, M. B., 1957, *Handb. Physik*, **32,** 440.
BLIN, J., 1954, *Thesis*, University of Paris ; 1955, *Defects in Crystalline Solids* (London: The Physical Society), p. 420 ; 1957, *Acta Met.*, **5,** 528.
BLIN, J., and GUINIER, A., 1951, *C.R. Acad. Sci., Paris*, **233,** 1288 ; 1953, *Ibid.*, **236,** 2150.
BRAMMER, W. G. 1955, *Ph.D. Thesis*, University of Wisconsin.
BUTTERWORTH, I., EGELSTAFF, P. A., LONDON, H., and WEBB, F. J., 1957, *Phil. Mag.*, **2,** 917.
DEXTER, D. L., 1953, *Phys. Rev.*, **90,** 1007.
EGELSTAFF, P. A., and PEASE, R. S., 1954, *J. sci. Instrum.*, **31,** 207.
FRANKS, A., and HOLDEN, J., 1955, *Nature, Lond.*, **176,** 1022.
NEYNABER, R. H., 1955, *Ph.D. Thesis*, University of Wisconsin.
ROBINSON, W. H., and SMOLUCHOWSKI, R., 1956, *J. appl. Phys.*, **27,** 657.
SEEGER, A., 1957 a, *Acta Met.*, **5,** 24 ; 1957 b, *Proc. Conf. Dislocations and Mech. Properties of Crystals, Lake Placid* (New York: J. Wiley), p. 506.
WEBB, M. B., 1956, *Ph.D. Thesis*, University of Wisconsin.
ZHURKOV, S. N., and SLUTSKER, A. I., 1957, *Zh. Tekh. Fiz.*, **27,** 1392.

Nuclear Alignment and the Beta Transition in Cobalt-58†

By P. Dagley, M. A. Grace, J. S. Hill and C. V. Sowter
The Clarendon Laboratory, Oxford

[Received March 8, 1958]

Abstract

A single crystal of nickel fluosilicate has been used for the low temperature alignment of cobalt-58. Angular distribution measurements of the 805 kev γ-radiation are consistent with the β-transition being pure Gamow–Teller, the Fermi admixture being given by

$$C_F^2|M_F|^2/\{C_F^2|M_F|^2+C_{GT}^2|M_{GT}|^2\}=-0{\cdot}003\pm0{\cdot}005.$$

§ 1. Introduction

The recent experiments relating to the violation of parity conservation in β-decay (Wu *et al.* 1957, Ambler, Hayward, Hoppes, Hudson and Wu 1957) have emphasized the importance of obtaining complete information on the character of β-transitions so as to provide a test of β-decay theory. In particular the presence of small admixtures of Fermi interaction in predominantly Gamow–Teller transitions can lead to interference terms which may radically alter the spatial asymmetry of β-rays in the ‘ parity ’ type of experiment. At the same time, the presence of such admixtures can also be detected in experiments which do not rely on the breakdown of parity conservation, such as the study of the anisotropy of γ-radiation from aligned nuclei in which the γ-emission is preceded by a β-transition. ^{58}Co which might exhibit such an admixture is so far the only isotope that has been studied by both methods and in this case the results of the two are in disagreement.

The decay scheme of ^{58}Co is given in fig. 1 (see, for instance, Frauenfelder *et al.* 1956) and shows that most of the disintegrations proceed via K-capture or positron emission directly to the 805 kev level in ^{58}Fe. The study of the weak branch through the 1·62 Mev state showed this state to be of spin 2 and the 815 kev γ-ray to be mixed with $\delta(E2/M1)=2{\cdot}2\pm0{\cdot}3$. The spin assignment to the other states is made on the basis of nuclear alignment experiments by Daniels *et al.* (1952). Recently the ground state spin of ^{58}Co has been confirmed by a paramagnetic resonance experiment by Dobrov and Jeffries (1957). Daniels *et al.* also showed the β-transition to be principally Gamow–Teller. A statistically more accurate result was obtained by Griffing and Wheatley (1956) who used the same technique. They showed that best agreement between the theoretical and observed γ-ray angular distributions is obtained for

$$\lambda=\frac{C_F^2|M_F|^2}{C_{GT}^2|M_{GT}|^2+C_F^2|M_F|^2}=0{\cdot}11\pm0{\cdot}4$$

---

† Communicated by the Authors.

C_F, C_{GT} are the Fermi and Gamow–Teller coupling constants and M_F, M_{GT} the corresponding nuclear matrix elements for the β-transition. A subsequent analysis of the measurements of Daniels *et al.* showed that a value of λ of $0{\cdot}1 \pm 0{\cdot}1$ would be consistent with their results: this figure is referred to in the paper of Griffing and Wheatley.

Fig. 1

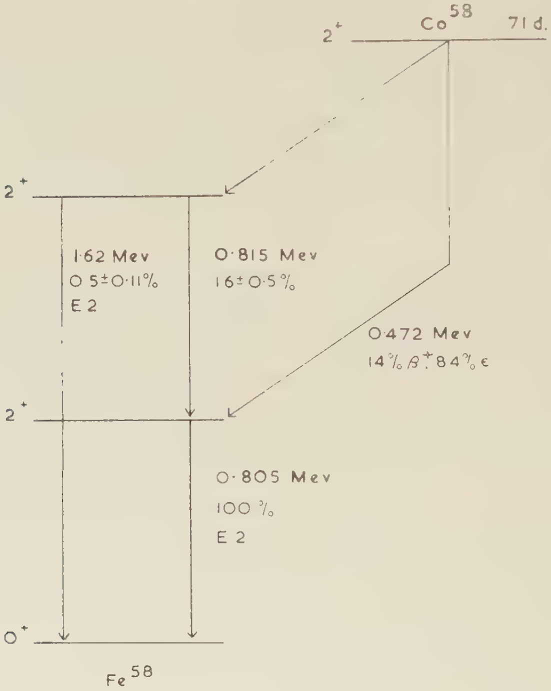

The decay scheme of cobalt-58.

In the ‘parity’ experiment of Ambler *et al.* the backward-forward asymmetry coefficient α was found to be $+0{\cdot}325 \pm 0{\cdot}047$ for the positrons from polarized ^{58}Co. This value is in agreement with that predicted by the two state neutrino theory for a pure GT transition $(+\frac{1}{3})$ and is incompatible with a value of λ greater than 0·03; this conclusion is supported by a similar experiment of Postma *et al.* (1957). Confirmation of this ‘parity’ result is provided by the β–γ circular polarization correlation measurements of Boehm and Wapstra (1957) who showed λ to be less than 0·06. Ambler, Hayward, Hoppes, and Hudson (1957) pointed out that the apparent discrepancy between the results of the γ-ray and the β-ray experiments might arise from the F–GT interference terms being largely imaginary but this hypothesis they showed to be untenable in the light of a β–γ correlation experiment on polarized ^{58}Co nuclei in which they found no evidence for such terms.

Since the establishment of a disagreement between these two types of experiment could be important in the development of future β-decay theory, it was decided to make a further study of λ by the γ-ray method under experimental conditions which avoided some of the defects of the earlier alignment experiments.

§ 2. DESIGN OF EXPERIMENT

The principle of the method for studying λ through the γ-ray angular distribution is as follows. The γ-ray intensity at an angle θ with the axis of alignment is expressible in the form (see, for instance, Gray and Satchler 1955)

$$W(\theta)=1+B_2U_2F_2P_2(\cos\theta)+B_4U_4F_4P_4(\cos\theta)$$

B_ν is a temperature dependent term describing the degree of alignment, and F_ν an angular correlation coefficient for the γ-ray transition. The character of the β-transition is contained in the terms U_ν which can be written as

$$U_\nu=\lambda U_\nu{}^{\mathrm{F}}+(1-\lambda)U_\nu{}^{\mathrm{GT}}$$

$U_\nu{}^{\mathrm{F}}$, $U_\nu{}^{\mathrm{GT}}$ being the values appropriate for Fermi and Gamow–Teller transitions. For ^{58}Co all these terms are known except λ and B_ν. Since in the simple case of completely anisotropic hyperfine structure (hfs) B_2, B_4 each depend only on the Boltzmann parameter $\beta(=A/2kT$ where A is the hfs constant; see below), it is sufficient to measure $W(\theta)$ for two values of θ and to compare these with the theoretical values in order to determine λ. It is usually convenient to choose to measure at the angles $\theta=0$ and $\frac{1}{2}\pi$ where both $P_2(\cos\theta)$ and $P_4(\cos\theta)$ are changing least rapidly. This was the method used in earlier alignment experiments, but these suffered from two defects:

(*a*) Since the experiments were carried out on a number of crystals arranged with their axes parallel thermal equilibrium amongst the constituents was not ensured and therefore the B_ν must be replaced by $\bar{B}_\nu$ where $\bar{B}_\nu$ is some average over all the crystals. Such a change in the calculated B_ν could lead to erroneous values for λ.

(*b*) The Tutton salt crystals used in the experiments have two alignment axes inclined at about 70° to each other, neither of which is coincident with a crystallographic axis. For ^{58}Co it is the axial direction in which the γ-ray intensity is most sensitive to the value of λ and therefore, since in the biaxial Tutton salt this direction is not accessible for study, the measurements with these crystals are less sensitive to λ than those on uniaxial crystals. In addition, the error introduced by uncertainty in the exact location of these alignment (tetragonal) axes makes the Tutton salt an unsatisfactory choice for this kind of measurement. A more favourable crystal would be one of the fluosilicate group which have a single axis of alignment coincident with one of the crystal axes.

The fluosilicates $M^{++}SiF_6 . 6H_2O$ form an isomorphous series in which M can be any divalent ion of the iron transition group. Experiments by Hill *et al.* (1958) using a magnetically diluted nickel salt of this series have shown that this can be cooled to temperatures of the order of 0·02°K by adiabatic demagnetization using H/T values of 25 kilo oersted/degree.

Fig. 2

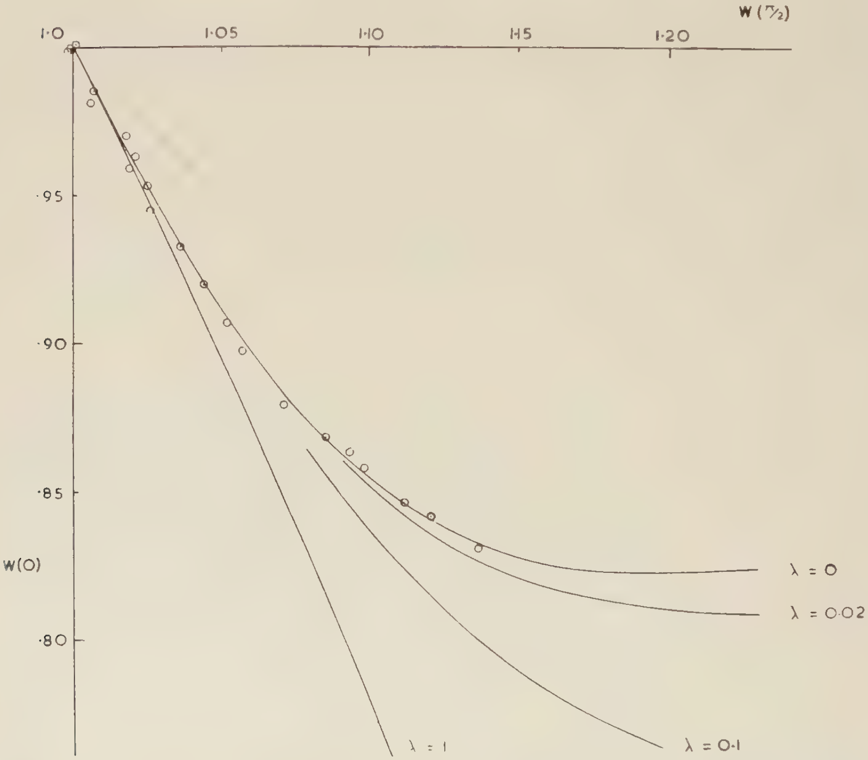

The normalized counting rate along the axis $W(0)$ is plotted against that in the equatorial plane $W(\frac{1}{2}\pi)$ for the 805 kev γ-ray from aligned ^{58}Co. The value 1 corresponds to the isotropic distribution. The solid curves show the expected dependence for different values of the β-transition mixing parameter

$$\lambda(=C_F{}^2|M_F|^2/C_F{}^2|M_F|^2+C_{GT}{}^2|M_{GT}|^2).$$

Only portions of the $\lambda=0{\cdot}1$ and 1 curves are shown.

Bleaney and Ingram (1951) have studied the paramagnetic resonance spectrum for Co^{++} in this lattice and have shown it to be describable by a spin Hamiltonian of the form

$$\mathscr{H}=AS_zI_z+B(S_xI_x+S_yI_y)+g\beta\mathbf{H.S}$$

where $S=\frac{1}{2}$ and $A=0{\cdot}0184\pm0{\cdot}0004$ cm^{-1}, $B=0{\cdot}0047\pm0{\cdot}0002$ cm^{-1} for stable cobalt: the sign of A is taken to be positive (Abragam and Pryce

1951). Thus at temperatures of the order of 0·01°K considerable alignment of the Co nuclei should occur in zero external magnetic field through the magnetic hfs (Bleaney 1951). The existence of the B term leads to a deviation from the uniform level spacing $\frac{1}{2}A$ and also to a mixing of the nuclear states. Both of these depend on the ratio B/A, a factor which is independent of the particular cobalt isotope. Thus for a given B/A the population functions B_ν can be evaluated in terms of β only. With these values a family of curves can be drawn showing the dependence of $W(0)$ on $W(\frac{1}{2}\pi)$, each member of the family corresponding to a single value of λ and each point on the curve corresponding to a different value of β. A number of these curves are shown in fig. 2 and indicate the substantial differentiation between small values of λ which can be obtained by this method. The sensitivity to λ comes from the great difference in the γ-ray intensities along the axis for the two cases: the minimum value of $W(0)$ for the Fermi transition is 0·06 whereas for the Gamow–Teller transition it is 0·822. It should be pointed out that the derivation of λ from a measurement of $W(0)$ and $W(\frac{1}{2}\pi)$ does not rely on any knowledge of the absolute temperature of the crystal but only on the validity of the spin Hamiltonian, the value of B/A and the sign of A.

§ 3. Experimental

Cobalt-58 was produced by the ^{58}Ni(n, p)^{58}Co reaction using the fast neutron flux of the A.E.R.E. pile. Carrier free cobalt was then separated chemically from the nickel. The cobalt was largely ^{58}Co, only about $\frac{1}{4}$% being due to ^{60}Co. This low yield is in accord with that predicted by Hughes (1954). A single crystal of (10% Ni, 90% Zn) $SiF_6 . 6H_2O$ weighing 3·1 g and containing about 70 μcuries of ^{58}Co was grown from active solution. The surfaces of the crystal were clear and its axis could be located accurately. This was then held in a small Perspex carriage and mounted with its axis horizontal on a rigid glass spill in the low temperature cryostat. Also mounted on the spill was a pill of $Mn(NH_4)_2(SO_4)_2 . 6H_2O$ which acted on cooling both as a guard ring for reducing the heat influx to the crystal through its support and as a ‘ getter ’ for mopping up the last traces of the exchange gas. After cooling by adiabatic demagnetization from initial fields of up to 35 kilo oersted at 0·9°K, scintillation counters fitted with 2 in. cylindrical NaI(Tl) phosphors were placed round the cryostat to record the counting rates on the axis of the crystal and in the equatorial plane. Each counter had an energy resolution of 8% for 660 kev γ-radiation and subtended a half angle of 9° at the crystal.

A pair of discriminators was set above and below the 805 kev photopeak. In this way account could be taken of the effect of the higher energy γ-radiation from ^{58}Co and from ^{60}Co contamination on the counting rate in the 805 kev channel. A pulse height analysis showed that the whole spectrum could be interpreted in terms of these components. These counting rates together with the magnetic temperature were followed for about 5 minutes and then the crystal was warmed up to about 1°K, the temperature of the helium bath. By demagnetizing from different initial fields the whole temperature range was covered.

The counting rates for any given value of the magnetic temperature were independent of whether this temperature was reached by direct demagnetization or by demagnetizing to a lower temperature and allowing the crystal to warm up. This shows that the temperature was sensibly homogeneous within the crystal over the measuring period of 5 minutes. Frequent tests throughout the series of runs were carried out which showed that no systematic trends, due, for instance, to instability or to fatigue of the counters, were influencing these readings. These tests took the form of demagnetizations from small fields in which case no cooling was produced and the isotropic distribution was obtained.

The counting rates for the channels on each counter normalized to the warm counting rates were then plotted one against the other and are shown in fig. 2. Each point is an average of a number of readings (about 20/point).

§ 4. Results and Discussion

It is seen that the uncorrected experimental points agree closely with the $\lambda=0$ curve. The results were treated quantitatively in the following way. Each experimental point can be treated as a measurement of the value of λ with a probable error and hence a weight arising from the counting statistics. In this way the average value of λ is found to be $+0\cdot003$ with a probable error based on the scatter of these points of $\pm0\cdot004$. This value is in agreement with that to be expected on the basis of the total number of counts ($\sim10^6$) for the coordinates of each point ($\pm0\cdot003$).

This value for λ now requires to be corrected for the following systematic effects:

(i) The finite aperture of the counters (9°) gives rise to a correction to λ of $-0\cdot003$ (see for instance Feingold and Frankel 1955).

(ii) The presence of pulses due to the 0·815 and 1·62 MeV γ-rays lying within the 0·805 MeV channel causes a correction which depends on the λ for this weak low energy β-transition (λ'). If $\lambda'=0$ the 1·62 MeV γ-ray involves no correction while the 0·815 MeV γ-ray causes a change in λ of $-0\cdot001$. If λ' is not zero but about 0·5 as the measurements of Griffing and Wheatley suggest then λ has to be corrected by $-0\cdot004$. For the present purposes we assume λ' to be zero.

(iii) The presence of ^{60}Co in the source was responsible for about 0·13% of the total number of counts in the 0·805 MeV channel. From the known values of A for ^{60}Co and ^{58}Co in this crystal the angular distribution of this radiation can be predicted and leads to a change in the value of λ of $-0\cdot001$.

(iv) The total thickness of the low temperature apparatus through which the γ-radiation had to pass was equivalent to a vertical cylinder of brass 0·35 cm thick which caused scattering of the γ-radiation. The discrimination level of the counter was such that it could not detect γ-radiation which had been singly scattered through angles greater than 30° with the corresponding degradation in energy. A calculation for a spherical scatterer of this thickness shows that scattering leads to a reduction in λ of 0·001. It is considered that this closely represents the experimental conditions and that a full numerical integration would not lead to a significantly different result. This has therefore been used in determining the best value for λ.

In addition to these there are the following sources of uncertainty:

(*a*) Possible misalignment of the crystal by 2° leads to an error in λ of $^{+0}_{-0\cdot002}$.

(*b*) The value of B/A is only known to 5% and this gives rise to an error of $\pm 0\cdot0015$.

Combining these corrections and errors we arrive at the result:

$$\lambda = -0\cdot003 \pm 0\cdot005.$$

This value is consistent with the complete absence of Fermi admixture and makes it unlikely that it exceeds 0·005.

§ 5. CONCLUSIONS

In the present experiment two possible sources of error which may have been present in the earlier ^{58}Co alignment experiments of Daniels *et al.* (1952) and of Griffing and Wheatley (1956) have been removed:

(i) The use of a single crystal rather than a large number of crystals eliminates any error arising from temperature inhomogeneity in the crystal.

(ii) The choice of a fluosilicate crystal with its single axis of alignment rather than the biaxial Tutton salt removes the necessity of determining the position of the tetragonal axes and increases the sensitivity of the γ-ray method to the parameters of the β-transition.

We conclude that the Fermi admixture is negligible, the value of γ being $-0\cdot003 \pm 0\cdot005$. This result is consistent with those obtained in the ‘ parity ’ type of experiment.

Note added in proof.—In subsequent experiments we have shown that the anisotropy of the 1·62 MEV γ-radiation is closely the same as that of the 0·805 MEV radiation. This result confirms the hypothesis that λ' is about zero and is incompatible with a value of λ' greater than 0·2.

ACKNOWLEDGMENTS

We are indebted to the Isotope Division, A.E.R.E., Harwell for kindly supplying the carrier free ^{58}Co. We are very grateful to Professor Bleaney and Dr. Kurti for many stimulating discussions. This work was carried out while three of us (P.D., J.S.H. and C.V.S.) were in receipt of maintenance grants from D.S.I.R.

References

Abragam, A., and Pryce, M. H. L., 1951, *Proc. roy. Soc.* A, **206,** 173.

Ambler, E., Hayward, R. W., Hoppes, D. D., and Hudson, R. P., 1957, *Phys. Rev.*, **108,** 503.

Ambler, E., Hayward, R. W., Hoppes, D. D., Hudson, R. P., and Wu, C. S., 1957, *Phys. Rev.*, **106,** 1361.

Bleaney, B., 1951, *Proc. phys. Soc. Lond.* A, **64,** 315.

Bleaney, B., and Ingram, D. J. E., 1951, *Proc. roy. Soc.* A, **208,** 143.

Boehm, F., and Wapstra, A. H., 1957, *Phys. Rev.*, **107,** 1462.

Daniels, J. M., Grace, M. A., Halban, H., Kurti, N., and Robinson, F. N. H., 1952, *Phil. Mag.*, **43,** 1297.

Dobrov, W., and Jeffries, C. D., 1957, *Phys. Rev.*, **108,** 60.

Feingold, A. M., and Frankel, S., 1955, *Phys. Rev.*, **97,** 1025.

Frauenfelder, H., Levine, N., Rossi, A., and Singer, S., 1956, *Phys. Rev.*, **103,** 352.

Gray, T. P., and Satchler, G. R., 1955, *Proc. phys. Soc. Lond.* A, **68,** 349.

Griffing, D. F., and Wheatley, J. C., 1956, *Phys. Rev.*, **104,** 389.

Hill, J. S., Meyer, H., and Milner, J. M., 1958, *Phil. Mag.*, **3** (to be published).

Hughes, D. J., 1954, *Nature, Lond.*, **173,** 396.

Postma, H., Huiskamp, W. H., Miedema, A. R., Steenland, M. J., Tolhoek, H. A., and Gorter, C. J., 1957, *Physica*, **23,** 259.

Wu, C. S., Ambler, E., Hayward, R. W., Hoppes, D. D., and Hudson, R. P., 1957, *Phys. Rev.*, **105,** 1413.

Taylor's Theorem for Shift Operators†

By R. A. SACK
Department of Theoretical Physics, University of Liverpool
and
British Rayon Research Association, Manchester

[Received February 6, 1958]

ABSTRACT

An expansion equivalent to Taylor's series is derived for functions of two operators of the form $F(A+B)$ where B is a shift operator with regard to A; the result is obtained as a special case of a theorem due to Kermack and McCrea. The development in powers of B involves finite differences of the function $F(A)$ instead of derivatives as in the case of commuting variables. Exponential functions can be factorized into two terms, each depending on one operator only.

The result allows a Gaussian potential energy to be expressed as a product of exponentials involving only creation and destruction operators. Explicit results are derived for the matrix elements of such a Gaussian function in the representations which diagonalize the Hamiltonians of the harmonic oscillator in one and two dimensions; they can be expressed in terms of Jacobi polynomials (finite hypergeometric series).

§ 1. INTRODUCTION

IN many problems it is of importance to determine how a function $F(A)$ of an operator A varies as A itself is altered. In the field of complex numbers this variation is determined by Taylor's theorem

$$F(x+h)=F(x)+\frac{h}{1!}\frac{dF}{dx}+\frac{h^2}{2!}\frac{d^2F}{dx^2}+\ldots=\exp\left(h\frac{d}{dx}\right)F(x), \qquad (1.1)$$

but this formula depends on the commutative law of multiplication. In consequence it cannot be used to express a function

$$F(w)=F(A+\lambda B) \quad . \quad . \quad . \quad . \quad . \quad . \quad . \quad . \qquad (1.2)$$

in powers of λ where A and B are non-commuting operators and λ is a complex number (a c-number), even if F has a well-defined meaning. Any formula analogous to (1.1) involves the whole algebra generated by A and B through the continued formation of commutators; the resulting equations either involve repeated integrals (Feynman 1951) or very cumbersome commutator expressions (Kubo 1952); they gain considerably in simplicity in representations in which the operator A is diagonal (Schafroth 1951).

---

† Communicated by the Author. Now at the Department of Theoretical Chemistry, University of Cambridge.

A formula for the expansion (1.2) has been derived by Kermack and McCrea (1931) which is applicable whenever A and B can be expressed as functions of two operators p and q which satisfy the simple commutation rule

$$[q, p]=qp-pq=1. \qquad (1.3)$$

This work is not well known even though one of their results

$$\exp(ap+bq)=\exp(ap)\exp(bq)\exp(\tfrac{1}{2}ab), \qquad (1.4)$$

where a and b are c-numbers, is widely used in field theory.

One particularly important case of non-commuting operators arises when one of them is a shift operator with regard to the other such that

$$[A, B]=AB-BA=aB. \qquad (1.5)$$

The Taylor expansion (1.2) for the case can easily be derived from the general formulae of Kermack and McCrea (1931). In § 2 their treatment will be briefly outlined and applied to the case of shift operators. Questions of convergence will be ignored as they have been fully discussed by Kermack and McCrea.

In certain quantum-mechanical problems it is necessary to consider potential energy functions which are essentially quadratic at large distances from a given centre, but near this centre have curvatures that do not correspond to their asymptotic behaviour and may even be negative. Such functions are most easily expressed as the sum of two terms, the first of which is purely quadratic and the second Gaussian. It will be shown in § 3 that the matrix elements for such a Gaussian function in the representation which diagonalizes the Hamiltonian of a harmonic oscillator can easily be calculated by repeated applications of the formulae derived in § 2.

§ 2. THE EXPANSION THEOREM INVOLVING SHIFT OPERATORS

The most important of the several expansion formulae derived by Kermack and McCrea (1931) can be written formally

$$F[q+\lambda f(p)]=F(q)+\frac{\lambda}{1!}HF(q)+\frac{\lambda^2}{2!}H^2F(q)+\ldots=\exp(\lambda H)F(q) \qquad (2.1)$$

where H is a symbolic operator acting on $F(q)$

$$H=f_1\frac{d}{dq}+\frac{1}{2!}\frac{df_1}{dp}\frac{d^2}{dq^2}+\frac{1}{3!}\frac{d^2f_1}{dp^2}\frac{d^3}{dq^3}+\ldots \qquad (2.2)$$

$$=f_2\frac{d}{dq}-\frac{1}{2!}\frac{df_2}{dp}\frac{d^2}{dq^2}+\frac{1}{3!}\frac{d^2f_2}{dp^2}\frac{d^3}{dq^3}-+\ldots \qquad (2.3)$$

The suffixes 1 and 2 attached to f indicate that in each term all the powers and derivatives of $f(p)$ premultiply or postmultiply respectively the appropriate derivatives of $F(q)$. This expansion is most easily derived if use is made of a theorem due to Dirac (1926, 1930)

$$qf(p)-f(p)q=df/dp. \qquad (2.4)$$

Total induction yields for positive integer m

$$q^m f(p) = f(p) q^m + \binom{m}{1} \frac{df}{dp} q^{m-1} + \binom{m}{2} \frac{d^2 f}{dp^2} q^{m-2} + \ldots \qquad (2.5)$$

The commutation rules (2.4) and (2.5) also apply if q is replaced by

$$w = q + \lambda f,$$

so that for any positive integer power w^n the first derivative becomes

$$\left.\begin{aligned} \frac{\partial(w^n)}{\partial\lambda} &= \sum_{m=0}^{n-1} w^m f w^{n-m-1} \\ &= \binom{n}{1} f w^{n-1} + \binom{n}{2} \frac{df}{dp} w^{n-2} + \binom{n}{3} \frac{d^2 f}{dp^2} w^{n-3} + \ldots = H(w^n) \end{aligned}\right\} . \qquad (2.6)$$

The alternative form (2.3) for H is proved in an analogous way; repeated application of (2.6) for a Taylor expansion in power of λ leads to (2.1).

The special commutation rules (1.5) for shift operators can be satisfied, in view of (2.4), by the choice

$$A = q, \qquad B = f(p) = \exp(ap). \quad . \quad . \quad . \quad . \quad . \quad (2.7)$$

In this case we can evaluate the operator H in (2.2)

$$H = B_1 \left(\frac{1}{1!} \frac{d}{dq} + \frac{a}{2!} \frac{d^2}{dq^2} + \ldots \right) = \frac{B_1}{a} [\exp(ad/dq) - 1] = \frac{B_1}{a} \Delta_a, \qquad (2.8)$$

where Δ_a is a finite difference operator acting on $F(A)$

$$\Delta_a F(A) = F(A + a) - F(A). \quad . \quad . \quad . \quad . \quad . \quad . \quad . \quad (2.9)$$

The alternative expression (2.3) leads to

$$H = -(B_2/a)\Delta_{-a}. \quad . \quad . \quad . \quad . \quad . \quad . \quad . \quad . \quad (2.10)$$

The suffixes 1 and 2 in (2.8) and (2.10) have the same meaning as in (2.2) and (2.3). The complete Taylor expansion for (1.2) becomes with the use of (2.1), (2.8) and (2.10):

$$F(A + \lambda B) = \exp[(\lambda B_1/a)\Delta_a] F(A) = \exp[-(\lambda B_2/a)\Delta_{-a}] F(A). \qquad (2.11)$$

For the special case of an exponential function

$$F(A) = \exp(\kappa A)$$

we have in view of (2.9)

$$\Delta_a F(A) = \exp[\kappa(A + a)] - \exp(\kappa A) = [\exp(\kappa a) - 1] F(A), \qquad (2.12)$$

so that (2.11) factorizes:

$$\exp[\kappa(A + \lambda B)] = \exp[(\lambda B/a)(e^{\kappa a} - 1)] e^{\kappa A} = e^{\kappa A} \exp[(\lambda B/a)(1 - e^{-\kappa a})], \quad . \quad . \quad . \quad (2.13)$$

In the limit $a \rightarrow 0$, the divided differences $\Delta_a F/a$ become derivatives and the expansion (2.11) and (2.13) become the corresponding Taylor series (1.1) for commuting variables.

§ 3. Matrix Elements for a Gaussian Potential Energy

A very common representation of dynamical variables in quantum mechanics is that which diagonalizes the Hamiltonian of the harmonic oscillator

$$H=\tfrac{1}{2}(p^2+q^2), \quad pq-qp=-i, \qquad \qquad (3.1)$$

where the units are chosen in such a way that $\hbar=\omega=1$. (The variables p and q in this section are not the same as in the first two sections; the commutation rule (3.1) is not identical with (1.3).) The eigenvalues for this Hamiltonian are well known to be

$$E=n=\tfrac{1}{2},\ \tfrac{3}{2},\ \tfrac{5}{2}\ldots \qquad \qquad (3.2)$$

If we try to evaluate the matrix elements for a Gaussian potential energy $\exp(-kq^2)$ in this representation, we are faced with the difficulty that the matrices for q^N become more and more complicated with increasing N. In contrast, the matrices for the powers and exponential functions of the creation and destruction operators

$$a^*=\tfrac{1}{2}(q-ip), \quad a=\tfrac{1}{2}(q+ip) \qquad \qquad (3.3)$$

retain a simple structure. In fact, if we use Dirac's bracket notation for the eigenstates of H, the matrix elements for a^* and a become

$$\langle n|a|s\rangle=\langle s|a^*|n\rangle=\delta_{s-n,1}[\tfrac{1}{2}(n+\tfrac{1}{2})]^{1/2} \qquad \qquad (3.4)$$

where $\delta_{m,n}$ is the Kronecker symbol

$$\delta_{mn}\begin{matrix}=1(m=n)\\ =0(m\neq n)\end{matrix}$$

(cf. Dirac 1947).

For powers of a^* and a the terms become accordingly

$$\langle n|a^N|s\rangle=\langle s|a^{*N}|n\rangle=\frac{\delta_{s-n,N}}{2^{N/2}}\left[\frac{(s-\frac{1}{2})!}{(n-\frac{1}{2})!}\right]^{1/2}. \qquad \qquad (3.5)$$

Furthermore

$$\langle n|a^*a|s\rangle=\tfrac{1}{2}\delta_{ns}(n-\tfrac{1}{2}), \quad \langle n|aa^*|s\rangle=\tfrac{1}{2}\delta_{ns}(n+\tfrac{1}{2}). \qquad \qquad (3.6)$$

Considerable simplification could therefore be achieved if the expression

$$V=\exp(-kq^2)=\exp[-k(a+a^*)^2] \qquad \qquad (3.7)$$

could be replaced by a product involving exponentials of a^2, a^{*2}, and aa^* or a^*a. From (3.1) and (3.3) we find the commutation rules

$$[a,\ a^*]=\tfrac{1}{2}, \qquad \qquad (3.8)$$

$$[aq,\ q^2]=[-a^*q,\ q^2]=q^2, \qquad \qquad (3.9)$$

$$[aq,\ a^2]=-a^2, \quad [a^*q,\ a^{*2}]=a^{*2}. \qquad \qquad (3.10)$$

The squares q^2, a^2 and a^{*2} therefore act as shift operators with regard to the products aq and a^*q, and the formulae derived in § 2 are immediately applicable. In particular we find from (2.13) and (3.9)

$$\exp(-\kappa a^*q)=\exp[\kappa(aq-q^2)]=\exp[(1-e^{\kappa})q^2]\exp(\kappa aq). \qquad \qquad (3.11)$$

Similarly from (2.13) and (3.10)

$$\exp(-\kappa a^*a)=\exp[-\kappa(a^*q-a^{*2})]=\exp(-\kappa a^*q)\exp[(e^\kappa-1)a^{*2}] \tag{3.12}$$

and

$$\exp(-\kappa aa^*)=\exp[-\kappa(aq-a^2)]=\exp[(e^\kappa-1)a^2]\exp(-\kappa aq). \tag{3.13}$$

Equating

$$k=e^\kappa-1,\quad \kappa=\log(1+k) \quad . \quad . \quad . \quad . \quad . \quad . \quad . \tag{3.14}$$

we obtain from (3.11)–(3.13)

$$\exp(-kq^2)=\exp(-\kappa a^*a)\exp(-ka^{*2})\exp(-ka^2)\exp(-\kappa aa^*). \tag{3.15}$$

Of the four factors on the right-hand side the first and last are diagonal matrices in view of (4.6) with elements

$$\langle n|\exp(-\kappa a^*a)|n\rangle=(1+k)^{-n/2+1/4},\quad \langle n|\exp(-\kappa aa^*)|n\rangle=(1+k)^{-n/2-1/4}. \tag{3.16}$$

The matrix elements of the other two exponentials are, in view of (3.5),

$$\langle s|\exp(-ka^{*2})|n\rangle=\langle n|\exp(-ka^2)|s\rangle=\frac{(-\frac{1}{2}k)^{(s-n)/2}}{[\frac{1}{2}(s-n)]!}\left[\frac{(s-\frac{1}{2})!}{(n-\frac{1}{2})!}\right]^{1/2} \tag{3.17}$$

provided $s-n$ is a non-negative even number, and zero otherwise. The matrix for $\exp(-kq^2)$ is thus reducible to two matrices involving states with $n=2l+\frac{1}{2}$ and $n=2l+\frac{3}{2}$ respectively ($l=0, 1, 2\ldots$). Use of (3.16) and (3.17) leads to the final result

$$\langle 2r+\tfrac{1}{2}|V|2s+\tfrac{1}{2}\rangle=\frac{(-)^{r+s}[(2r)!(2s)!]^{1/2}}{(1+k)^{r+s+1/2}} \times\left\{\frac{(\frac{1}{2}k)^{r+s}}{0!r!s!}+\frac{(\frac{1}{2}k)^{r+s-2}}{2!(r-1)!(s-1)!}+\ldots\right\} \tag{3.18}$$

$$\langle 2r+\tfrac{3}{2}|V|2s+\tfrac{3}{2}\rangle=\frac{(-)^{r+s}[(2r+1)!(2s+1)!]^{1/2}}{(1+k)^{r+s+3/2}} \times\left\{\frac{(\frac{1}{2}k)^{r+s}}{1!r!s!}+\frac{(\frac{1}{2}k)^{r+s-2}}{3!(r-1)!(s-1)!}+\ldots.\right\}. \tag{3.19}$$

Written in ascending powers of k, this becomes for $r\geqslant s$

$$\langle 2r+\tfrac{1}{2}|V|2s+\tfrac{1}{2}\rangle=\frac{(-)^{r+s}[(2r)!(2s)!]^{1/2}}{(1+k)^{r+s+1/2}} \times\left\{\frac{(\frac{1}{2}k)^{r-s}}{(2s)!(r-s)!}+\frac{(\frac{1}{2}k)^{r-s+2}}{1!(2s-2)!(r-s+1)!}+\ldots\right\} \tag{3.20}$$

$$\langle 2r+\tfrac{3}{2}|V|2s+\tfrac{3}{2}\rangle=\frac{(-)^{r+s}[(2r+1)!(2s+1)!]^{1/2}}{(1+k)^{r+s+3/2}} \times\left\{\frac{(\frac{1}{2}k)^{r-s}}{(2s+1)!(r-s)!}+\frac{(\frac{1}{2}k)^{r-s+2}}{1!(2s-1)!(r-s+1)!}+\ldots\right\}. \tag{3.21}$$

For $s>r$ the expressions are equivalent to (3.20), (3.21) with r and s interchanged.

The derivation (3.8)–(3.15) applies equally in the case of a Gaussian potential energy in several dimensions as any creation and destruction operator relating to one direction commutes with all the operators relating to a normal direction. In particular, for an isotropic two-dimensional oscillator

$$H=\tfrac{1}{2}(p_x^2+p_y^2+q_x^2+q_y^2) \quad . \quad . \quad . \quad . \quad . \quad . \quad . \qquad (3.22)$$

the eigenstates can be classified according to their energy n and momentum m

$$H|n,m\rangle=n|n,m\rangle,\ (q_xp_y-q_yp_x)|n,m\rangle=m|n,m\rangle \quad . \quad . \qquad (3.23)$$

$$m=0,\pm 1,\pm 2\ldots,\quad n=|m|+1,|m|+3,\ldots \quad . \quad . \quad . \qquad (3.24)$$

(cf. Pauling and Wilson 1935). For a potential energy

$$V=\exp\left[-k(q_x^2+q_y^2)\right]=\exp\{-k[(a_x+a_x^*)^2+(a_y+a_y^*)^2]\} \qquad (3.25)$$

the only non-vanishing matrix elements occur between states of constant m. The matrix elements for $(a_x\pm ia_y)$ and $(a_x^*\pm ia_y^*)$ have been derived by Moffitt and Liehr (1957) (cf. also Longuet-Higgins *et al.* 1957); they are

$$\left.\begin{aligned}\langle n,m|a_x-ia_y|n+1,m+1\rangle&=\langle n+1,m+1|a_x^*+ia_y^*|n,m\rangle\\&=[\tfrac{1}{2}(n+m+1)]^{1/2}\\\langle n,m|a_x^*-ia_y^*|n-1,m+1\rangle&=\langle n-1,m+1|a_x+ia_y|n,m\rangle\\&=[\tfrac{1}{2}(n-m-1)]^{1/2}\end{aligned}\right\} \qquad (3.26)$$

whereas all the other terms vanish. From this follows

$$\langle n,m|a_x^2+a_y^2|n+2,m\rangle=\langle n+2,m|a_x^{*2}+a_y^{*2}|n,m\rangle=\tfrac{1}{2}[(n+1)^2-m^2]^{1/2} \qquad (3.27)$$

$$\langle nm|a_xa_x^*+a_ya_y^*|nm\rangle-\tfrac{1}{2}=\langle nm|a_x^*a_x+a_y^*a_y|nm\rangle+\tfrac{1}{2}=n. \qquad (3.28)$$

The results can be expressed somewhat more simply if we confine our attention to non-negative m (for negative m the results are entirely analogous); then the matrix elements of the relevant exponentials become with the use of (3.27)

$$\left.\begin{aligned}&\langle 2r+m+1,m|\exp\left[-k(a_x^{*2}+a_y^{*2})\right]|2s+m+1,m\rangle\\&\langle 2s+m+1,m|\exp\left[-k(a_x^2+a_y^2)\right]|2r+m+1,m\rangle\end{aligned}\right\}$$

$$=\frac{(-k)^{r-s}}{(r-s)!}\left[\frac{r!(r+m)!}{s!(s+m)!}\right]^{1/2}. \qquad (3.29)$$

The final result is then, in view of (3.15), (3.25), (3.28) and (3.29),

$$\langle 2r+m+1,m|V|2s+m+1,m\rangle=\frac{(-)^{r+s}[r!s!(r+m)!(s+m)!]^{1/2}}{(1+k)^{r+s+m+1}}$$

$$\times\left\{\frac{k^{r+s}}{0!m!r!s!}+\frac{k^{r+s-2}}{1!(m+1)!(r-1)!(s-1)!}+\frac{k^{r+s-4}}{2!(m+2)!(r-2)!(s-2)!}+\ldots\right\}$$

$$. \quad . \quad . \qquad (3.30)$$

$$=\frac{(-k)^{r+s}}{(1+k)^{r+s+m+1}m!}\left[\frac{(r+m)!(s+m)!}{r!\,s!}\right]^{1/2}{}_2F_1(-r,-s;m+1;k^{-2}) \quad . \qquad (3.31)$$

where ${}_2F_1$ denotes the hypergeometric function (cf. Whittaker and Watson 1927). The occurrence of non-positive integers as the first two parameters ensures the breaking off of the series, the resulting polynomials are known as Jacobi polynomials. The expressions (3.18) and (3.19) correspond to (3.30), (3.31) if m is taken to be $-\frac{1}{2}$ and $\frac{1}{2}$ respectively.

These formulae could also have been derived by the use of the generating function of Laguerre polynomials (cf. Pauling and Wilson 1935).

ACKNOWLEDGMENTS

The problem discussed in § 2 has been brought to the writer's attention by Professor H. Fröhlich and that of § 3 by Dr. J. A. Pople, both of whom he wishes to thank. He also wishes to thank Professor M. H. L. Pryce and Dr. G. R. Alcock for useful advice, and the British Rayon Research Association for their support.

REFERENCES

DIRAC, P. A. M., 1926, *Proc. Camb. phil. Soc.*, **23,** 412; 1930, *The Principles of Quantum Mechanics*, 1st edn., (Oxford : The Clarendon Press), p. 34; 1947, *Ibid.*, 3rd edn. (Oxford : The Clarendon Press).

FEYNMAN, R. P., 1951, *Phys. Rev.*, **84,** 108.

KERMACK, W. O., and MCCREA, W. H., 1931, *Proc. Edinb. math. Soc.*, **2,** 220.

KUBO, R., 1952, *J. chem. Phys.*, **20,** 770.

LONGUET-HIGGINS, H. C., PRYCE, M. H. L., ÖPIK, U., and SACK, R. A., 1958, *Proc. roy. Soc.* A, **244,** 1.

MOFFITT, W., and LIEHR, A. D., 1957, *Phys. Rev.*, **106,** 1195.

PAULING, L., and WILSON, E. B., 1935, *Introduction to Quantum Mechanics* (New York : McGraw-Hill Book Co.).

SCHAFROTH, M. R., 1951, *Helv. phys. Acta*, **24,** 645.

WHITTAKER, E. T., and WATSON, G. N., 1927, *A Course of Modern Analysis*, 4th edn. (Cambridge : University Press).

Restricted Random Walks and the Use of Moments†

By R. A. Sack
Department of Theoretical Physics, University of Liverpool
and
British Rayon Research Association, Manchester

[Received February 6, 1958]

Abstract

It is shown that the method of moments can be applied to many problems of random walks on lattices with inequivalent sites. The method is illustrated by two simple examples.

The theory of the random walk in one or more dimensions when there is no correlation between successive steps is well established and makes use of Laplace's method of characteristic functions for a complete specification of the results. The same method applies if the possible positions after each step are confined to a lattice, i.e. a discrete set of points, provided all the lattice points are equivalent.

The method of characteristic functions is not applicable in its simple form whenever an explicit correlation exists between two or more successive steps or for walks on lattices in which the points are not all equivalent. In such cases recourse must be made to the more refined theory of Markov chains (cf. Montroll 1947, Daniels 1952, Hammersley 1953).

In many cases a less complete description of the results is required, in particular if the only quantities of interest are the mean displacement and the mean square deviation therefrom or the parameters specifying the asymptotic Gaussian distribution which is obtained after a large number of steps. In such cases the use of moments provides a more elementary, and usually simpler, method of derivation of the results for uncorrelated steps than the method of characteristic functions. For motion in one dimension the nth moment m_n relating to a single step is defined as

$$m_n = \sum_i p_i x_i^n = m_0 E(x^n) \quad . \quad . \quad . \quad . \quad . \quad . \quad . \quad . \qquad (1)$$

where p_i is the probability that the displacement x will be of magnitude x_i and $E(f)$ denotes the expectation value for the function f. The nth moments $[M_n]_N$ of the distribution for the algebraic sum

$$X_{(N)} = x_{(1)} + x_{(2)} + \ldots x_{(N)}$$

---

† Communicated by the Author. Now at the Department of Theoretical Chemistry, University of Cambridge.

of N successive displacements $x_{(k)}$ satisfy the well-known recurrence relations

$$[M_n]_{N+1} = \sum_{\nu=0}^{n} \binom{n}{\nu} [M_{n-\nu}]_N m_\nu \, ; \; [M_n]_1 = m_n. \qquad (2)$$

This formula is most simply derived from the definition

$$X_{(N+1)} = X_{(N)} + x_{(N+1)},$$

the binomial theorem and the equation

$$E(X_{(N)}{}^{n-\nu} . x_{(N+1)}{}^{\nu}) = E(X_{(N)}{}^{n-\nu}) . E(x_{(N+1)}{}^{\nu}) \qquad (3)$$

which expresses the independence of the distributions for $X_{(N)}$ and $x_{(N+1)}$.

The zero'th moments m_0 and $[M_0]_N$ are unity in most applications; a smaller value of m_0 corresponds to the possibility that the moving particle is eliminated from the system, the quantity $1-m_0$ is then called the probability of absorption. A somewhat different case is found if the p_i are interpreted as transition probabilities in a fixed time interval; in this case there may be a non-zero probability that the particle remains on the same lattice point, but m_0 will be unity if there is no absorption.

Extension of (2) to random walks in several dimensions is straightforward. Thus for a two-dimensional walk we may define

$$m_{n,n'} = \sum_i p_i x_i^n y_i^{n'}, \qquad (4)$$

and the recurrence formula analogous to (2) becomes

$$[M_{n,n'}]_{N+1} = \sum_{\nu=0}^{n} \sum_{\nu'=0}^{n'} [M_{n-\nu,\, n'-\nu'}]_N \, m_{\nu,\nu'} \, ; \qquad (5)$$

the generalization to more dimensions is obvious.

The purpose of the present note is to point out that the method of moments is often applicable even for random walks on lattices with non-equivalent sites, provided that steps are uncorrelated in the sense that given the starting point of a step the transition probabilities do not depend on how this point has been reached. The relations (3) and hence (2) remain true for all values of n for which the moments $m_\nu \, (\nu \leqslant n)$ defined in (1) are constants of the lattice, independent of the starting point of the step. In particular if the moments up to second order are the same for all lattice points the asymptotic distribution after a large number of steps can be calculated by the usual methods. Similar considerations apply to (4) and (5) for walks in several dimensions.

The usefulness of the method will be illustrated by two examples:

(i) *A one-dimensional example*

A particle can move on a linear lattice, the distance between neighbouring points being alternately a and $2a$. Within a standard time interval the particle can move to either adjoining site or remain where it is. The probability of its performing the longer or shorter step are p and $2p$ respectively, and $1-3p$ is the probability that it will not move. The moments for a single time interval are thus

$$m_0=1,\ m_1=\pm(p.2a-2p.a)=0,\ m_2=6pa^2 \quad . \quad . \quad . \quad (6\,a)$$

for all sites, whereas

$$m_3=\pm[p.(2a)^3-2p.a^3]=\pm 6pa^3 \quad . \quad . \quad . \quad . \quad (6\,b)$$

depends on the starting point. Formula (2) yields immediately

$$[M_0]_N=1;\ [M_1]_N=0;\ [M_2]_N=6Npa^2. \quad . \quad . \quad . \quad (6\,c)$$

(ii) *Random walk on a hexagonal close-packed lattice*

In the lattice structure each site has 12 nearest neighbours at a distance a. The sites are arranged in parallel layers composed of nets of equilateral

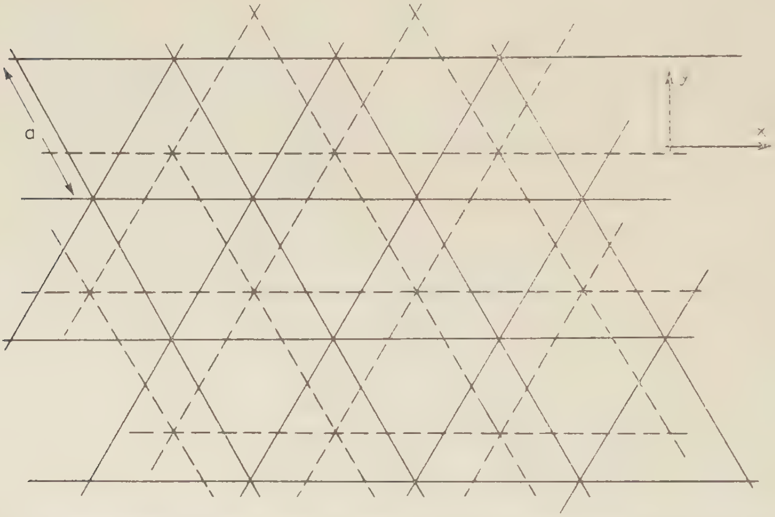

Sites of a hexagonal close-packed lattice. The intersections of the full lines and of the broken lines are the normal projections of the lattice sites in alternate layers on to a plane parallel to the layers.

triangles; the sites of one layer lie above the geometric centres of alternate triangles of the adjoining layers, but the lines connecting corresponding sites of next nearest layers are normal to the layers.

Assume that a particle can carry out an uncorrelated random walk in such a way that in a standard time interval it can move to any nearest neighbour site with a probability $p/6$ or $q/6$ according to whether the motion is within a layer or to an adjoining layer; the probability that it remains on the same site is $1-p-q$. The sites are not equivalent; in rectangular Cartesian coordinates (x, y, z) with the xy-plane parallel to the layers and the x-axis parallel to one set of sides of the triangles the components of the possible steps within the same layer are

$$(\pm a, 0, 0) \ (\pm \tfrac{1}{2}a, \ \pm \tfrac{1}{2}\sqrt{3}a, 0)$$

for all lattice sites, and for steps to adjoining layers $(0, a/\sqrt{3}, \ \pm a\sqrt{\tfrac{2}{3}})$ and $(\pm \tfrac{1}{2}a, \ -\tfrac{1}{2}a/\sqrt{3}, \ \pm a\sqrt{\tfrac{2}{3}})$ for sites in even planes and their negatives for sites in odd planes. The moments for a single interval are thus in a self-explanatory notation

$$m_x = m_z = m_{xz} = m_{yz} = m_{xy} = 0 \qquad \ldots \ldots \quad (7\,a)$$

for reasons of symmetry, also

$$m_y = \pm \tfrac{1}{6}q(2.a/\sqrt{3} - 4.\tfrac{1}{2}a/\sqrt{3}) = 0, \qquad \ldots \ldots \quad (7\,b)$$

$$\left.\begin{aligned} m_{xx} &= \tfrac{1}{6}p(2a^2 + 4.\tfrac{1}{4}a^2) + \tfrac{1}{6}q(4.\tfrac{1}{4}a^2) = (\tfrac{1}{2}p + \tfrac{1}{6}q)a^2, \\ m_{yy} &= \tfrac{1}{6}p(4.\tfrac{3}{4}a^2) + \tfrac{1}{6}q(2.\tfrac{1}{3}a^2 + 4.\tfrac{1}{12}a^2) = (\tfrac{1}{2}p + \tfrac{1}{6}q)a^2, \\ m_{zz} &= \tfrac{1}{6}q(6.\tfrac{2}{3}a^2) = \tfrac{2}{3}qa^2. \end{aligned}\right\} \qquad (7\,c)$$

The inequivalence of sites in alternate layers shows itself only in the third and higher moments. For N intervals the non-vanishing second moments are thus in view of (4)

$$[M_{xx}]_N = [M_{yy}]_N = (\tfrac{1}{2}p + \tfrac{1}{6}q)Na^2; \ [M_{zz}]_N = \tfrac{2}{3}qNa^2. \qquad \ldots \quad (8)$$

As these results depend only on the products pN and qN, they are equally valid for a continuous process in time in which p and q denote transition rates and N the time t. In view of the Einstein (1905) relation

$$[M_{xx}]_t = 2D_{xx}t, \text{ etc.} \qquad \ldots \ldots \quad (9)$$

the diffusion constants D_{xx}, D_{yy}, D_{zz} are given by the moments in (7 *c*) divided by two. The results (8) have been derived by Hammersley (1953) by means of a complicated application of the theory of Markov chains.

ACKNOWLEDGMENTS

The writer wishes to thank Mr. J. M. Hammersley and Professor H. E. Daniels for informative discussions and advice. This work formed part of the fundamental research programme of the British Rayon Research Association.

REFERENCES

DANIELS, H. E., 1952, *Proc. roy. Soc. Edinb.*, A, **63**, 290.
EINSTEIN, A., 1905, *Ann. Phys.*, **17**, 549.
MONTROLL, E. W., 1947, *Ann. math. Statist.*, **18**, 18.
HAMMERSLEY, J. M., 1953, *Compos. math.*, **11**, 171.

The Growth of Inorganic Salt Whiskers from Solution†

By P. Charsley and P. E. Rush
Research Laboratory, Associated Electrical Industries Limited,
Aldermaston Court, Aldermaston, Berkshire

[Received March 3, 1958]

Abstract

Whiskers of sodium chloride, potassium chloride, copper sulphate and sodium nitrate, grown from aqueous solution, have been studied by optical and electron microscopy. The results lead to the conclusion that growth is in two stages: an initial linear growth and subsequent whisker thickening by two-dimensional nucleation. This picture of whisker growth is in accordance with a theory which has been proposed by Sears. Certain direct electron microscope results suggest that the mechanism of whisker thickening is responsible for the known decrease in strength with increasing diameter.

§ 1. Introduction

There are two distinct methods by which whiskers can be grown from solution. In one method, carried out by Newkirk and Sears (1955) and Gordon (1957), the whisker grows totally immersed in the solution. The second method, as developed by Gyulai (1948) and Kato (1955), produces whiskers connected to the parent solution only at their bases: the solution is retained in a porous plate or exists as a film of solution on a large crystal.

One of the most interesting properties of whiskers, their high mechanical strength, was demonstrated for the case of sodium chloride whiskers by Gyulai (1954). Some of the whiskers of about 1 μ diameter had breaking strengths of about 100 kg/mm^2 but thicker whiskers had progressively decreasing strengths, as their diameters increased.

In the present work the final shapes and surface structures of whiskers of several inorganic salts, grown by the method Gyulai, have been studied using the electron microscope. The surface structures can in some respects be explained in terms of the growth mechanism.

§ 2. Method of Growth and Optical Observations

Pieces of a refractory boat were soaked in a concentrated solution of the salt under investigation, either sodium chloride, potassium chloride, sodium nitrate or copper sulphate, and then allowed to dry out very slowly at room temperature (20–25°c). The whiskers varied in diameter between 0·1 μ and 20 μ and grew several millimetres in length.

---

† Communicated by Dr. G. A. Geach.

Observations of sodium chloride whiskers under a low-powered microscope, showed that growth was preceded by an induction period of about a day after which whiskers grew to a length of about 1 mm in 15 hours. There was some evidence that, towards the end of growth in length, thickening occurred. In many cases the whiskers were seen to grow out from small sodium chloride crystals on the surface of the refractory boat. Sodium chloride whiskers were usually quite straight and unbranched and kinks were rare; occasionally whiskers in the form of right-angled crosses were observed. Whiskers of the three other substances investigated were more frequently kinked and branched.

§ 3. Electron Diffraction

The orientations of sodium and potassium chloride whiskers were determined by electron diffraction. Out of 20 sodium chloride whiskers examined 19 had [100] orientations and one had a [110] orientation. A similar number of potassium chloride whiskers examined all had a [110] orientation.

Although the electron diffraction specimens were up to 1 μ thick, extended cross-grating patterns were observed and Kikuchi lines were absent. It was concluded that the whiskers were not perfect crystals but were distorted.

§ 4. Carbon Replica Observations

Single stage carbon replicas were made of sodium and potassium chloride and copper sulphate whiskers, shadowed $\tan^{-1}\frac{1}{2}$ with gold-palladium, in order to study their shapes and surface structures. Most of this work was done on sodium chloride whiskers with a smaller amount on potassium chloride and copper sulphate.

4.1. *Sodium Chloride*

It was found that the whiskers could be broadly classified into three groups on the basis of their size and surface structure. In the first group are those whiskers, or sections of whiskers, which have diameters of about 1 μ or less. The whisker cross sections were irregular and varied along the length; the surfaces were smooth and rounded. Two examples of this type are shown in figs. 1 and 2, Pl. 20; in each case the thin section is more rounded than the thicker section which is faceted and regular.

The thick section of the whisker in fig. 2 is typical of the second group in which the whisker cross sections were regular and constant for considerable lengths. These whiskers were typically a few microns in diameter. A square cross section bounded by {100} planes was most common but occasionally cross sections which were apparently triangular were seen as in fig. 3, Pl. 20. It is possible that the triangular whisker had a [111] orientation.

The most commonly observed whiskers, in contrast to the groups already discussed, showed many growth layers. These whiskers were of a lath-shaped cross section between 1 and 10 μ in width and with width to thickness ratios up to 3 : 1. Two parallel faces were {100} planes (developed to various extents) and the whisker cross section was completed by the irregular termination of growth layers. Typical examples of this type are shown in figs. 4 and 5, Pl. 20; in fig. 5 many fine lines can be seen on the side of the central ridge indicating that this part of the whisker has been built up by layer growth. The growth layers observed were very variable in height and, where it could be decided, they were initiated at the centre of a face, as in fig. 6, Pl. 20.

4.2. *Potassium Chloride*

A large proportion of these whiskers were smooth thin laths of irregular width a few microns wide and a fraction of a micron thick, as in fig. 7, Pl. 21; they only exhibited faint growth markings. They were frequently kinked; in some cases at angles of 60° corresponding to the angle between ⟨110⟩ growth directions. Another type was a more regular, straight, trapeziform whisker as shown in fig. 8, Pl. 21.

4.3. *Copper Sulphate*

The most commonly observed whiskers of copper sulphate were only a few tenths of a micron in diameter and appeared to be square in cross section as in fig. 9, Pl. 21. Only short lengths of such whiskers were observed, probably as a result of fracture in the preparation of the replicas. The tangled appearance of copper sulphate whiskers, as seen in the optical microscope, is probably a result of many thin fibres which coalesce at various points; some support for this idea is given by the replica shown in fig. 10, Pl. 21. Since the whiskers were always sensibly straight, as seen on the electron micrographs, they must break in a brittle manner and do not kink like sodium chloride whiskers (Gyulai 1954).

Occasionally thick copper sulphate whiskers were seen and in these cases they were irregular and rounded and exhibited growth layers.

§ 5. WHISKER DISINTEGRATION IN THE ELECTRON BEAM

When sodium and potassium chloride whiskers were subjected to an intense electron beam in the microscope interesting effects were observed. In fig. 11, Pl. 21 is shown the result of irradiating a sodium chloride whisker about 7 μ wide; the whisker has almost disintegrated and a pattern of rectangles of different opaqueness has been revealed. Effects similar to fig. 11 were always seen during the disintegration of sodium or potassium chloride whiskers providing they were greater than about 1 μ in width. Although the whisker axes were different for these two substances (§ 3) the rectangles were always oriented parallel to [100].

Electron irradiation of sodium chloride whiskers a few tenths of a micron in width never resulted in a regular pattern during disintegration.

Figure 12, Pl. 21 is typical of our observations on this class of whisker; although the transparency is not uniform there are no clear lines of demarcation and there is no pattern.

§ 6. Discussion

For all three kinds of whiskers investigated by electron microscopy a general picture of growth in two stages seems satisfactory. Initially there is a rapid linear growth of a thin whisker and later growth results in a thickening of the whisker by layer growth. In the case of sodium chloride, for which a more detailed picture has been obtained, the initial thin whisker is irregular and rounded in cross section and layer growth develops {100} planes to varying extents. The difference between whiskers of the second and third groups can be attributed to the different thickness of the growth layers resulting from small differences in conditions of growth.

Gyulai (1954) and Kato (1955) reported that whiskers of this type grow from the tip, so that it is probable that the initial growth in length is a result of one or more axial screw dislocations. Some support for this may be found in the absence of Kikuchi lines in the electron diffraction patterns; although misorientation as a result of layer growth could also extinguish Kikuchi lines it is probable that most of the electron diffraction specimens had not thickened to any extent.

The observations of the way in which whiskers thicken support the theory of growth proposed by Sears (1957). On this theory solute is transported to the whisker tip by the hydrodynamic flow of a thin adherent film of solution; the driving force for the flow is the gradient of surface tension resulting from a gradient in the concentration of the adherent film. As the solution travels up the whisker from the base its supersaturation steadily increases, falling again at the tip where the supersaturation would remain small. The maximum supersaturation along the whisker increases as the whisker grows in length until two-dimensional nucleation can occur on the whisker surface, resulting in a thickening of the whisker by layer growth. The onset of layer growth will inhibit the further growth in length of the whisker. In contrast to the growth of lead nitrate crystals by layer growth (Williams 1957) two-dimensional nucleation on sodium chloride crystals occurs at the centre of a face and not at the edges. This difference, however, may merely be a result of considerable differences in growth conditions.

The possibility that the observed growth layers arise from dislocations which have a screw component normal to the whisker axis, has been rejected for two reasons: firstly, the number of centres of nucleation is sometimes improbably high ($>10^8/\text{cm}^2$); secondly, the observation of whisker crosses, in the case of sodium chloride, can be interpreted as due to screw dislocations formed at the growing tip giving rise to two collinear branches. Thus screw dislocations transverse to the axis do not give rise to layers but branches during the growth of sodium chloride whiskers.

The thickness of the adherent film of solution, necessary for the whiskers to grow at the observed rate, can be calculated using the equation derived by Sears[†]. Taking the diameter of the growing whiskers to be $1\,\mu$ and supposing that the whiskers grow 1 mm in 15 hours, the film thickness is about 60 Å, which is not an unreasonable figure.

It is not proposed to attempt a complete explanation of the mechanism by which whiskers disintegrate in an intense electron beam; it is probable that evaporation takes place from the crystal surface which the electrons enter. Nevertheless, the size effect observed in these experiments, which corresponds to that whisker diameter below which no layer growth could be expected, is significant. The correspondence implies that layer growth creates a structure in the crystal which is not produced by the initial linear growth. Since sodium chloride whiskers only have a high strength when they are of about $1\,\mu$ in diameter it is suggested that the structure created during layer growth is responsible for a lowering of the mechanical strength.

ACKNOWLEDGMENTS

The authors wish to thank various members of this Laboratory for useful discussion, Dr. G. A. Geach for his continued encouragement and Dr. T. E. Allibone, F.R.S., Director of this Laboratory, for permission to publish this paper.

REFERENCES

GORDON, J. E., 1957, *Nature, Lond.*, **179,** 1270.
GYULAI, Z., 1948, *Z. Phys.*, **125,** 1; 1954, *Ibid.*, **138,** 317.
KATO, N., 1955, *J. phys. Soc. Japan*, **10,** 1024.
NEWKIRK, J. B., and SEARS, G. W., 1955, *Acta. Met.*, **3,** 110.
SEARS, G. W., 1957, *J. chem. Phys.*, **26,** 1949.
WILLIAMS, A. P., 1957, *Phil. Mag.*, **2,** 317.

[†] The equation as given by Sears (1957) is somewhat incorrect. The equation for the film thickness τ should be:

$$\tau = \left\{ \frac{\rho \eta r}{2M\sigma^* t} \cdot \frac{dc}{d\gamma} \right\}^{1/2} \frac{l}{C_0}$$

where l is the length of whisker of radius r which grows in a time t; ρ is the density of the whisker; η is the viscosity of the saturated solution; M is the molecular weight of the solute; C_0 is the equilibrium concentration of the solution; σ^* is the critical supersaturation for two-dimensional nucleation and $d\gamma/dc$ is the rate of change of surface tension with concentration.

Annealing in Slip Bands in Copper Fatigued at 90°K†

By D. Hull
Atomic Energy Research Establishment, Harwell

[Received January 16, 1958 ; and in revised form March 6, 1958]

Abstract

The number of slip bands formed during the fatigue of O.F.H.C. copper at 90°K and 293°K have been compared. For equivalent stresses to cause failure in 2×10^6 cycles, more slip bands are formed at 90°K than at 293°K. The number of slip bands formed increases with the length of the test. When specimens are fatigued at 90°K, and heated to room temperature at intermediate stages, the rate of increase of slip bands is much smaller than for specimens kept entirely at 90°K. The intermediate heating effectively makes the slip bands softer than the surrounding regions so that on further fatiguing slip is localized near or within the slip band. The critical temperature for the intermediate heating, above which the annealing occurs, is approximately 180°K. The results are attributed to point defect hardening during the annealing treatment.

§ 1. Introduction

McCammon and Rosenberg (1957) have found a marked temperature-dependence of the fatigue life of metals. They reported that the stresses required to fracture copper in 2×10^6 cycles at 293, 90, 20 and 4·2°K were 1·2, 1·75, 2·4 and $2{\cdot}55 \times 10^9$ dynes cm^{-2} respectively. It is well known that in fatigue large slip movements to and fro are localized in slip bands and that eventually fatigue cracks are formed in these bands. The temperature-dependence of fatigue life is probably related to the changes with temperature of the ease of formation of slip bands and the amount of slip in each band. In an investigation into the appearance of slip bands formed at different temperatures (Hull 1958) it was observed that slip bands became finer and more closely spaced as the temperature of fatiguing was decreased. Closer study of the difference in the number of slip bands in specimens fatigued at 293 and 90°K, after different lengths of time, indicated that some changes occurred in the slip bands when specimens fatigued at 90°K were heated to 293°K for examination. It was found that fewer slip bands formed on subsequent fatiguing at 90°K than were expected. This effect has now been examined in detail and the results are described here.

§ 2. Experimental

The fatigue tests were made in the apparatus used by McCammon and Rosenberg (1955). Specimens of O.F.H.C. copper, approximately

---

† Communicated by Dr. A. H. Cottrell, F.R.S.

1/32 in. thick, were shaped as shown in the figure (*a*). The specimens were annealed at 600°c for 4 hours *in vacuo* and then electropolished before fatiguing.

The number of slip bands formed on the specimen after fatiguing was measured by determining the distribution of slip bands over the whole specimen. Counts were made of the number of slip bands in one quadrant of the eyepiece of an optical microscope (magnification × 500, area of one quadrant 3×10^{-4} cm^2). This was scanned over the specimen in the way illustrated in the figure (*a*). The average of the three results across the

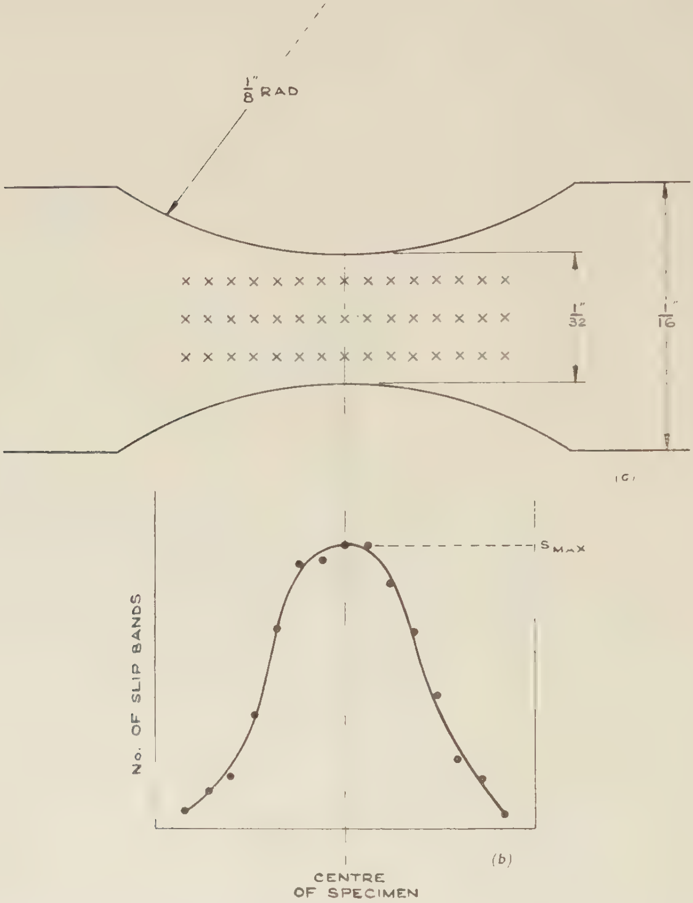

(*a*) Shape of specimen used illustrating the way in which the surface was scanned to determine the slip band distribution. The number of slip bands was counted in the microscope at all the points marked (X).

(*b*) A typical slip band distribution curve of a fatigued specimen.

specimen was plotted against the length of the specimen. The figure (*b*) is a typical distribution of slip bands. The value $S_{\max}$, marked in the figure (*b*), was taken as a measure of the number of slip bands formed.

The specimens were fatigued at 293 and 90°K. After fatiguing at 90°K for 10^4 cycles some specimens were annealed at temperatures between 293 and 140°K and then refatigued for a further 2×10^4 cycles at 90°K. The annealing was carried out by immersing the specimens in a bath of precooled acetone. The temperature could be kept constant to within 3 degrees for over an hour. The specimens had to be removed from the fatigue apparatus for examination, but could be replaced without distortion. All the annealing treatments, except those at 293°K, were made *in situ*.

§ 3. Results

The O.F.H.C. copper used in the present work showed the same dependence of fatigue life on temperature as the H.C. copper used by McCammon and Rosenberg, but the actual fatigue curves were slightly lower. For a life of 2×10^6 cycles the stresses required for failure at 293, 90, 20 and 4·2°K were 1·0, 1·6, 2·2 and $2{\cdot}4\times10^9$ dynes cm^{-2}; when these same stresses were applied in unidirectional tension, then $1{\cdot}0\times10^9$ dynes cm^{-2} produced an extension of 1·9% at 293°K, $1{\cdot}6\times10^9$ dynes cm^{-2} an extension of 5·3% at 90°K and $2{\cdot}2\times10^9$ dynes cm^{-2} gave an extension of 8% at 20°K.

When a specimen was fatigued at 293°K at a stress of $1{\cdot}0\times10^9$ dynes cm^{-2} for 10^4, 3×10^4 and 10^5 cycles the value of $S_{\max}$ increased progressively as shown in the table. This was repeated at 90°K with a stress of $1{\cdot}6\times10^9$ dynes cm^{-2}, but in this case the specimen had to be warmed to room temperature to be examined after each fatigue (i.e. after 10^4, 3×10^4 and 10^5 cycles) and then recooled. The table shows that after 10^4 cycles at 90°K many more slip bands have been formed than with an equivalent stress at 293°K. After 3×10^4 and 10^5 cycles there were more slip bands, but the differences are less pronounced. To avoid the effect of heating the specimens to room temperature at intermediate stages of the fatigue test for examination, three separate specimens were fatigued at 90°K for 10^4, 3×10^4 and 10^5 cycles respectively. The increase in $S_{\max}$ (see table) are quite different from the increases that occur with intermediate heating; the interruption of the fatiguing for room temperature examination has resulted in a marked decrease in the number of slip bands formed subsequently. The changes are due probably to a thermally activated process. To determine the temperature range in which this occurs a number of specimens were fatigued at 90°K for 10^4 cycles and then annealed at temperatures between 190 and 140°K for one hour, followed by a further fatigue of 2×10^4 cycles at 90°K. The results which are summarized in the table show that for annealing temperatures below 167°K, the value of $S_{\max}$ is approximately the same as for specimens given 3×10^4 cycles without an anneal. For annealing temperatures above 190°K $S_{\max}$ is approximately the same as for specimens heated to 293°K. The annealing effect occurs, therefore, between 167 and 190°K. Annealing at 393°K has the same effect as an anneal at 293°K.

The intermediate annealing of specimens fatigued at 90°K also affects the thickness of the slip band formed. At room temperature, fatigue produces a few broad slip bands which gradually thicken by formation of further slip steps adjacent to the band. A number of new bands are formed between these broad bands. At 90°K a large number of fine bands are formed and there is more emphasis on formation of new bands than on thickening of existing bands. However, if the specimen is warmed to 293°K after fatiguing at 90°K further fatigue at 90°K causes the existing bands to thicken.

Values of $S_{\max}$ After Different Fatigue and Annealing Treatments

Number of cycles	10^4	3×10^4	10^5
Fatigue at 293°K	5	13	26
Fatigue at 90°K on one specimen warming to 293°K for examination between each fatigue period	19	26	35
Fatigue at 90°K using three different specimens, one for each fatigue period	19	66	~90
Fatigue at 90°K to 10^4 cycles. Anneal at 148°K and then fatigue to 3×10^4 cycles	—	65	—
As above. Anneal at 157°K	—	68	—
As above. Anneal at 167°K	—	69	—
As above. Anneal at 190°K	—	31	—
Fatigue at 90°K on one specimen heating to 393°K between each fatigue period and then examining	20	26	36

§ 4. DISCUSSION

Comparing the effect of increasing the length of the fatigue test on the number of slip bands formed, we see that at 293°K a relatively small number of bands form and that these become broader and increase in numbers slowly. At 90°K a larger number of bands form which do not broaden appreciably, and new bands form between the existing bands. The essential difference appears to be that at 293°K further slip can occur close to existing bands throughout the test, but at 90°K the bands rapidly become resistant to further slip and new bands form between them. The larger number of slip bands formed at 90°K than at 293°K at the beginning of the test (10^4 cycles) is due partially to the larger amount of plastic strain, as shown by the tensile tests, in specimens fatigued at $1{\cdot}6 \times 10^9$ dynes cm^{-2} at 90°K than in specimens fatigued at $1{\cdot}0 \times 10^9$ dynes cm^{-2} at 293°K. The results resemble closely those of Brown (1951) for aluminium. He found that in direct tension many more slip bands were formed at 90°K than at 293°K and 543°K. At the higher temperatures further slip occurred in planes adjacent to the existing bands far more readily than at 90°K. This is most probably due to cross slip which is a thermally activated process occurring when specimens are deformed in the parabolic hardening or Stage III region of the stress–strain curve. More cross slip occurs in the existing slip bands at higher temperatures and so produces broader bands. In the fatigue experiments a constant cyclic stress was applied in a range where cross slip is expected and this may be responsible also for the formation of broader bands at 293°K than at 90°K in this case.

The annealing treatment after fatigue at 90°K effectively makes the existing slip bands softer relative to the surrounding material so that on further fatigue at 90°K slip remains localized in these slip bands. This can be achieved either by hardening the regions between the slip bands, which would produce an overall increase in hardness of the specimen, or by softening the regions close to and within the bands, which would result in softening of the specimen. Broom and Ham (private communication) have recently observed that a specimen fatigued at 90°K and then heated to room temperature had a higher yield stress when extended in tension at 90°K than a specimen which was fatigued at 90°K and extended at 90°K without intermediate heating. The observation indicates that hardening of regions between the slip bands occurs on annealing. The hardening between the slip bands will be an additional effect to cross slip in determining the width of the bands formed at different temperatures. Broom and Ham (1957) reported that more fatigue hardening occurs at 293°K than at 90°K which suggests that slip will be more localized into bands at the higher temperatures.

Electrical resistivity measurements at low temperatures by MacCrone, McCammon and Rosenberg (private communication) show that considerable annealing of the extra resistivity produced by fatiguing copper at 90°K occurs in the region of 170°K. This is in the same temperature range at which the present effects are first observed. Since electrical resistivity is relatively insensitive to dislocation regrouping compared with the rearrangement of point defects (Nowick 1955), it is probable that the annealing effects are due to point defects.

Hardening of regions between the slip bands could result from diffusion of defects in the lattice to free dislocations, thus pinning them. It is unlikely that at temperatures as low as 167–190°K vacancies will move more than a few atomic spaces, but this may be sufficient to take them to dislocations. More complex defects, such as divacancies (Henderson and Koehler 1956), are expected to be more mobile than single vacancies.

In conclusion, the difference in the number and width of slip bands formed at 293 and 90°K is due probably to the larger amounts of cross slip and greater hardening at the higher temperature. The effect of heating to above 167 to 190°K, after fatigue at 90°K, on the number of slip bands formed on subsequent fatigue at 90°K is thought to result from point defect hardening particularly between the existing slip bands.

ACKNOWLEDGMENTS

This work was carried out at the Clarendon Laboratory, Oxford. The author wishes to thank Dr. A. H. Cottrell and Dr. H. M. Rosenberg for encouragement and advice.

REFERENCES

BROWN, A. F., 1951, *J. Inst. Metals*, **80**, 115.
BROOM, T., and HAM, R. K., 1957, *Proc. roy. Soc.* A, **242**, 166.
HENDERSON, J. W., and KOEHLER, J. S., 1956, *Phys. Rev.*, **104**, 626.
HULL, D., 1958, *J. Inst. Metals* (to be published).
MCCAMMON, R. D., and ROSENBERG, H. M., 1955, *Conf. Phys. des Basses Temps, Paris*, P. 482 ; 1957, *Proc. roy. Soc.* A, **242**, 203.
NOWICK, A. S., 1955, *Acta Met.*, **3**, 312.

The Influence of Vacancies upon the Internal Friction of Polycrystalline Copper†

By R. S. BARNES, N. H. HANCOCK and E. C. H. SILK
Atomic Energy Research Establishment, Harwell

[Received February 15, 1958]

ABSTRACT

Neutron irradiation, gamma irradiation and quenching all change the internal friction of pure polycrystalline rods of copper. Only if the rods are initially given an anneal near the melting point for many hours do these three treatments give consistent and similar results, and then the logarithmic decrement is reduced. It is concluded from the results that it is the vacancies introduced by each of the three treatments which pin the dislocation lines by diffusing to them, and that unless the purity of the copper is high their effect can be obscured.

§ 1. INTRODUCTION

The internal friction of pure metals in the kilocycle per second frequency range is drastically reduced, and the Young's Modulus correspondingly increased, by the introduction of small quantities of impurity (Weertman and Salkovitz 1955, Takahashi 1956, Weinig and Machlin 1956). Recently irradiation and quenching have been shown individually to produce a similar reduction in the internal friction and an increase in the Young's Modulus. Electron bombardment of polycrystalline copper at -180°C increases the Young's Modulus, a dose of $4{\cdot}5\times10^{15}$ 1 MeV electrons/cm^2 producing almost the maximum (i.e. complete) change obtainable for large doses, if there is an intervening room temperature anneal (Dieckamp and Sosin 1956). Neutron or gamma irradiation of copper single crystals produces comparable changes in the Young's Modulus with 10^{12} neutrons/cm^2 and 10^{15} gamma photons/cm^2 respectively (Thompson *et al.* 1955, Thompson and Holmes 1956, 1957). The internal friction of gold decreases when it is cooled in air from 900°C (Roswell and Nowick 1957) and the amplitude dependence is reduced. Levy and Metzger (1955) report that after quenching from 640°C, the decrease in the internal friction of aluminium occurs slowly at room temperature.

This paper describes some experiments designed to compare the effect of three different ' treatments '—neutron irradiation, gamma irradiation and quenching upon the internal friction of polycrystalline copper.

---

† Communicated by Dr. A. H. Cottrell, F.R.S.

§ 2. Experimental Method

The apparatus used was essentially the same as that described by Förster (1937). Each sample, in the form of a rod 0·5 cm diameter and 7·5 cm long, was hung horizontally in two cotton stirrups placed 1 cm from each end, i.e. about 0·6 cm outside the nodes when the rod was vibrating in its fundamental mode. One of the cotton stirrups was used to induce the rod to vibrate transversely and the other to detect the oscillations. Calibration of the detection system (consisting of the cotton stirrup, the piezo-electric pick-up, the head amplifier and the main amplifier) enabled the strain amplitude of the rod to be estimated.

The advantage of this apparatus over other types lies in the ease of demounting and replacing rods (sometimes radioactive) with the minimum of deformation. This was an essential requirement as the rods had to be removed from the apparatus either for irradiation or quenching, and carelessness in handling the rods was found to alter their internal friction.

The rods normally have two resonances, up to 100 c/sec apart, which have been ascribed to the maximum and minimum moments of inertia of cross sections of the rod (Russell and Boag 1953). Each rod was always rotated in its stirrups until the amplitude of vibration at one of these frequencies was dominant. The rod was then always measured while so oriented in the stirrups so that this resonance was used. The logarithmic decrement (Δ) was determined by measuring the frequency width of the resonance peak ($\delta\nu$) at half the amplitude at the resonant frequency ($\nu = 3300$ c/s approximately) $\Delta = (\pi/\sqrt{3})(\delta\nu/\nu)$.

§ 3. Experiments

The material used throughout the investigation was Johnson Matthey spectroscopically standardized copper which has a stated impurity content of about 8 parts per million of lead, silver, iron and nickel together, and less than 5 parts per million of other elements spectroscopically detectable. This material was received in the worked state, when it had the values of internal friction almost independent of strain shown as curve (*a*) in fig. 1.

Several rods were annealed *in vacuo* successively for one hour at the temperatures 200, 400, 600, 800 and 1000°c. No appreciable change in the logarithmic decrement occurred until the last of these anneals when the values shown in fig. 1 (*b*) were obtained. These values compare with those for polycrystalline copper used by other workers.

Some preliminary experiments were performed with rods initially annealed for one hour *in vacuo* at 1000°c. It was found that whereas their decrements decreased slightly upon neutron irradiation, both gamma irradiation and quenching produced slight increases in decrement. The results, however, were not consistent from one rod to another. It was thought that the low initial decrement of these rods and the inconsistent results were due to impurities in the copper.

Eventually an annealing procedure was evolved which consistently gave rods with logarithmic decrements higher than that shown as curve (*c*) in fig. 1. This consisted of initially acid etching the rods and then annealing them for 48 hours at 1050°C in a silica tube vacuum furnace. In an attempt to avoid the introduction of impurities the rods were placed upon a rack made of spectrographically pure graphite rods. During the anneal the pressure was maintained at less than 10^{-5} mm of mercury. The rods were allowed to cool slowly with the furnace. The grain size of the copper after this treatment was about 0·3 cm. By performing several high temperature anneals on a given rod it was possible to obtain logarithmic decrements as high as that shown as curve (*d*) in fig. 1.

Fig. 1

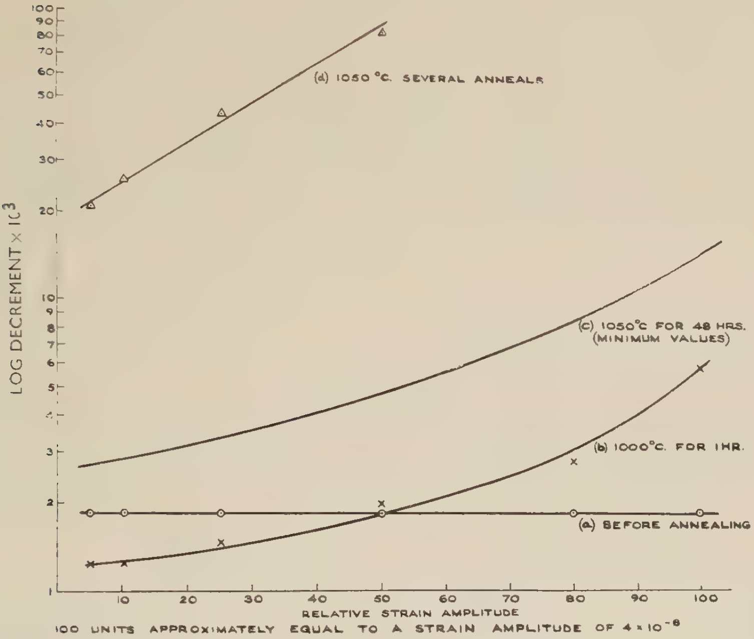

Logarithmic decrement versus strain amplitude for the copper rods before and after various heat treatments.

One rod which had been annealed in this way was etched in stages in dilute nitric acid to two-fifths of its original diameter. After each reduction in diameter the logarithmic decrement was measured. There was no change in the values, suggesting that the internal friction was homogeneous throughout the rod.

Some rods were annealed at temperatures up to 500°C *in vacuo* and slowly cooled. Their values of internal friction were retained.

Rods which had received identical initial anneals giving them high values of logarithmic decrement were irradiated with neutrons or gamma rays or quenched and the effect upon their internal friction compared.

§ 4. Results

Figure 2 shows graphs for three of the polycrystal rods which were used to investigate the effect of neutron irradiation (number 77) gamma irradiation (number 75) and quenching (number 81). For each rod the graphs show, firstly the initial values of logarithmic decrement versus strain amplitude, secondly the final values after the treatment and lastly the values after an anneal for 2 hours at 400°c *in vacuo*. As soon as possible after the irradiation or quenching treatment the rods were replaced in the cotton stirrups and the logarithmic decrement at a low strain amplitude measured at intervals. These values for rod numbers 77 and 75 are plotted

Fig. 2

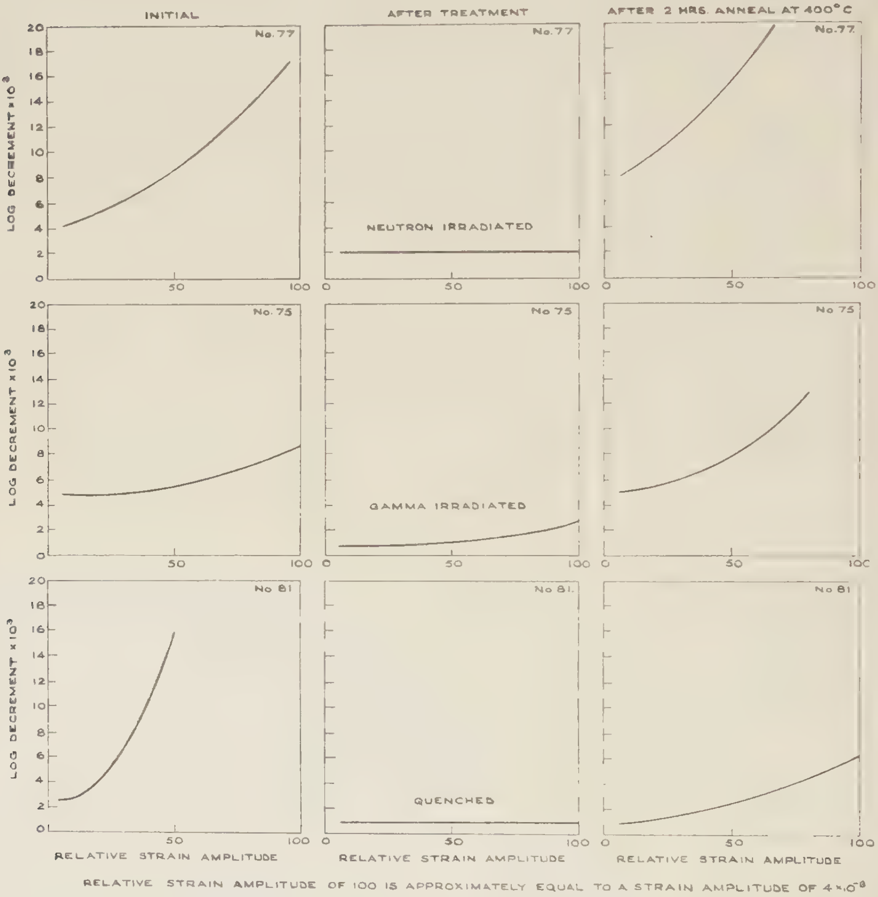

Logarithmic decrement versus strain amplitude for three copper rods number 77 irradiated with neutrons, number 75 irradiated with gamma rays and number 82 quenched.

versus the time after treatment in fig. 3. A similar graph for rod number 55 (quenched to room temperature in silicone fluid from 530°c) is given for comparison.

Fig. 3

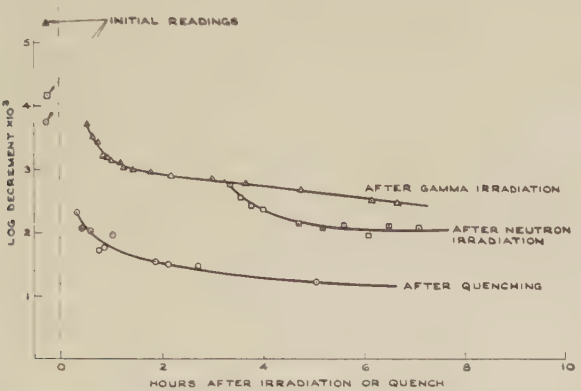

Logarithmic decrement measured at small strain amplitude versus time after (*a*) neutron irradiation (*b*) gamma irradiation and (*c*) quenching.

The individual treatments given the rods were as follows :

Rod Number 77. *Neutron Irradiation*

The rod was gently placed in an aluminium container packed with cotton wool which was then lowered into a vertical hole in BEPO where it was held for 15 minutes and then removed. The rod received a dose of 4×10^{14} thermal neutrons/cm² while still at room temperature (it is assumed that it received an equal dose of fast neutrons); it was not in BEPO long enough to take up the temperature of the reactor (about 60°c).

Rod Number 75. *Gamma Irradiation*

This rod, also carefully packed, was placed 2 cm from a 300 curie ^{60}Co source and left there for 168 hours. It is estimated to have received a dose of 6×10^{16} gamma photons/cm² while at room temperature.

Rod Number 81. *Quenched*

This rod was heated to 1044°c for 8 minutes while held in a molybdenum cage. It was then gently lowered from the furnace to cool for 3 minutes in argon and then in silicone fluid at room temperature.

The critical condition at which each of the three treatments produced a complete decrease in the logarithmic decrement was estimated to be approximately (*a*) a dose of 3×10^{14} fast neutrons/cm²; (*b*) a dose of 10^{17} gamma photons/cm²† and (*c*) a quench in silicone fluid from a temperature of 550°c.

---

† It should be noted that the gamma photon dose given rod 75 (see fig. 2) was less than this critical value and that the minimum value of logarithmic decrement has not been reached.

The temperature at which the logarithmic decrement recovered was determined by performing a series of anneals. Those rods which had received the above critical treatments all recovered at about 400°C. For conditions less than critical, the values recovered at temperatures as low as 100°C, while for conditions above critical the recovery temperature was above 400°C.

§ 5. DISCUSSION

At frequencies above a kilocycle per second the estimated damping due to reorientation effects, thermoelasticity and grain boundary sliding is much smaller than the value which is observed and, since grain boundary sliding is of little importance, single crystal and polycrystalline material of the same purity will have very similar values of logarithmic decrement. The internal friction of metals measured at these frequencies is considered to be due to the motion of dislocation lines within the crystals. The oscillatory motion of these dislocation lines (and hence the internal friction) will be very sensitive to the free length of the dislocation loops, which will normally be less than the distance between dislocation nodes due to the presence of pinning agents along the dislocation line. The breakaway of the dislocations from these pinning agents at large stress amplitudes has been used to explain the marked amplitude dependence of the internal friction which appears above a critical stress amplitude (Nowick 1950, Marx and Koehler 1950, Granato and Lücke 1956). Any discontinuity in the lattice which will attract a dislocation line to it can act as a pinning agent. Thus impurities, interstitial atoms and vacancies can act in this way. For the free length to be greater than 10^{-5} cm the atomic concentration of impurities on dislocation lines must be less than 10^{-8}. Thus, in even the most pure materials, the free length of the dislocation loops will be limited.

The impurities in the copper used initially obscured the effects due to irradiation and quenching presumably because of the heavy pinning by impurity atoms and by their trapping of point defects.

Experiments have shown that an increase in the impurity content increases the critical stress at which the internal friction becomes amplitude dependent and reduces the value of the amplitude independent part (Weertman and Salkovitz 1955, Takahashi 1956). Thus the changes brought about by the high temperature vacuum anneal, i.e. a decrease in the critical stress and raising of the amplitude independent part (see fig. 1) correspond to a *reduction* in the impurity content of the copper.

The curve (*d*) of fig. 1 shows values of the logarithmic decrement at a given strain amplitude comparable with those given for single crystals. The initial values of the internal friction of copper used by various workers have been listed by Kamentsky (1956) who showed that the values of the logarithmic decrement at low strain amplitude range from 7×10^{-6} to $4{\cdot}8 \times 10^{2}$, the higher values being generally associated with single crystals and with the higher purity material. The higher internal friction of single crystal copper is probably due to the removal of some of the impurities from the material by the single pass zone-refining which occurs during the Bridgman method of single crystal growth.

Removal of the surface layers (even to a depth of 0·15 cm), does not alter the logarithmic decrement of a rod. This suggests that any impurity extracted during the high temperature anneal had been removed homogeneously. Thus its diffusion coefficient in copper at 1050°c must be greater than 10^{-7} cm^2/sec. However, spectroscopic analysis before and after the anneal at 1050°c did not detect any change in the metallic impurities. This indicates that the anneal is not reducing the impurity content of the copper but it is possible that the impurities aggregate so that their spacing along dislocation lines is greatly increased.

Retention of the high value of damping during the subsequent anneals at temperatures up to 500°c suggests that the high damping does not result from some unstable configuration of the dislocation lines.

Gamma irradiation and quenching can hardly introduce impurities into the copper rods, and the atomic concentration of zinc introduced by the thermal neutrons is less than 10^{-8}. The internal friction after both neutron and gamma irradiation and subsequent annealing at 400°c is higher than it was initially, which suggests no increase in the impurity content.

The similarity in behaviour of rods which have been quenched to those which have been irradiated indicates that the same process is producing the effect with all three treatments. Dislocation lines could be produced by internal stress during the quench and it has been suggested that neutron bombardment can lead to the introduction of dislocations; however, it is most unlikely that gamma photons could do this. Whereas interstitial atoms and vacancies must be produced in equal numbers by both the irradiation treatments the number of interstitial atoms produced by the quench will be 20 orders of magnitude less. The only fundamental process which is common to all three is the introduction of vacancies.

The internal friction of copper single crystals measured at -195°c was not altered by 15 minutes neutron irradiation while at -195°c. Only after pulse annealing for several hours at 23°c did the internal friction decrease (Barnes and Hancock 1958). This experiment suggested that the number of interstitial atoms produced (which might be expected to be mobile at -195°c) was not modifying the value of internal friction and that whatever agent lowered it could only do so while the temperature was above 0°c.

The movement of vacancies to the dislocation lines can explain the decrease of damping. Vacancies introduced either by quenching or irradiation will diffuse to dislocation lines at room temperature and pin them. The decay of the logarithmic decrement observed at room temperature after the treatments suggests that the vacancies introduced diffuse slowly to the dislocation lines at room temperature.

The atomic concentration of vacancies produced by the critical conditions for each treatment can be estimated. These values are approximately (*a*) 10^{-7} for neutron irradiation, assuming that each primary knock-on produces 100 permanently displaced atoms (*b*) 10^{-7} for gamma irradiation assuming a cross section for the displacement of copper atoms of 1 barn for the gamma photons† and (*c*) 2×10^{-7} for the quench assuming an activation energy of formation of vacancies of 1·1 ev and that all these vacancies are retained during the quench. There is remarkable agreement between these figures, which adds to the evidence that vacancies are responsible for the pinning. These figures suggest that the dislocation damping is greatly reduced only when the atomic concentration of vacancies in the material is about 10^{-7}, i.e. when there is one vacancy for each atomic site along the dislocation lines in the crystal if the density of dislocation lines is $10^8/\text{cm}^2$.

§ 6. CONCLUSIONS

The main source of variation in the logarithmic decrement of different rods appears to be their purity, very high values being associated with pure material. It is essential that very pure material be used if the dislocation pinning behaviour of agents other than impurities is to be studied.

The similarity in the internal friction behaviour, after either neutron irradiation, gamma irradiation, or quenching suggests that the pinning agent produced by all three is vacancies. This view is upheld by the suppression of an internal friction change when irradiated at −195°c and the slow decrease in the decrement observed at room temperature after each treatment.

ACKNOWLEDGMENTS

The authors wish to thank Dr. A. H. Cottrell for helpful discussions and Miss Y. J. Berglin and Mr. D. J. Mazey for their assistance.

REFERENCES

BARNES, R. S., and HANCOCK, N. H., 1958, *Phil. Mag.*, **3,** 527.
DIECKAMP, H., and SOSIN, A., 1956, *J. appl. Phys.*, **27,** 1416.
DUGDALE, R. A., 1955, *Report of Bristol Conference on Defects in Crystalline Solids* (London : Physical Society).
GRANATO, A., and LÜCKE, K., 1956, *J. appl. Phys.*, **27,** 583, 789.
FÖRSTER, F., 1937, *Z. Metalk.*, **29,** 109.
KAMENTSKY, L. A., 1956, *Cornell Univ. tech Rep.*, AFOSR–TN–56–425.
LEVY, M., and METZGER, M., 1955, *Phil. Mag.*, **46,** 1021.
MARX, S., and KOEHLER, J. S., 1950, *Pittsburg Symposium on the Plastic Deformation of Crystalline Solids* (Washington : Office of Naval Research), p.171.
NOWICK, A. S., 1950, *Pittsburg Symposium on the Plastic Deformation of Crystalline Solids* (Washington : Office of Naval Research).
RUSSELL, M. C. B., and BOAG, J. C., 1953, *A.E.R.E.*, EL/M77.
ROSWELL, A. E., and NOWICK, A. S., 1957, *Acta Met.*, **5,** 228.
TAKAHASHI, S., 1956, *J. Phys. Soc. Japan*, **11,** 1253.
THOMPSON, D. C., and HOLMES, D. K., 1956, *J. appl. Phys.*, **27,** 713 ; 1957, *J. Phys. Chem. Solids*, **1,** 275.
THOMPSON, D. C., HOLMES, D. K., and BLEWITT, T. H., 1955, *J. appl. Phys.*, **26,** 1188.
WEINIG, S., and MACHLIN, E. S., 1956, *J. appl. Phys.*, **27,** 734.
WEERTMAN, J., and SALKOVITZ, E. L., 1955, *Acta Met.*, **3,** 1.

---

† The 1·1 and 1·3 MEV gamma photons from the decay of cobalt-60 produce electrons by Compton collisions each able to displace a copper atom (Dugdale 1955).

The Effects of Neutron Irradiation upon the Internal Friction of Copper Single Crystals at Liquid Nitrogen Temperatures†

By R. S. Barnes and N. H. Hancock
Atomic Energy Research Establishment, Harwell, Berkshire

[Received February 15, 1958]

Abstract

The internal friction of copper single crystals remains unaffected by a short neutron bombardment at −195°c if no warning is allowed before measurement. Successive pulse anneals produce no marked change until 23°c is reached, when the internal friction is greatly reduced.

§ 1. Introduction

The internal friction of metals normally decreases rapidly during neutron bombardment at room temperature, the fast neutron dose associated with 10^{15} thermal neutrons cm^2 in BEPO being sufficient to complete the change in polycrystalline copper (Barnes *et al.* 1958). Thompson *et al.* (1957) have recently reported that the internal friction of a copper single crystal is reduced during irradiation, even at about 21°K, but at this temperature the change was not completed after a dose of 2×10^{15} fast neutrons/cm^2. An experiment designed to investigate the annealing behaviour of copper single crystals after neutron irradiation at liquid nitrogen temperature, is described here.

§ 2. Experimental Details

The two single crystals (referred to as crystals 1 and 2) were grown by the Bridgman technique from Johnson Matthey spectroscopically standardized copper and were 8·5 cm long and 0·5 cm in diameter. Their internal friction was measured using an apparatus essentially the same as that described by Förster (1937) and shown in block diagram form in fig. 1. The single crystal rod was suspended horizontally by two cotton threads tied permanently near to each end. One of these cottons was used to induce the rod to vibrate transversely and the other to detect the oscillations. Measurements at −195°c were made by surrounding the crystal and its supporting threads in a metal jacket, that part of the jacket around the crystal itself being immersed in liquid nitrogen. The jacket was evacuated to avoid ice formation on the rod and threads, and to prevent the condensation of atmospheric oxygen. The logarithmic decrement (Δ) was determined by oscillating the crystal in its fundamental mode and measuring the frequency width of the resonance peak $\delta\nu$ at half the amplitude at the resonant frequency ν, $\Delta = (\pi/\sqrt{3})(\delta\nu/\nu)$. The strain amplitude of the crystal during oscillation was estimated by calibrating the detection system (consisting of the thread, the piezo-electric crystal pick-up, the head amplifier, and the main amplifier).

---

† Communicated by Dr. A. H. Cottrell, F.R.S.

Fig. 1

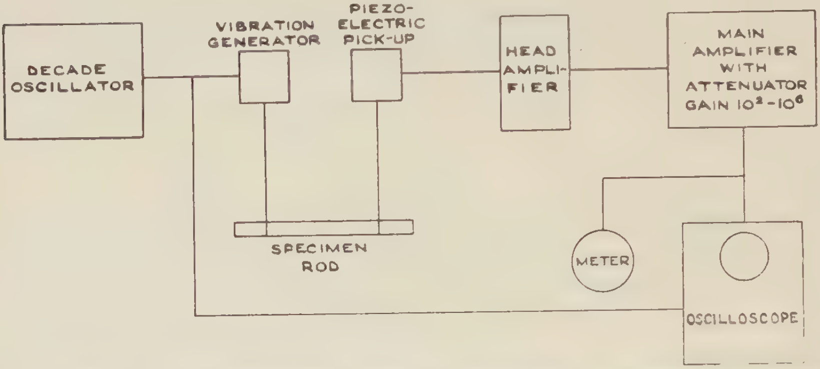

Block diagram of the apparatus used to measure the internal friction and Young's modulus of the single crystal rods.

The logarithmic decrements of both crystals were measured at room temperature at various strain amplitudes up to about 10^{-7}. Crystal 1 was then deformed in torsion (maximum strain 2×10^{-2}) and remeasured after several days when the values had stabilized. After measuring the logarithmic decrement of both crystals at -195°C they were gently transferred by their attached threads into a Dewar flask where they were completely immersed in liquid nitrogen. This flask was gently lowered into a vertical hole in BEPO (measured thermal neutron flux $1\cdot2\times10^{12}$ cm^2 sec) and held there for 15 minutes. It was left for several hours after removal to allow the radioactivity to decay. Crystal 1 was then quickly transferred from the flask back into the measuring apparatus which had already been cooled with liquid nitrogen. To prevent the crystal heating during this transfer, a loosely fitting aluminium tube had been placed around it before the first measurement; the suspending threads passing through two holes in the tube. The logarithmic decrement at -195°C was measured again and remeasured after each of several pulse anneals, the final of these being at room temperature (23°C) when values were also measured during the anneal. Crystal 2, which had meanwhile been kept immersed in liquid nitrogen, was then similarly treated.

§ 3. RESULTS

The results of the measurements on crystals 1 and 2 are given in figs. 2 and 3 respectively.

The final values measured at room temperature after irradiation at -195°C (see figs. 2 and 3) are comparable with those obtained after neutron irradiation of a crystal to the same dose at room temperature. Tables 1 and 2 show that the logarithmic decrement measured at -195°C decreases appreciably only after the anneal at room temperature.

Fig. 2

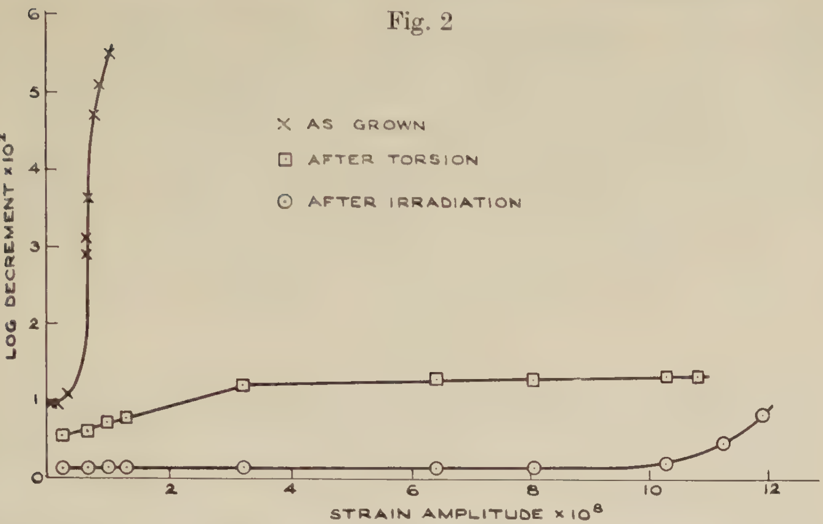

Logarithmic decrement at various strain amplitudes measured at room temperature for crystal 1.

Fig. 3

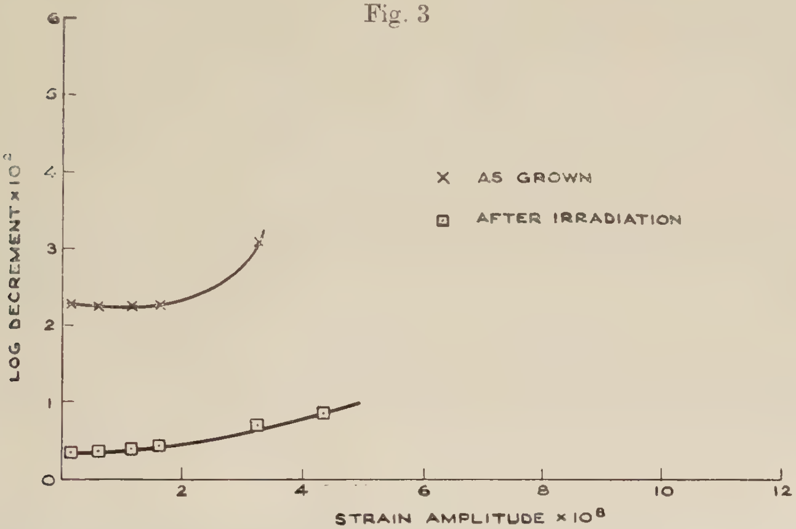

Logarithmic decrement at various strain amplitudes measured at room temperature for crystal 2.

Table 1. Table of the Logarithmic Decrements Extrapolated to Zero Strain Amplitude Measured after the Sequence of Anneals for Crystal 1

Temperature of measurement °c	Logarithmic decrement × 10^3						
	As grown	After torsion	After irradiation	After 1 hour at −114°c	After 1 hour at −60°c	After $1\frac{1}{3}$ hours at 0°c	After 20 hours at 23°c
23	9·5	5·5	—	—	—	—	1·5
−195	2·5	2·0	2·0	2·0	2·0	2·0	1·0

Table 2. Table of the Logarithmic Decrements Extrapolated to Zero Strain Amplitude Measured after the Sequence of Anneals for Crystal 2

Temperature of measurement °c	Logarithmic decrement × 10^3					
	As grown	After irradiation	After 1 hour at −98°c	After 22 min at −60°c	After 20 min at 0°c	After 113 min at 23°c
23	22·5	—	—	—	—	3·5
−195	3·5	3·1	3·4	4·2	4·2	2·5

§ 3. Discussion

These results are similar to that of Dieckamp and Sosin (1956) who found that a room temperature anneal could complete a Young's Modulus change in copper that was begun by electron bombardment at −180°c.

It is generally accepted that the internal friction measured in the kilocycle per second frequency range is due to the oscillatory motion of dislocations lines and that it is drastically reduced by the introduction of pinning agents along the dislocation lines. That the damping is not appreciably affected by the fast neutron dose associated with 10^{15} thermal neutrons/cm^2 at −195°c, suggests that insufficient extra pinning points are introduced. As interstitial atoms are thought to be mobile at −195°c they must either have little ability to pin dislocation lines which seems unlikely, or they very rarely reach the dislocation lines. The latter would occur if they precipitate as platelets in the crystal, or are trapped at impurities; as crowdions perhaps (Lomer and Cottrell 1955). However, on warming to a temperature greater than about 0°c the internal friction is reduced, suggesting that the dislocation lines become heavily pinned. This temperature range is that in which vacancies are thought to be mobile in copper (Broom and Ham 1957) which suggests that vacancies move to the dislocation lines at these temperatures and pin them. The experiment thus supplies evidence that vacancies are the important pinning agents introduced during the irradiation.

References

Barnes, R. S., Hancock, N. H., and Silk, E. C. H., 1958, *Phil. Mag.*, **3**, 519.
Broom, T., and Ham, R. K., 1957, *Symposium on Vacancies and Other Point Defects in Metals and Alloys* (London : Institute of Metals).
Dieckamp, H., and Sosin, A., 1956, *J. appl. Phys.*, **27**, 1416.
Förster, F., 1937, *Z. Metall.*, **23**, 109.
Lomer, W. M., and Cottrell, A. H., 1955, *Phil. Mag.*, **46**, 711.
Thompson, D. O., Blewitt, T. H., and Holmes, D. K., 1957, *J. appl. Phys.*, **28**, 742.

Direct Observation of the Strain Field Produced by Coherent Precipitated Particles in an Age-Hardened Alloy†

By R. B. Nicholson and J. Nutting
Department of Metallurgy, Cambridge University

[Received February 23, 1958]

Abstract

Transmission electron micrographs of aged aluminium 4%-copper foils have shown unusual contrast near precipitated particles. This is interpreted in terms of Bragg diffraction from regions distorted by elastic coherency strains between the precipitate and the matrix.

The first phase precipitated when a supersaturated solid solution decomposes is usually coherent with the matrix, i.e. there is complete continuity between the atom planes of the precipitate and the matrix. If the normal lattice parameters of the two phases are not equal, high elastic strains may be generated near the interface and localized lattice distortion occurs in both the precipitate and the matrix (Nabarro 1940). The strains in the matrix are thought to account for some of the hardening produced by this type of precipitation process.

When a supersaturated solid solution of aluminium 4%-copper is aged at low temperatures the first formed precipitates are discs, one atom thick, of copper aligned on the {100} planes of the aluminium matrix. These discs are known as G.P. [1] zones and their formation brings about hardening of the alloy. At higher ageing temperatures or after longer ageing times G.P. [2] zones form and a further increase in hardness occurs. It is thought that the G.P. [2] zones consist of alternate copper and aluminium rich layers of atoms parallel to the {100} planes of the matrix. The crystal structure of G.P. [2] has been shown to be tetragonal with $a=b=4{\cdot}04$ Å whilst the c parameter varies between 8·0 Å and 7·6 Å depending on the precise heat treatment. When first formed the c parameter of the G.P. [2] zones is 8·0 Å and this changes to 7·6 Å as the zones become larger (Silcock *et al.* 1953). The structure may be considered as two collapsed cubic aluminium unit cells. Both the G.P. [1] and G.P. [2] zones are therefore coherent precipitates.

We have recently observed some unusual contrast effects in the electron optical images from thin foils of an aged Al 4%-Cu alloy, which we believe are a result of coherency strains.

Samples of an Al 4%-Cu alloy, in the form of thin sheets, were solution heat treated and water-quenched to produce a supersaturated solid solution.

---

† Communicated by the Authors.

They were then aged for 16 hr at 130°c to give a structure consisting entirely of G.P. [1] zones and for 5 hr at 160°c to give a structure consisting chiefly of G.P. [2] zones. These are the structures predicted from x-ray diffraction studies on identical specimens by Silcock *et al.* (1953). Thin foils 200 Å to 500 Å thick were prepared from the sample using the technique described by Nicholson *et al.* (1958) and were examined by transmission in the Siemens Elmiskop I operating at 80 kv.

The microstructure observed after the ageing treatment at 160°c is shown in fig. 1, Pl. 22. The G.P. [2] zones form as discs along the {100} planes of the matrix and as the surface of the foil is about (101) the discs parallel to (010) are seen as needles about 20 Å thick and 300 Å long. In this case the precipitate diameter is about equal to the thickness of the foil. Under these circumstances the contrast may arise from two sources: the preferential scattering of the electrons due to the greater mass thickness of the copper rich zones, and Bragg diffraction from the crystal planes of the zone. For this orientation no diffracted beams are collected by the 20 micron aperture of the objective lens and a dark image results. The discs parallel to (100) and (001) are not observed because their resolved thickness in the plane of the incident beam is insufficient to produce either type of contrast. If the foil is appreciably thicker than the precipitate diameter and if the orientation of the foil surface is nearly (001) unusual contrast effects can be obtained by slightly tilting the specimen using the stereo holder. At a critical angle of tilt some of the G.P. [2] zones appear lighter than the matrix, whilst there are dark regions in the matrix adjacent to some of the precipitates. A typical micrograph is shown in fig. 2, Pl. 22.

In other parts of the same grain the regions adjacent to the precipitates appear lighter than the matrix on one side of the precipitate and darker on the other side. This effect is shown in fig. 3, Pl. 23. The extreme sensitivity to orientation and the possible reversal of the contrast indicate that these effects are diffraction phenomena similar to those observed around dislocations in thin metal foils by Hirsch *et al.* (1956). It follows that the aluminium lattice adjacent to the G.P. [2] zone is displaced so that the crystal is no longer perfect.

In view of the results of Silcock *et al.* (1953) on the crystallography of the G.P. [2] zones it may be assumed that the distortion of the matrix lattice planes adjacent to the precipitate is as shown in fig. 4. This requires an induced tetragonality of the face-centred cubic lattice of the matrix in a direction normal to the faces of the G.P. [2] zones.

Using this model, a possible explanation of the unusual contrast effects can be made in terms of double diffraction. Dark field micrographs have shown that in certain orientations the G.P. [2] precipitates give strong diffracted beams. The use of a 20 micron objective aperture makes it impossible for any of the primary diffracted beams to contribute to the bright field image (Menter 1956). However, it has been shown by Pashley *et al.* (1958) that double diffraction by two crystal lattices is possible even when the depth of one of them is only 50 Å. If the depth of the metal foil is greater than the diameter of the precipitate a primary diffracted beam from the aluminium lattice may be diffracted a second time by the G.P. [2] lattice. Alternatively the order of diffraction may be reversed, as this depends solely on whether the precipitate is at the top or bottom of the foil. A simple calculation shows that doubly diffracted beams from any important sets of crystallographic planes will fall inside the objective aperture and will contribute to the bright field image of the precipitate.

Fig. 4

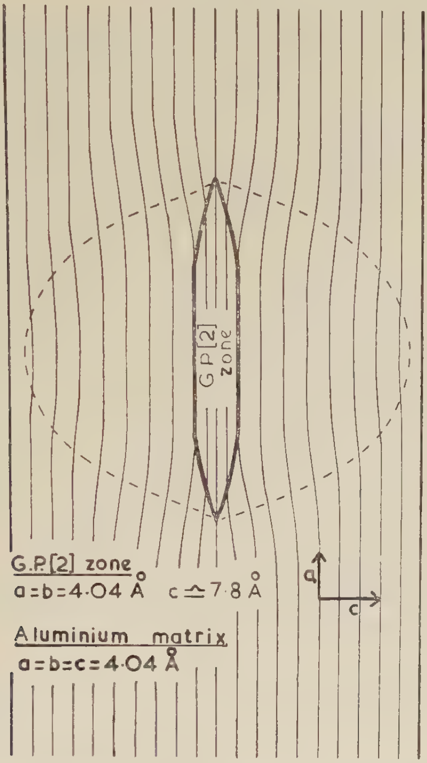

Diagram showing distortion of (100) planes near G.P. [2] zone. The dotted line indicates the approximate extent of the induced tetragonality (not to scale).

It has been found by Pashley *et al.* (1957, 1958) that the doubly diffracted beam may interfere with the undeviated beam to give unusual contrast effects in the bright field image. If there are two infinite diffracting lattices a moiré pattern is produced but it is difficult to predict the precise effect when one of the lattices is in the form of a thin vertical disc as in the present experiments. In fact the precipitates appear black, white or as in a few cases in fig. 2, Pl. 22, a double line of white and black. Thus the contrast probably depends on the exact diffracting conditions arising from the size and relative position of the precipitate.

A similar argument may be advanced to explain the abnormal contrast in the regions of the matrix adjacent to the precipitate. In this case the lattice displacement extends over a comparatively large area, therefore the difference in lattice parameter is very small. If the two lattices were infinite a very large moiré spacing would result and this may explain why the small regions do not show the banded contrast characteristic of moiré patterns. As before these regions may appear dark or light but for reasons which are not fully understood there is sometimes no contrast near a precipitate or contrast on one side only.

So far it has not been possible to obtain direct proof of double diffraction in these foils. The difficulties arise from the weakness of the doubly diffracted beam (due to the very small volume of the foil which is contributing to the beam) and its proximity to the very intense undeviated beam. The angular separation of the two beams is less than 10^{-3} radians. However, indirect proof is provided by two phenomena. No contrast effects are observed when there is only one diffracting lattice, i.e. when the precipitate diameter exceeds the maximum thickness of the foil (about 500 Å), yet at this stage the precipitates are still fully coherent and large local strains would be expected. Secondly the contrast effects always disappear towards the edge of the specimen. An example of this is shown in fig. 5, Pl. 23 where the edge is just beyond the right-hand side of the picture. The mode of preparation of these foils necessarily involves the production of a thin wedge rather than a uniform thin film. This disappearance of the contrast effects in and near the precipitates is again associated with a reduction in foil thickness and the consequent elimination of the two superposed lattices.

If this explanation is correct the contrast effects observed near the precipitates arise from coherency strains induced by the tetragonality of the G.P. [2] structure. The nature of these strains is of considerable importance due to their influence on dislocation movement. With increasing size of the G.P. [2] zones and greater density of precipitation the strain to be accommodated in the matrix becomes larger and eventually the whole of the regions between the precipitates will be strained. This effect is shown in fig. 5, Pl. 23.

The formation of G.P. [1] zones which is associated with the first increase in hardness during the ageing of a supersaturated solid solution should also give rise to small coherency strains. Figure 6, Pl. 24 shows a typical micrograph from the sample aged for 16 hr at 130°C. The G.P. [1] discs can be seen in only one orientation and appear as needles 4 to 6 Å thick and about 80 Å in diameter. The very great density of precipitation leads to strains between the precipitates. The contrast effects produced by these strains can be seen in the micrograph. As in fig. 3, Pl. 23 and fig. 4 the thickness of the foil exceeds the precipitate diameter so that there is also abnormal contrast in some of the G.P. [1] precipitates.

Further experiments to determine the magnitude of the coherency strains associated with the formation of the G.P. zones are in progress and it is hoped to correlate the results with the age-hardening behaviour of this alloy.

ACKNOWLEDGMENTS

The authors would like to thank Professor G. W. Austin, O.B.E., for his interest and encouragement. One of them (R.B.N.) gratefully acknowledges financial support from the Department of Scientific and Industrial Research.

REFERENCES

HIRSCH, P. B., HORNE, R. W., and WHELAN, M. J., 1956, *Phil. Mag.*, **1,** 677.
MENTER, J. W., 1956, *Proc. roy. Soc.* A, **236,** 119.
NABARRO, F. R. N., 1940, *Proc. roy. Soc.* A, **175,** 519.
NICHOLSON, R. B., THOMAS, G., and NUTTING, J., 1958, *Brit. J. appl. Phys.*, **9,** 25.
PASHLEY, D. W., BASSETT, G. A., and MENTER, J. W., 1957, *Nature, Lond.*, **179,** 752 ; 1958, *Proc. roy. Soc.* A (to be published).
SILCOCK, J. M., HEAL, T. J., and HARDY, H. K., 1953, *J. Inst. Met.*, **82,** 239.

CORRESPONDENCE

The Remanent Magnetization of Single Domain Ferromagnetic Particles: II. Mixed Uniaxial and Cubic Anisotropies

By D. G. Tonge and E. P. Wohlfarth
Department of Mathematics, Imperial College, London

[Received February 17, 1958]

In a previous paper (Wohlfarth and Tonge 1957) some theoretical results were obtained for the remanent magnetization of single domain particles having mixed uniaxial anisotropies. This work has now been extended to the problem of the remanence of particles whose anisotropy is made up of a uniaxial and a cubic magnetocrystalline component. This situation arises, for example, in iron particles which have an additional shape or strain anisotropy.

Let the direction cosines of the magnetization vector I_0 be α, β, γ and of the direction of uniaxial anisotropy l, m, n, both referred to the cube axes. Then the total anisotropy energy is

$$E=K(\alpha^2\beta^2+\beta^2\gamma^2+\gamma^2\alpha^2)-s(\alpha l+\beta m+\gamma n)^2, \quad . \quad . \quad . \quad (1)$$

where K, which may be positive or negative, is the usual cubic anisotropy constant, and s the uniaxial anisotropy constant which is here taken positive (negative values have also been considered). The remanence can be calculated from (1) by using the method of Gans (1932). This would necessitate locating the stationary directions of the magnetization vector as dependent on l, m, n and μ, where

$$\mu=s/K, \quad . \quad . \quad . \quad . \quad . \quad . \quad . \quad . \quad . \quad . \quad (2)$$

followed by an averaging process, to give the reduced remanence

$$j_r=I_r/I_0, \quad . \quad . \quad . \quad . \quad . \quad . \quad . \quad . \quad . \quad . \quad (3)$$

as a function of l, m, n, and $|\mu|$. It has been found that the problem of locating these stationary directions is so laborious that its complete solution in the absence of a high speed computer is impracticable. Instead, only special cases of (1) have been considered, and the general case has been discussed qualitatively, leading to a fairly clear understanding of what a complete solution of the problem would give. A summary of the results is given in this note.

When $\mu=0$, (1) leads to 6 or 8 minimum directions for $K+$ or $-$ respectively. As $|\mu|$ increases these minima move towards the direction $[l, m, n]$, and in general they reach this direction only when $|\mu| \to \infty$. It has been found, however, that for values of $|\mu|$ as low as 2 or 3, the angles which the minimum directions make with $[l, m, n]$ are quite small. For the special cases for which the directions $[l, m, n]$ are given by

(A) $[111], K > 0$; (A′) $[111], K < 0$;
(B) $[110], K > 0$; (B′) $[110], K < 0$;
(C) $[100], K > 0$; (C′) $[100], K < 0$;

the number of minimum directions reduces to 2 at finite values of $|\mu|$, μ_c say. These values of μ_c are:

(A)	(A′)	(B)	(B′)	(C)	(C′)
$\frac{2}{3}$	0·22	1	$\frac{2}{3}$	1	1

The case (C′) was considered in one instance (magnetic field applied parallel to [100]) by Akulov (1933), who could not, of course, carry out an averaging process.

The value of j_r is, in general, above $\frac{1}{2}$, but the deviations from $\frac{1}{2}$ will be small when the minimum directions are close to $[l, m, n]$, which, as already stated, happens for $|\mu|$ as low as 2 or 3. For the special cases (A), (A′) . . . (C′) just discussed, $j_r = \frac{1}{2}$ for $|\mu| \geqslant \mu_c$.

Complete calculations of a curve relating j_r with $|\mu|$ are possible without excessive labour only for (C) and (C′), and the results are shown in the figure which also shows μ_c for (A), (A′), (B), (B′).

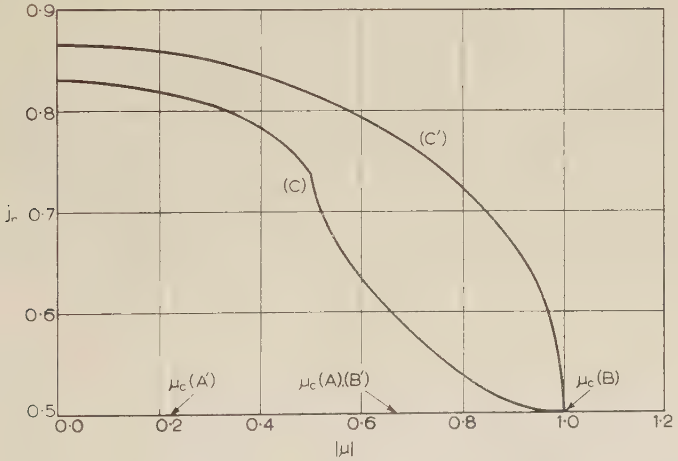

To complete the discussion it would be necessary to average j_r, $|\mu|$ curves over all values of l, m, n. Although this is not at present possible, the above results show that the averaged j_r, $|\mu|$ curve will not deviate appreciably from $\frac{1}{2}$ for values of $|\mu|$ appreciably above 1, which is the point where the coercive forces arising from the cubic and uniaxial anisotropies *separately* are equal.

References

Akulov, N., 1933, *Z. Phys.*, **81**, 790.
Gans, R., 1932, *Ann. Phys., Lpz.*, **15**, 28.
Wohlfarth, E. P., and Tonge, D. G., 1957, *Phil. Mag.*, **2**, 1333.

Grüneisen's Law and the Third Law of Thermodynamics

By Martin J. Klein and Solomon J. Glass
Department of Physics, Case Institute of Technology, Cleveland, Ohio

[Received February 17, 1958]

In one of the many papers (Simon 1951) in which the late Sir Francis Simon explored and clarified the Third Law of Thermodynamics he raised the following question : under what conditions can one prove that the vanishing of the specific heat as T approaches zero implies the Third Law ? Simon himself pointed out that the theorem is true for the ideal quantum gas, and this case has since been discussed in greater detail by Landsberg (1954). The purposes of this note are to show that the theorem is true for another class of systems, those satisfying the Grüneisen equation of state, and to discuss some of the implications of this result.

The Grüneisen equation of state can be written in the form

$$p=-\frac{dU_0}{dV}+\frac{\gamma}{V}(U-U_0) \quad . \quad . \quad . \quad . \quad . \quad . \quad . \quad (1)$$

where p is the pressure, V is the volume, and U is the internal energy of the system. $U_0(V)$ is the internal energy at absolute zero and $\gamma(V)$ is Grüneisen's ' constant ' (see Slater 1939 or Born and Huang 1954).

From (1) it follows immediately that $(\partial p/\partial T)_V$ is equal to $(\gamma/V)(\partial U/\partial T)_V$, i.e. to $\gamma C_V/V$ where C_V is the heat capacity at constant volume. If we express $(\partial p/\partial T)_V$ in terms of the standard quantities β, the volume coefficient of thermal expansion, and κ, the isothermal compressibility, we obtain the result

$$(\partial p/\partial T)_V=\beta/\kappa=\gamma C_V/V \quad . \quad . \quad . \quad . \quad . \quad (2)$$

which is the usual Grüneisen law. Since $(\partial p/\partial T)_V$ is equal to $(\partial S/\partial V)_T$, where S is the entropy, it follows that if, as T approaches zero, C_V approaches zero, then also $(\partial S/\partial V)_T$ must approach zero. In other words for a system obeying Grüneisen's law the vanishing of C_V as T approaches zero implies the Third Law.

The class of systems satisfying the Grüneisen equation of state is certainly non-trivial. It will be satisfied by any collection of harmonic oscillators all of whose frequencies ν depend on volume in the same way, and γ is then $-(d \ln \nu/d \ln V)$ (Slater 1939). More generally Grüneisen's equation will be satisfied by any collection of harmonic oscillators in a crystal regardless of how their frequencies depend on volume, at sufficiently low temperatures and at sufficiently high temperatures (Borns 1923). At intermediate temperatures Barron's theory (1955, 1957) indicates that γ will appear to vary with T from its low temperature limit to its high temperature limit. (The experimental situation here is not clear: Bijl and Pullan (1955) find a pronounced variation in γ for several metals, but their experimental method is questioned by Simmons and Balluffi (1957) who find much less variation.) In any case at sufficiently low temperatures the Grüneisen equation should apply to the crystal lattice, and that is sufficient for Third Law considerations.

In conclusion we may point out that the ideal gas, for which the theorem was previously discussed, also satisfies the Grüneisen relation (2) with a γ equal to 2/3 (Simon 1951). It would be interesting to be able to establish Simon's theorem for systems of more complex character than the ideal gas or ideal crystal lattice.

REFERENCES

BARRON, T. H. K., 1955, *Phil. Mag.*, **46,** 720; 1957, *Ann. of Phys.*, **1,** 77.
BIJL, D., and PULLAN, H., 1955, *Physica*, **21,** 285.
BORN, M., 1923, *Atomtheorie des festen Zustandes* (Leipzig : Teubner).
BORN, M., and HUANG, K., 1954, *The Dynamical Theory of Crystal Lattices* (Oxford : University Press).
LANDSBERG, P. T., 1954, *Phil. Mag.*, **45,** 1129.
SIMMONS, R. O., and BALLUFFI, R. W., 1957, *Phys. Rev.*, **108,** 278.
SIMON, F. E., 1951, *Z. Naturf.*, **6a,** 397.
SLATER, J. C., 1939, *Introduction to Chemical Physics* (New York : McGraw-Hill).

The Evolution of the Extra-galactic Nebulae and the Origin of Meta-galactic Radio Noise

By C. E. R. BRUCE
Electrical Research Association Laboratory, Leatherhead, Surrey

[Received February 12, 1958]

IN their paper ' On the Identification of Radio Sources ', Baade and Minkowski (1954) referring to the ' jet ' in the globular nebula NGC 4486, remark that " no possibility exists at this time of forming any hypothesis on the formation of the jet, the physical state of its material, and the mechanism which connects the existence of the jet with the observed radio emission ". May I point out that many years ago—some years before the recognition of radio astronomy indeed—I put forward a hypothesis which led to the expectation that such ' jets ' would exist in some Type E nebulae (Bruce 1944). The hypothesis was that such extensive atmospheres as exist in globular and elliptical nebulae, and in late type stars, would become the site of radial electric fields, which would increase until breakdown occurs.

Since then I have shown (Bruce 1955 a, b) that a mechanism does exist which will lead to the generation of these electric fields in gaseous atmospheres, namely the charging of dust particles or grains by asymmetrical impacts and the separation of the charged particles in a gravitational field. The necessary grains are known to be present in our own and other galaxies, and to be orientated in a particular direction in any one place as they would be by an electric field.

Applied to the long-period variable stars the theory of electric fields and discharges accounts satisfactorily for the general nature of the outbursts in these stars, the times involved, the nature of the light changes and of the gas movements (Bruce 1956, 1957 a).

It is shown in an E.R.A. Report (Bruce 1957 b) that the discharge hypothesis similarly accounts for many phenomena observed in the extragalactic nebulae, in addition to the 'jet' or discharge channel in NGC 4486, and that there would appear to be sufficient reason to accept the occurrence of electrical discharges to resolve the nebular theoretical impasse, just as it has successively resolved the corresponding impasses on the terrestrial and stellar scales.

REFERENCES

BAADE, W., and MINKOWSKI, R., 1954, *Ap. J.*, **119,** 215.

BRUCE, C. E. R., 1944, *A New Approach in Astrophysics and Cosmogony* (London); 1955 a, *Observatory*, **75,** 82; 1955 b, *Phil. Mag.*, **46,** 1123; 1956, *C.R. Acad. Sci. Paris*, **242,** 2101; 1957 a, *Observatory*, **77,** 107, 153; 1957 b, E.R.A. Report Ref. Z/T 117.

The Small Angle Scattering of High Energy Photons in Uranium

By J. MOFFATT and M. W. STRINGFELLOW
Clarendon Laboratory, Oxford

[Received March 24, 1958]

WE have measured differential cross sections for the scattering of photons of mean energy 90 MEV in uranium through angles ranging from 1·2 to 4·5 milliradians. The X-ray beam from the Oxford synchrotron operating at 110 MEV peak energy was collimated to 2 mm diameter at a distance of 4 m from the machine target. The scattering angle was defined by an annular aperture 8 m from the target. A total absorption Čerenkov counter and biased discriminator were used as a threshold detector for high energy photons. The uranium scatterer, placed immediately behind the 2 mm collimator, was 11·0 g/cm² thick, and electrons produced in the scatterer were removed by a magnetic field. A large background due to scattering by the air near the annular collimator was eliminated by evacuating the space between this collimator and the scatterer, and cosmic ray background was reduced by gating the counter on during the x-ray pulse. The experimental results are shown in the figure.

Inelastic scattering of photons can occur by the Compton effect and by secondary processes such as pair production followed by Bremsstrahlung. The differential Compton cross section is 7·3 barn/steradian and is substantially constant over the small angles investigated. The energy loss of Compton scattered photons is so small that the counter did not discriminate between Compton and elastic scattering. The intrinsic angular distributions of pair production and Bremsstrahlung are narrow enough to give a significant variation in the yield of secondary photons with angle, but, by using a thick scatterer, this variation is reduced to a few per cent over the range of angles of interest in this experiment due to broadening of the distribution by multiple scattering of the pair electrons. The number of secondary photons counted varies very rapidly with discriminator bias, but a rough theoretical estimate gave an effective cross section only slightly greater than the Compton cross section for the bias used.

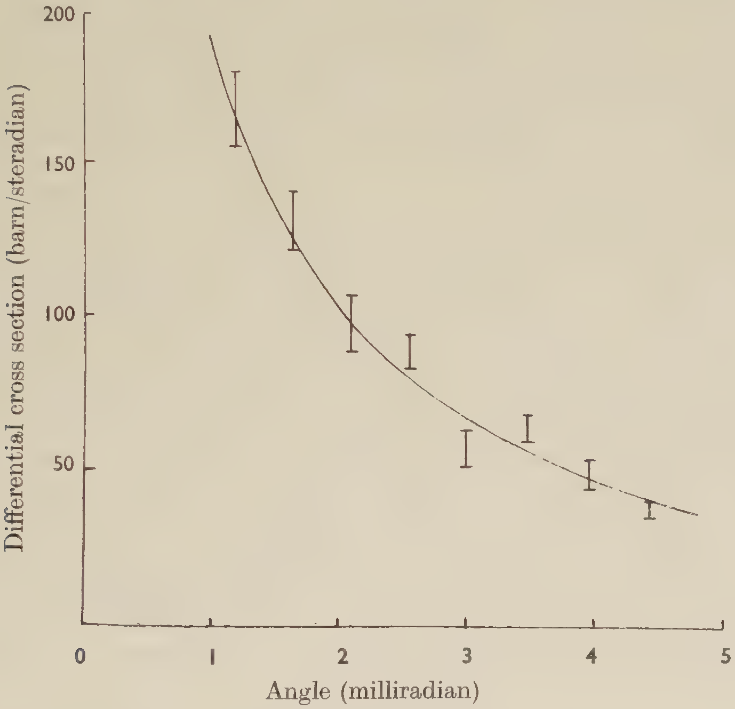

Angular distribution of scattered photons. The full curve is calculated from Bethe and Röhrlich's formula increased by 18 barn/steradian. Probable errors are shown for the experimental data.

The forward peak in the experimental distribution is therefore presumably due to elastic scattering processes. Of these, nuclear Thomson scattering is negligible, probably of the order of 3×10^{-5} barn steradian. There is at present no complete theory of Rayleigh scattering at high energies. However, simple form factor calculations (Franz 1935) lead to a differential cross section of 6 barn/steradian at the smallest angle for which measurements were made. This is more than an order of magnitude smaller than the observed elastic scattering, and it is extremely unlikely that corrections for relativistic effects and binding in the intermediate state could change the cross section to this extent. We conclude therefore that the main contribution to elastic scattering is Delbrück or potential scattering in the Coulomb field of the nucleus.

Although it thus appears that Rayleigh scattering is small compared with Delbrück scattering at 90 MEV, it may still modify the total scattering significantly by interference. However, in the absence of a satisfactory theory of Rayleigh scattering, we have compared the experimental data with calculations of Delbrück scattering alone made by Bethe and Röhrlich (1952). The full curve in the figure shows the calculated cross sections superimposed on a uniform (inelastic) cross section of 18 barn/steradian, chosen to give the best fit to the experimental points. The agreement is within experimental error.

Previous evidence for the existence of Delbrück scattering (e.g. Goldzahl and Eberhard 1957) has been sought by comparing measured scattering cross sections for lead at energies of the order of 1 MEV with calculations of Rayleigh and Thomson scattering. At these energies, Delbrück scattering is small and the uncertainties in the theory of Rayleigh scattering make unambiguous separation of the different elastic processes very difficult. The present results seem to give definite evidence for the existence of Delbrück scattering, and that the calculations of Bethe and Röhrlich are at least approximately correct.

REFERENCES

BETHE, H., and RÖHRLICH, F., 1952, *Phys. Rev.*, **86,** 10.
FRANZ, W., 1935, *Z. Phys.*, **98,** 314.
GOLDZAHL, L., and EBERHARD, P., 1957, *J. Phys. Radium,* **18,** 33.

REVIEWS OF BOOKS

The Exploration of Space by Radio. By R. Hanbury Brown and A. C. B. Lovell. (Chapman and Hall, 1957.) [Pp. 207.] 35*s*.

This is a very good book. It is clearly written, attractively produced, and moderate in price. All branches of radio astronomy are described, including the scintillations of radio stars produced by the terrestrial ionosphere, and radio observations of the aurora. The emphasis is on work carried out at the Jodrell Bank Experimental Station.

The value of the book would be increased by the addition of a full bibliography. In some of the chapters full references are given to the original papers, but in others the author's name only is given. There are a few misprints, and fig. 33 (*a*) is wrongly drawn. These are small points which could easily be put right in a later edition. B. H. B.

Die Photographische Empfindlichkeit. By J. W. Mitchell. (Helwich: Darmstadt.) [Pp. 35.] D.M. 8.40.

The silver halides belong to that class of silver salts which decompose when irradiated with light of the appropriate wavelength. The importance of the silver halides lies in the fact that they are used in photographic emulsions. A theory for the formation of the silver latent image was first proposed by Mott and Gurney and in this article Dr. Mitchell discusses how the Mott–Gurney theory must be modified to bring it into line with the present day experimental evidence. It is now evident that crystal imperfections play a decisive role in the formation of the latent image and this is discussed in relation to crystal growth and optical and chemical sensitization. The present theory of silver formation differs from that proposed by Mott and Gurney in the positions assigned to the energy levels of silver sulphide, latent image specks and visible silver particles relative to the energy bands of the silver halide crystal. On this basis the latent image speck grows by first adsorbing a silver ion which traps a conduction electron during exposure and accepts electrons from reducing molecules during development.

The new theory presented in this excellent review owes much to the work of Dr. Mitchell and his colleagues at Bristol. It describes not only the formation of the latent image but most of the physical and chemical aspects of photographic sensitivity. B. L. E.

The Scientific Papers of Sir Geoffrey Ingram Taylor. Vol. I. Mechanics of Solids. Edited by G. K. Batchelor. (Cambridge: University Press.) [Pp. x+593.] 75*s*.

This fine volume containing the scientific papers of Sir Geoffrey Ingram Taylor on the Mechanics of Solids is a fitting record of his outstanding work on this subject from 1917 until the present day. The Editor, Dr. G. K. Batchelor, and the Cambridge University Press are to be congratulated on its production. N. F. M.

BOOK NOTICES

Games and Decisions. By R. D. LUCE and H. RAIFFA. (London : Chapman & Hall.) [Pp. xi+509.] Price 70*s.*

Proceedings of the Third Midwestern Conference on Solid Mechanics held at the University of Michigan, April 1 *and* 2, 1957. Edited by A. M. KUETHE. (Ann Arbor : University of Michigan Press.) [Pp. vi+250.] Price $5.50.

Proceedings of the Fifth Midwestern Conference on Fluid Mechanics held at the University of Michigan, April 1 *and* 2, 1957. Edited by A. M. KUETHE. (Ann Arbor : University of Michigan Press.) [Pp. viii+388.] Price $8.00.

Combination of Observations. By W. M. SMART. (Cambridge University Press.) [Pp. xiv+253.] Price 35*s.*

Nuclear Masses and their Determination. Proceedings of the Conference held in the Max Planck Institut für Chemie, Mainz, 10–12 July 1956. Edited by H. HINTENBERGER. (London : Pergamon Press.) [Pp. ix+267.] Price 84*s.*

Year Book of the Physical Society 1957. (London : Physical Society.) [Pp. 132.] Free to Members ; price to non-members 12*s.* 6*d.*, postage 7*d.*

Integral Equations. By F. G. TRICOMI. (Pure and Applied Mathematics, Volume V.) (London and New York : Interscience Publishers.) [Pp. viii+238.] Price $7.00.

Differential Equations : Geometric Theory. By S. LEFSCHETZ. (Pure and Applied Mathematics, Volume VI.) (London and New York : Interscience Publishers.) [Pp. x+364.] Price $9.50.

Mécanique Statistique des Fluides. By D. MASSIGNON. (Paris : Dunod.) [Pp. xiv+263.] Price 3,900 frs.

Electronic Theories of Organic Chemistry. By J. W. BAKER. (Oxford : Clarendon Press.) [Pp. vii+224.] Price 30*s.*

[The Editors do not hold themselves responsible for the views expressed by their correspondents.]

Fig. 2

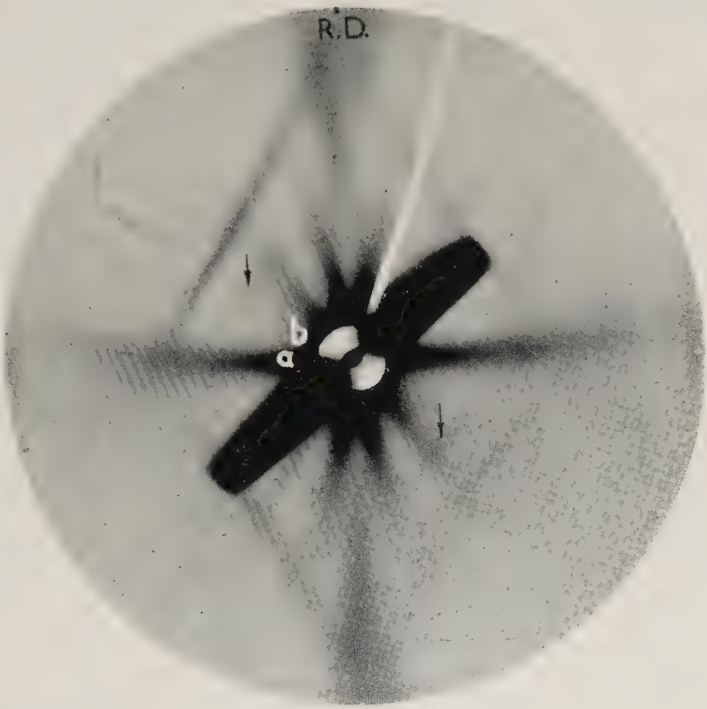
R.D.
b
a

Fig. 8

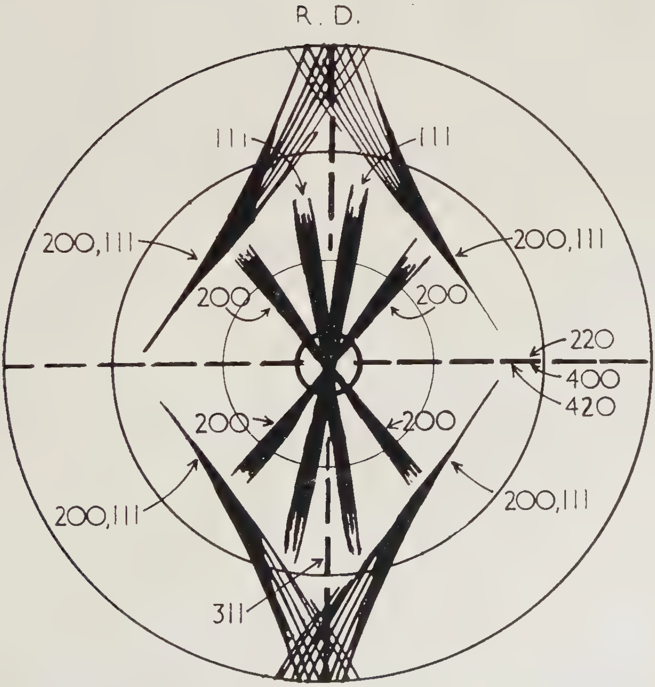
R. D.
111
111
200,111
200,111
200
200
220
400
420
200
200
200,111
200,111
311

Fig. 4

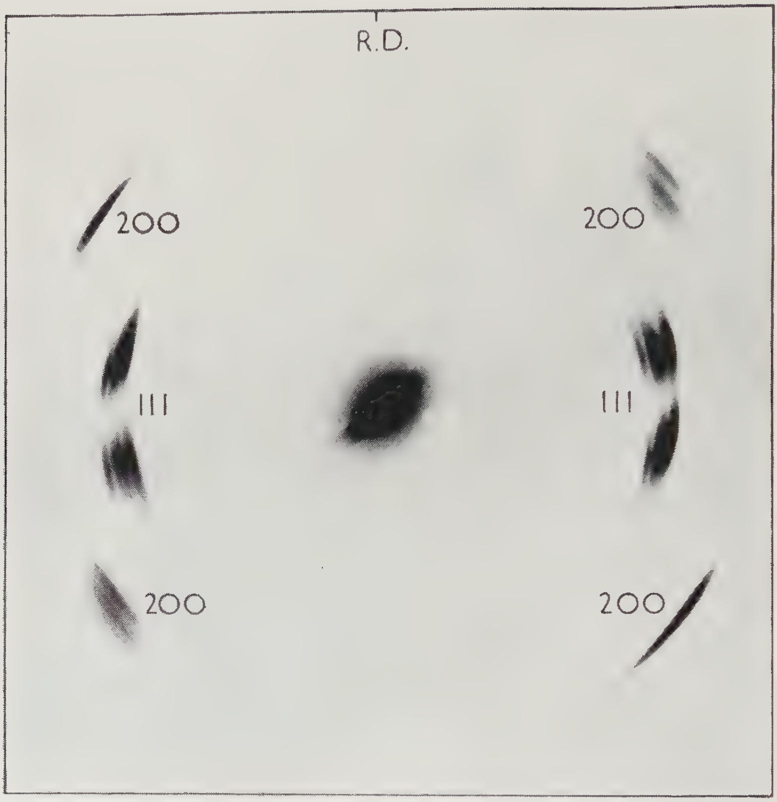

Fig. 5

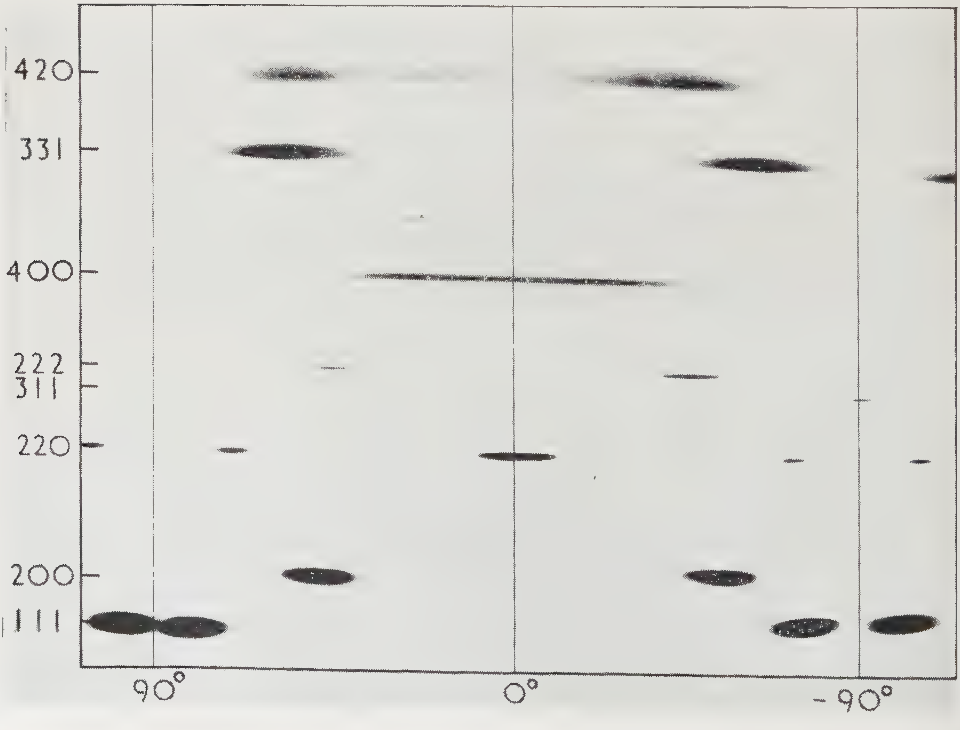

Fig. 9

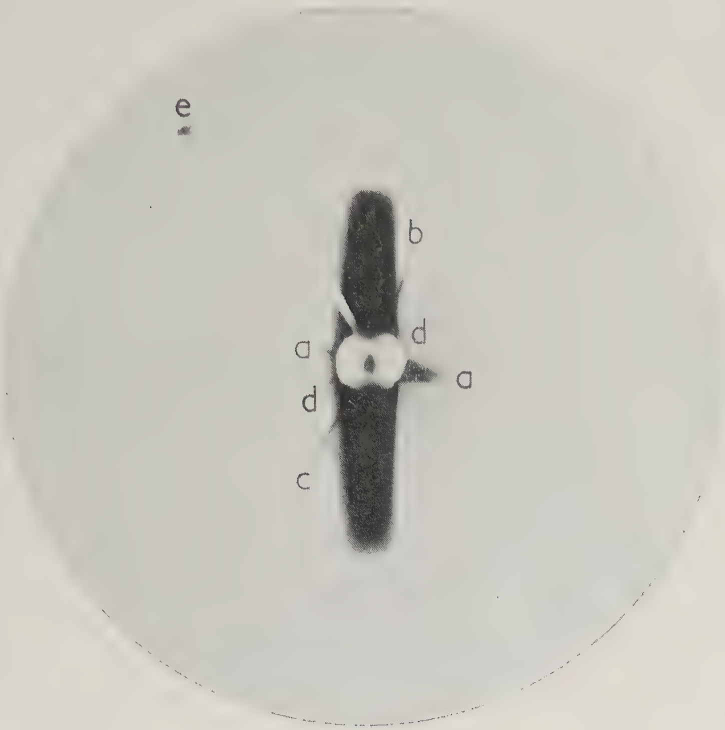

Fig. 10

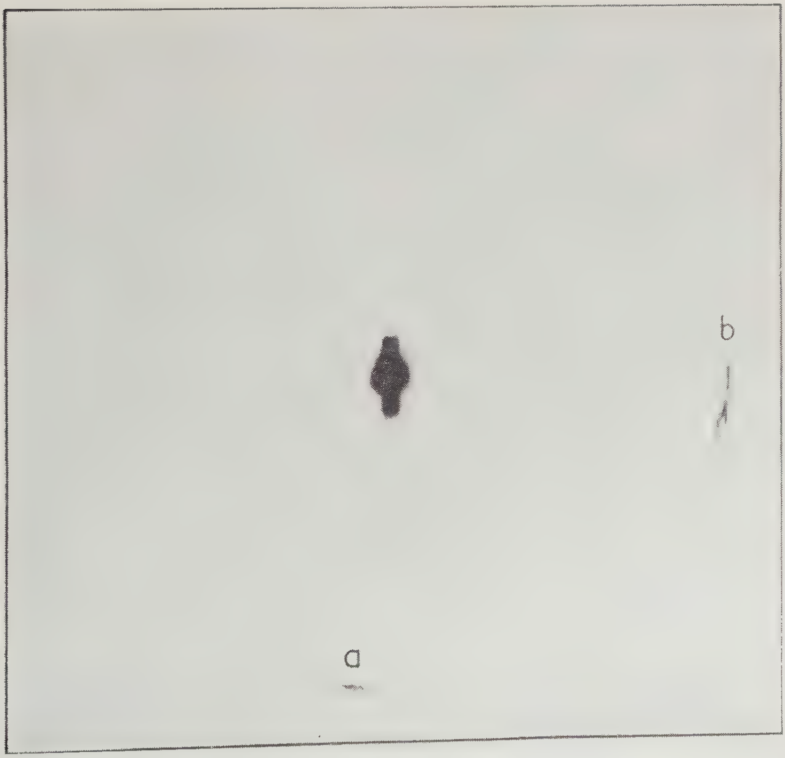

Fig. 11

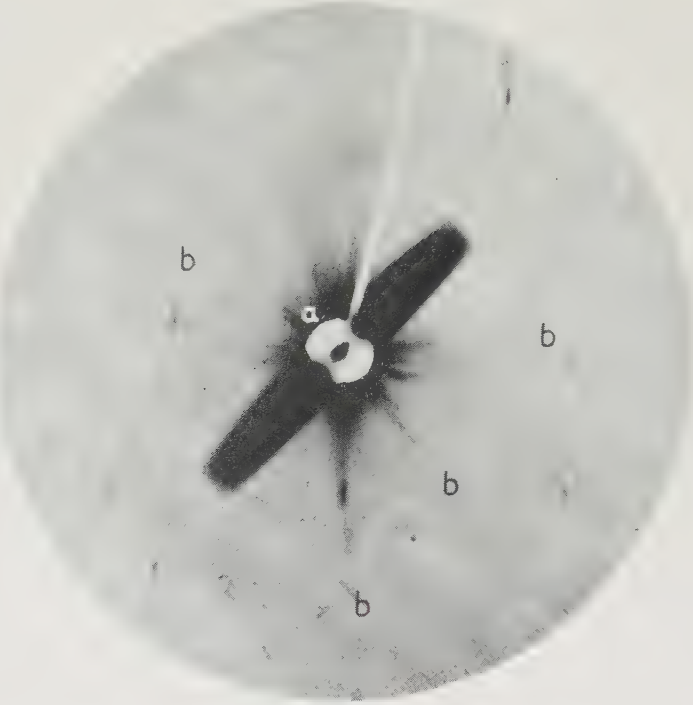

Fig. 12

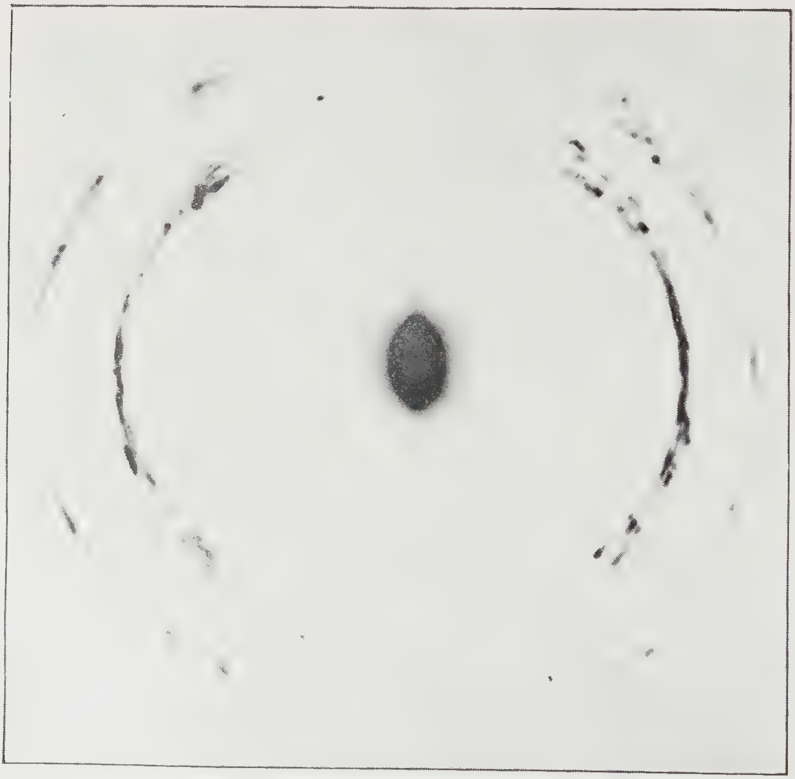

Fig. 13

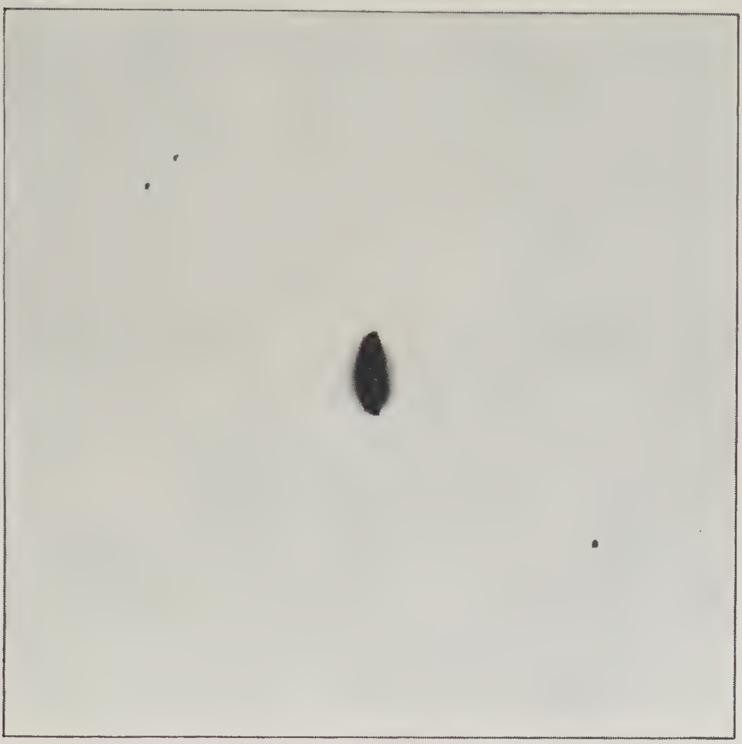

Fig. 14

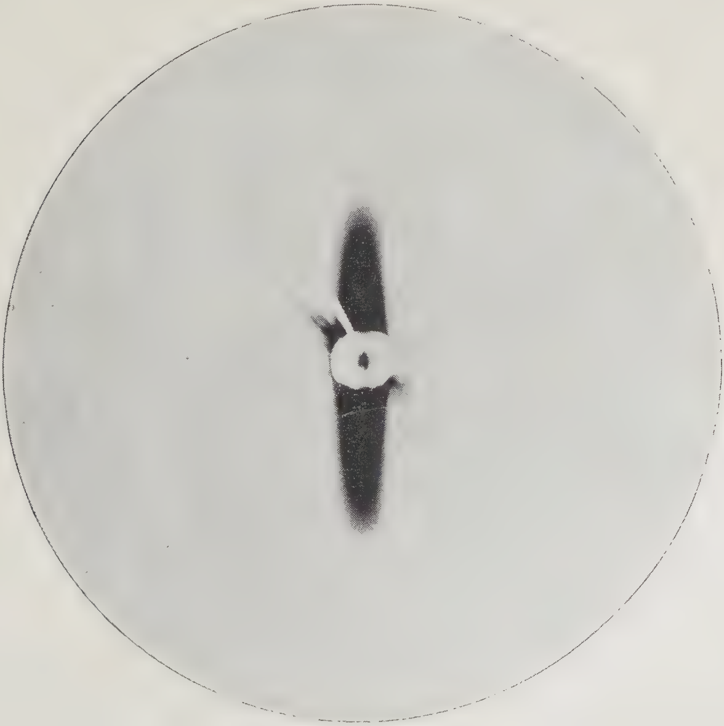

Fig. 15

CAPTIONS TO PLATES

Fig. 2

The small angle scattering from cold rolled commercial copper. The round beam stop, which obscures angles less than 1½°, was removed for ¼ second to expose the direct beam. The beam stop is supported by a wire, the shadow of which can be seen. The large rectangular region has been blackened by parasitic radiation. The arrows indicate the positions of weak streaks due to reflections of the type 222, 311.

Fig. 8

Small angle scattering pattern from cold rolled commercial copper predicted entirely from the pole figures, figs. 6 and 7 (continuous lines) and from fig. 5 (broken lines). The directly measured pattern is shown in fig. 2. The concentric circles represent scattering at 1½° (size of beam stop) 5°, 10°, 15° (largest angle observed).

Fig. 4

Large angle transmission photograph taken in the point focusing instrument showing the strong preferred orientation in the cold rolled commercial copper. The central blackening results from the direct beam, which also causes some spreading of the reflections.

Fig 5.

Bragg reflections from cold rolled commercial copper. The geometry of the photograph is described in § 2.2.1.

Fig. 9

The small angle scattering from a single grain of aluminium deformed 18% in tension.

Fig. 10

Large angle transmission photograph of aluminium deformed in tension (the same specimen as in fig. 9).

Fig. 11

Small angle scattering from fatigued pure copper. The letters ‘ b ’ indicate scattering of the type 200, 111.

Fig. 12

Large angle transmission photograph of fatigued pure copper (the same specimen as in fig. 11).

Fig. 13

Large angle transmission photograph of fatigued commercial copper. The specimen produced no observable small angle scattering.

Fig. 14

Small angle scattering from a single grain of fatigued aluminium.

Fig. 15

Large angle photograph of fatigued aluminium (same specimen as in fig. 14).

Fig. 1

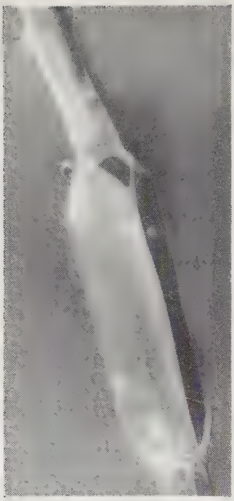

×3000

Fig. 2

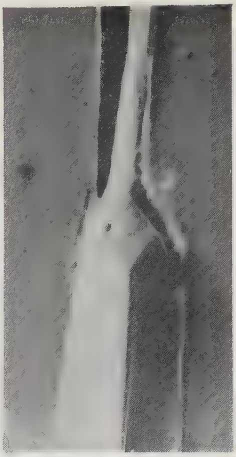

×5000

Fig. 3

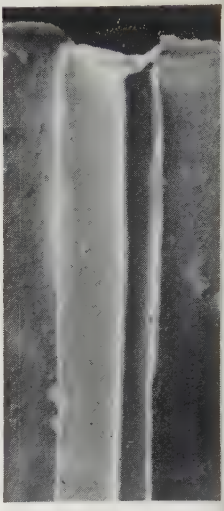

×3700

Fig. 4

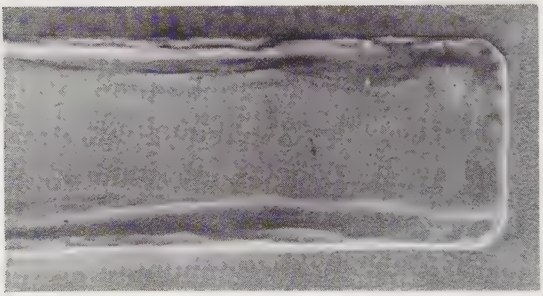

×5000

Fig. 5

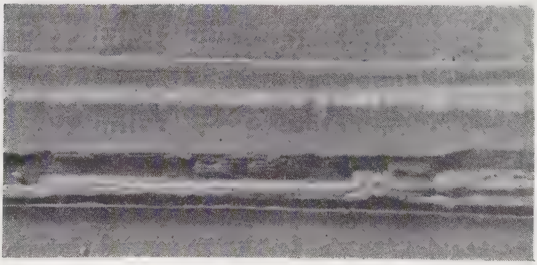

×6600

Fig. 6

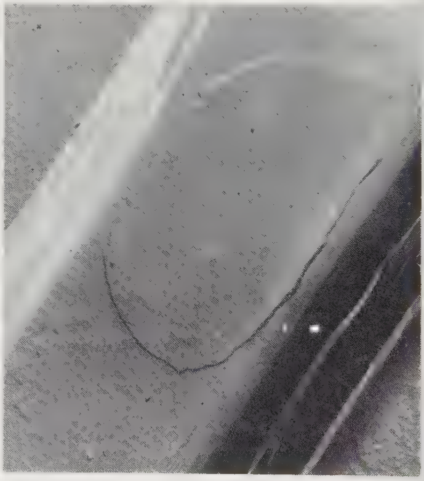

×5100

Figs. 1–6. Carbon replicas of sodium chloride whiskers grown from solution.

Fig. 7

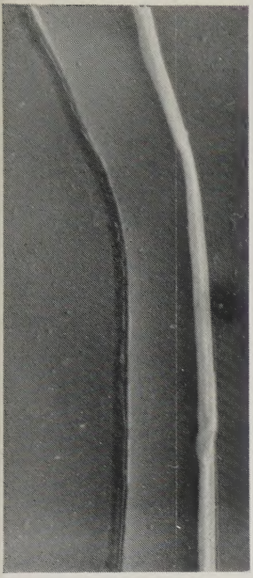

× 5000

Fig. 8

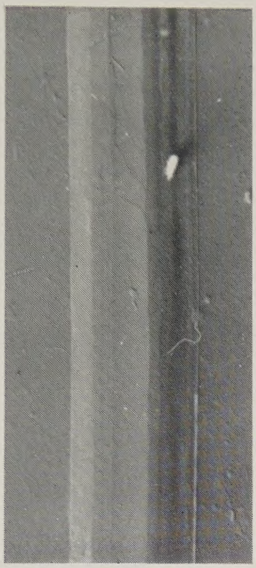

× 8600

Fig. 9

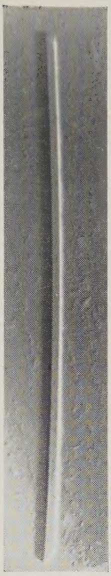

× 4600

Fig. 10

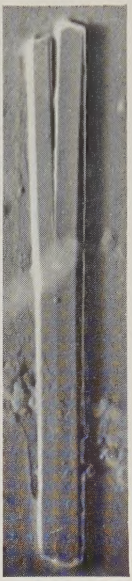

× 10 800

Carbon replicas of potassium chloride whiskers (figs. 7 and 8) and copper sulphate whiskers (figs. 9 and 10).

Fig. 11

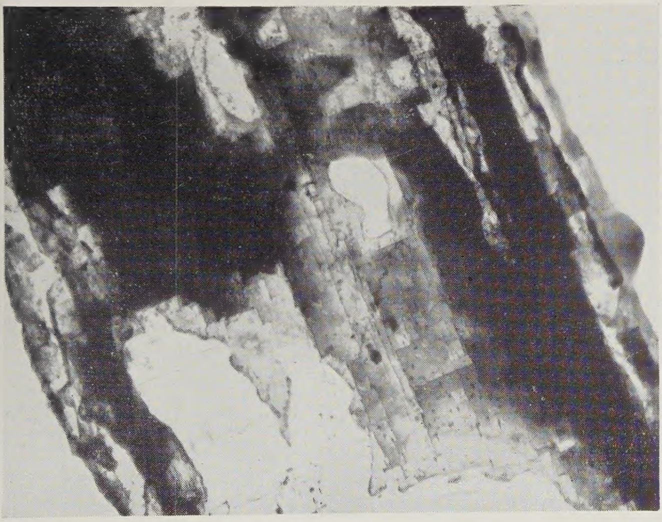

× 12 000

Fig. 12

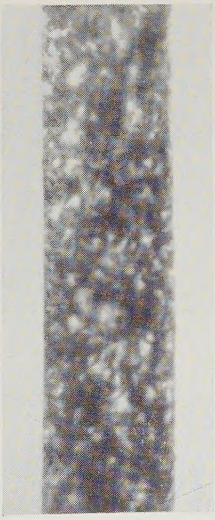

× 77 500

Figures 11 and 12. Direct electron micrographs of sodium chloride whiskers after exposure to the electron beam.

Fig. 1

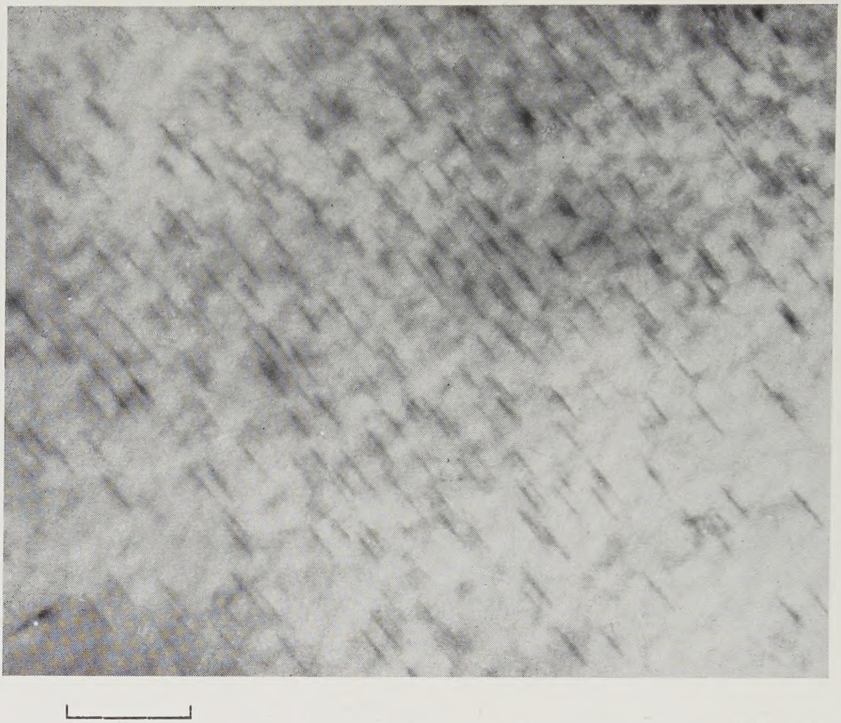

Thin foil Al 4%-Cu aged 5 hr at 160°c. (×160 000.)

Fig. 2

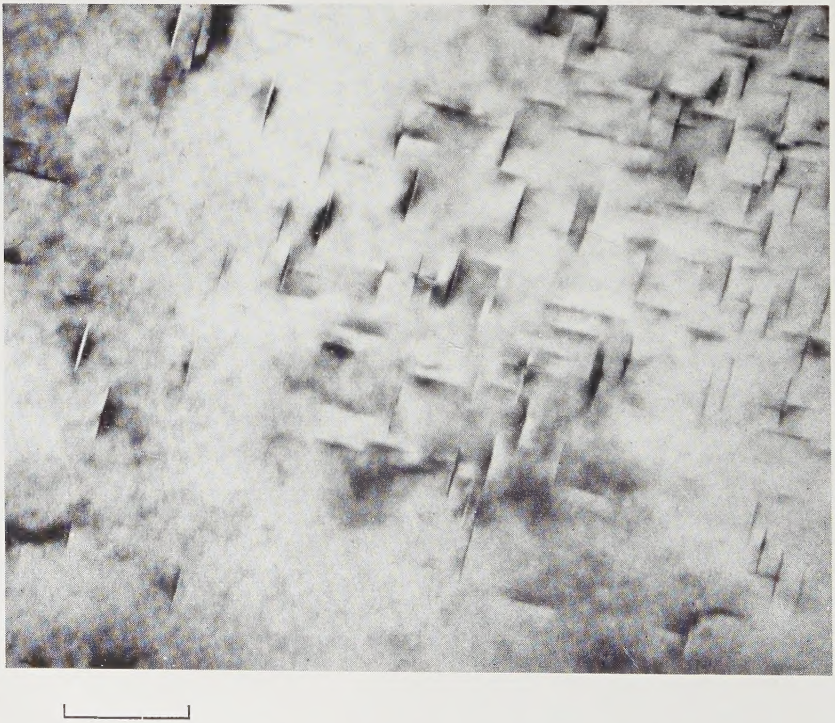

Thin foil Al 4%-Cu aged 5 hr at 160°c. (×160 000.)

Fig. 3

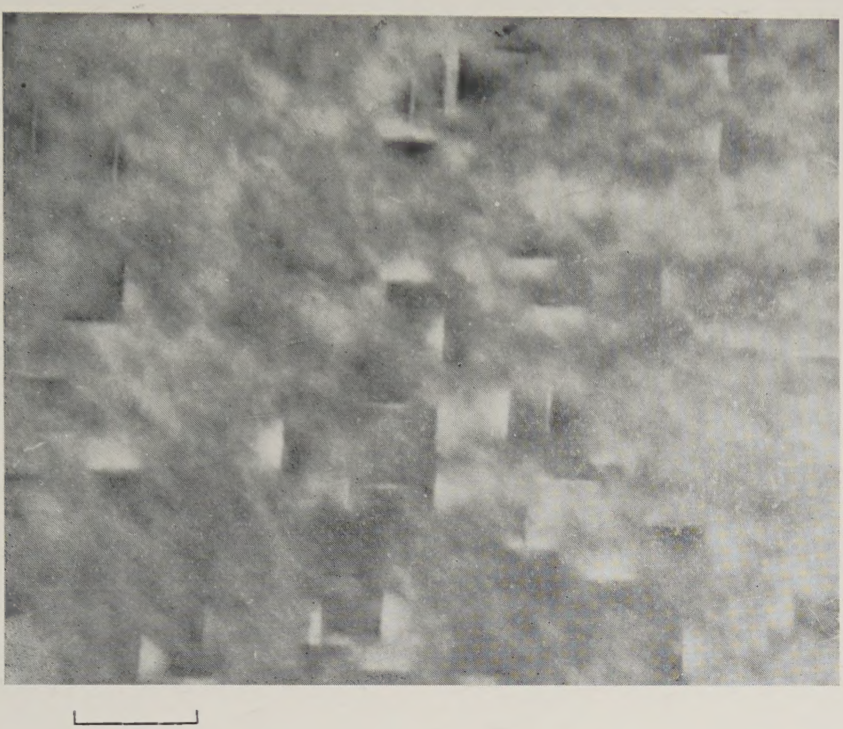

Thin foil Al 4%-Cu aged 5 hr at 160°c. (×160 000.)

Fig. 5

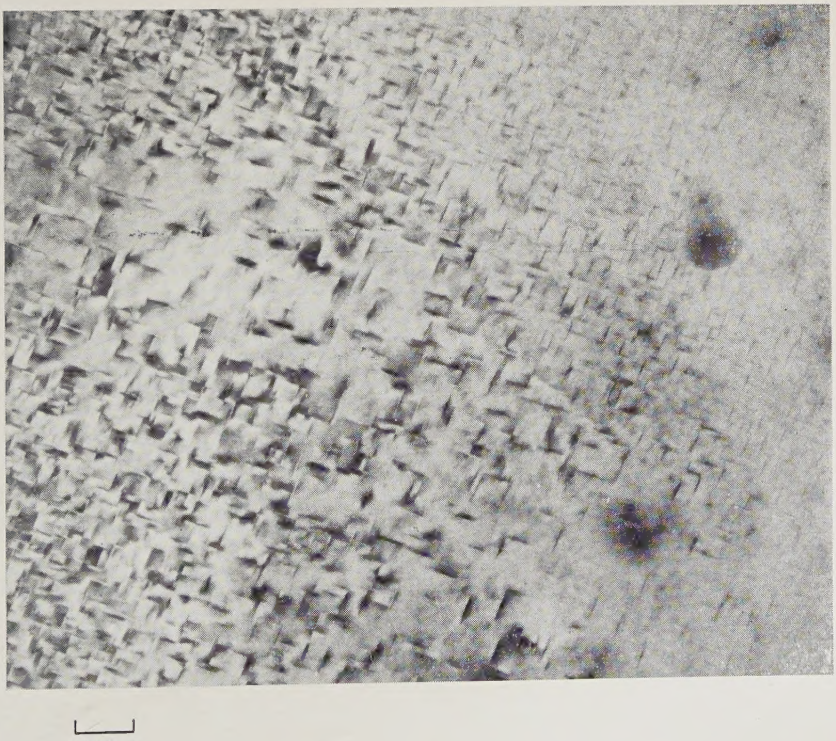

Thin foil Al 4%-Cu aged 5 hr at 160°c. (×80 000.)

Fig. 6

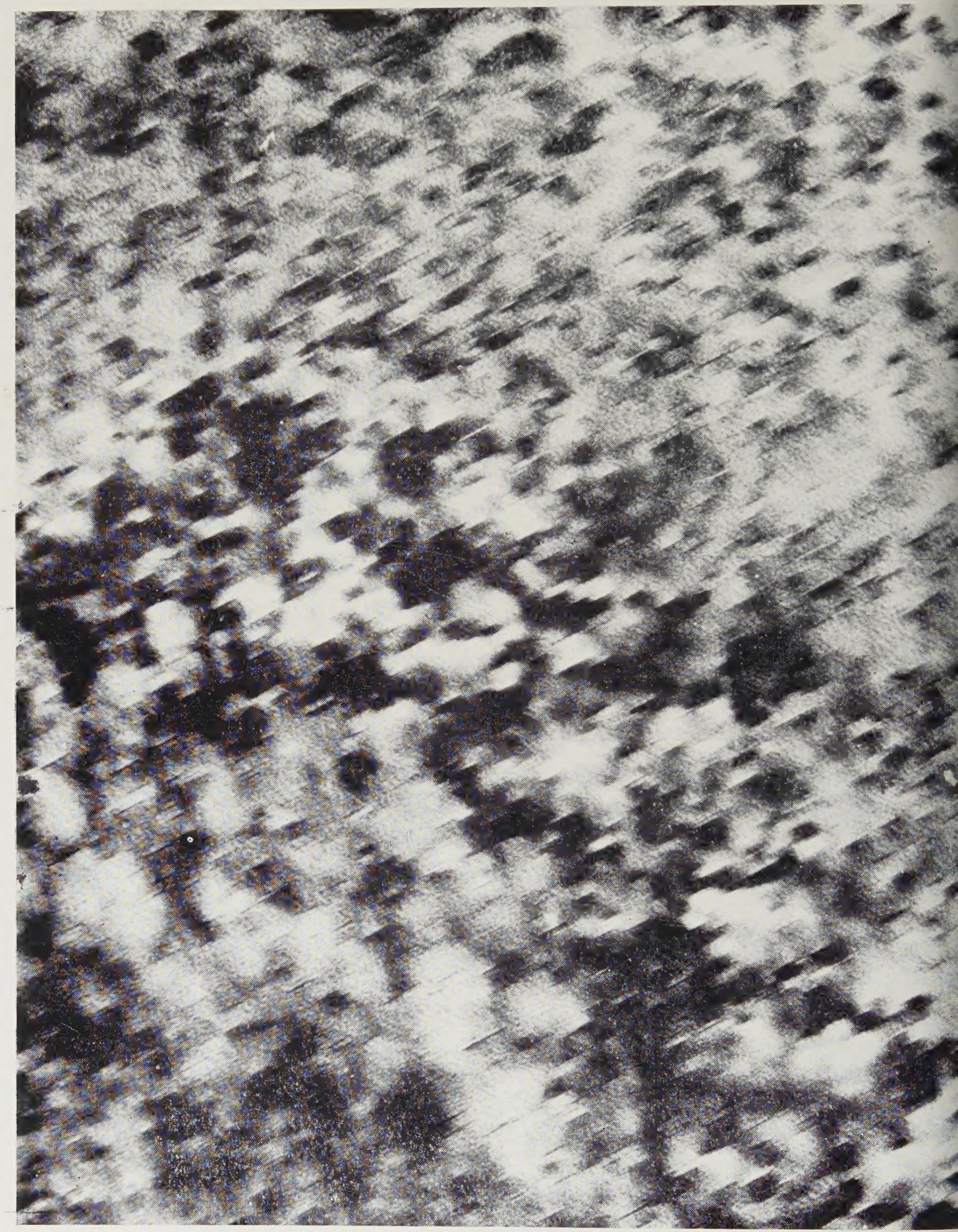

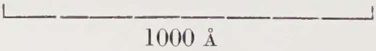

Thin foil Al 4%-Cu aged 16 hrs at 130°c to produce G.P. [1] zones. (×500 000.)